

ISSN 1408-7073

RMZ – MATERIALS AND GEOENVIRONMENT

PERIODICAL FOR MINING, METALLURGY AND GEOLOGY

RMZ – MATERIALI IN GEOKOLJE

REVIJA ZA RUDARSTVO, METALURGIJO IN GEOLOGIJO

Historical Review

More than 80 years have passed since in 1919 the University Ljubljana in Slovenia was founded. Technical fields were joint in the School of Engineering that included the Geologic and Mining Division while the Metallurgy Division was established in 1939 only. Today the Departments of Geology, Mining and Geotechnology, Materials and Metallurgy are part of the Faculty of Natural Sciences and Engineering, University of Ljubljana.

Before War II the members of the Mining Section together with the Association of Yugoslav Mining and Metallurgy Engineers began to publish the summaries of their research and studies in their technical periodical Rudarski zbornik (Mining Proceedings). Three volumes of Rudarski zbornik (1937, 1938 and 1939) were published. The War interrupted the publication and not until 1952 the first number of the new journal Rudarsko-metalurški zbornik - RMZ (Mining and Metallurgy Quarterly) has been published by the Division of Mining and Metallurgy, University of Ljubljana. Later the journal has been regularly published quarterly by the Departments of Geology, Mining and Geotechnology, Materials and Metallurgy, and the Institute for Mining, Geotechnology and Environment.

On the meeting of the Advisory and the Editorial Board on May 22nd 1998 Rudarsko-metalurški zbornik has been renamed into “RMZ - Materials and Geoenvironment (RMZ -Materiali in Geokolje)” or shortly RMZ - M&G.

RMZ - M&G is managed by an international advisory and editorial board and is exchanged with other world-known periodicals. All the papers are reviewed by the corresponding professionals and experts.

RMZ - M&G is the only scientific and professional periodical in Slovenia, which is published in the same form nearly 50 years. It incorporates the scientific and professional topics in geology, mining, and geotechnology, in materials and in metallurgy.

The wide range of topics inside the geosciences are welcome to be published in the RMZ -Materials and Geoenvironment. Research results in geology, hydrogeology, mining, geotechnology, materials, metallurgy, natural and antropogenic pollution of environment, biogeochemistry are proposed fields of work which the journal will handle. RMZ - M&G is co-issued and co-financed by the Faculty of Natural Sciences and Engineering Ljubljana, and the Institute for Mining, Geotechnology and Environment Ljubljana. In addition it is financially supported also by the Ministry of Higher Education, Science and Technology of Republic of Slovenia.

Editor in chief

Table of Contents – Kazalo

Characterization of titanium and stainless steel medical implants surfaces

Karakterizacija površin medicinskih vsadkov iz titana in nerjavnih jekel

BOMBAČ, D., BROJAN, M., KRKOVIČ, M., TURK, R., ZALAR, A. 151

Hot forming of Zn and ZnCuTi, ZnPb alloys

Toplo preoblikovanje Zn in zlitin ZnCuTi ter ZnPb

FAJFAR, P., TURK, R., BRESKVAR, B., TERČELJ, M. 165

Varjenje močno legiranih jekel z oplaščenimi elektrodami

Welding of high-alloy steels with covered electrodes

KEJŽAR, R., KOSEC, L., KEJŽAR U. 179

Določitev meje T/J z analizo stabilnih izotopov $\delta^{13}\text{C}$ in $\delta^{18}\text{O}$ (Krim, Slovenija)

Determination of T/J boundary by $\delta^{13}\text{C}$ and $\delta^{18}\text{O}$ stable isotope analysis (Krim Mountain, Slovenia)

MILER, M., PAVŠIČ, J., DOLENEC, M. 189

Foraminiferal suborder Robertinina from the Badenian of Kozjansko (Eastern Slovenia)

Foraminiferni podred Robertinina iz badenija na Kozjanskem (vzhodna Slovenija)

OBLAK, K. 203

Geological characteristics of the terrain along Vc corridor between Sava river and Sarajevo town

BAŠAGIĆ, M., ŠKRIPKIĆ, N., SKOPLJAK, F. 217

Environmental protection and investment costs as factors of road placement

Okolje in investicijski stroški kot dejavnika za umeščanje cestne trase v prostor

KOČEVAR, H., ŠETINC, M. 223

Designing a national groundwater quantity monitoring network on groundwater bodies with alluvial aquifers in Slovenia

Načrtovanje državne mreže za spremljanje količin podzemne vode na vodnih telesih podzemne vode z aluvialnimi vodonosniki

- SOUVENT, P., MIKULIČ, Z., ANDJELOV, M., SAVIĆ, V. 235

A contribution to construction monitoring with simultaneous application of various types of observations

Prispevek k spremljanju objektov s simultanimi meritvami različnih tipov

- VULIĆ, M., URANJEK, G. 247

Distance reduction with the use of UDF and Mathematica

Redukcija dolžin z uporabo MS Excel-ovih lastnih funkcij in programa Mathematica

- VULIĆ, M., BRECELJ, U. 265

Predstavitev Oddelka za materiale in metalurgijo Naravoslovnotehniške fakultete na sejmu GIFA, METEC, THERM PROCESS in NEWCAST 2007

- KORES, S., PETRIČ, M., VONČINA, M. 287

- Author's Index, Vol. 54, No. 2** 291

- Instructions to Authors** 292

- Template** 295

No. of indexing of RMZ-M&G in singular Databases

- Število indeksiranih člankov iz RMZ-M&G v posameznih bazah 302

Characterization of titanium and stainless steel medical implants surfaces

Karakterizacija površin medicinskih vsadkov iz titana in nerjavnih jekel

DAVID BOMBAC¹, MIHA BROJAN², MATIJA KRKOVIČ³, RADOMIR TURK¹, ANTON ZALAR^{1,4}

¹ University of Ljubljana, Faculty of Natural Sciences and Engineering, Aškerčeva cesta 12, SI-1000 Ljubljana, Slovenia; E-mail: david.bombac@ntf.uni-lj.si, rado.turk@ntf.uni-lj.si

² University of Ljubljana, Faculty of Mechanical Engineering, Aškerčeva cesta 6, SI-1000 Ljubljana, Slovenia; E-mail: miha.brojan@fs.uni-lj.si

³ University Medical Center, Zaloška cesta 7, SI-1525 Ljubljana, Slovenia;
E-mail: matija.krkovic@kclj.si

⁴ Jozef Stefan Institute, Jamova cesta 39, SI-1000 Ljubljana, Slovenia;
E-mail: anton.zalar@ijs.si

Received: March 25, 2007

Accepted: September 28, 2007

Abstract: Medical implants made from titanium and stainless steel have been used widely and successfully for various types of trauma and orthopaedic reconstructions. It is believed that oxide films covering implant surfaces are of crucial importance for biocompatibility and successful osseointegration. The aim of this study is to investigate the surfaces of new and used commercial medical implants made from titanium and stainless steel. The surfaces were studied by Auger electron spectroscopy (AES) and Atomic force microscopy (AFM).

Izvleček: Medicinski vsadki narejeni iz titana in nerjavnega jekla so uspešno uporabljeni v kirurški praksi pri rekonstrukcijah v travmatologiji in ortopediji. Splošno prepričanje je, da so oksidne plasti, ki prekrivajo površine, bistvenega pomena pri biokompatibilnosti in uspešni oseointegraciji. Cilj te študije je preiskava površin komercialnih novih in že uporabljenih medicinskih vsadkov narejenih iz titana in nerjavnih jekel. Površine so bile preiskane z Augerjevo elektronsko spektroskopijo (AES) in mikroskopijo na atomsko silo (AFM).

Key words: medical implants, AES, depth profiling, AFM, roughness

Ključne besede: medicinski vsadki, AES, profilna analiza, AFM, hrapavost

INTRODUCTION

Implants used in medicine for bone osseosynthesis have to satisfy functional demands defined by the working environment of human body. Ideally, they should have biomechanical properties comparable to those of autogenous tissues without any adverse effects. The principal requirements are corrosion resistance, biocompatibility, biofunctionality, bioadhesion, etc. Geometry, roughness and other characteristics of the implant surface also importantly influence the surface-tissue interaction, which is considered to be dynamic. In the first few seconds after the contact has been made, there are only water, dissolved ions, and free biomolecules in the closest proximity of the surface, but no cells. The composition of the body liquid changes continuously as inflammatory and healing processes precede, causing changes in the composition of the adsorbed layer of biomolecules on the implant surface until it is balanced. Cells and tissues eventually contact the surface and, depending on the nature of the adsorbed layer, they respond in specific ways that may further modify the adsorbed biomolecules^[1].

Currently commercially pure (CP-Ti), titanium alloy TiAl6V4 and stainless steel AISI 316L are the most popular alloys used for the trauma and orthopaedic medical implants and are normally covered with a thin protective film, which largely determines the surface properties of an implant. On stainless steel a layer of the surface oxide is formed either during manufacturing or intentionally passivated in various media. Passivation is the spontaneous formation of a surface film on a metal which inhibits

further corrosion. A metal is passive when it behaves nobler than it is in a given solution as a result of the protective surface film, usually an oxide. As the name indicates, the metal is then said to be passive to corrosion. Passivation of AISI 316L steel can be performed either thermally, electrochemically, or in nitric acid. Very good corrosion resistance of medical grade stainless steel is derived from the protective layer of chromium oxide type Cr_2O_3 , that forms on the surface. If surface is damaged, e.g. scratched the oxide layer reforms almost instantly and can be referred to as "self-healing"^[2]. This surface oxide provides the ultimate interface with tissue after implantation and behaves differently compared to bare metallic surface. The corrosion process is responsible for cell toxicity and stimulates fibroblast growth, protein, and platelet adhesion. Metallic implants can interact with living tissue in 3 ways: (1) by electron exchange – redox reaction, (2) by proton exchange – hydrolysis, and (3) by complex formation – metal ion-organic molecule binding. The behaviour of stainless steel is dominated by its nickel component, which induces all 3 reactions, whereas none have been observed with titanium^[3]. Studies by other authors reported the surface oxide on commercially available titanium implant systems, consisted mainly of TiO_2 , and the oxide structure was found to be noncrystalline^[4-6]. This thin oxide film, naturally formed on a titanium substrate, is presumably responsible for the excellent biocompatibility of titanium implants due to a low level of electronic conductivity^[7], a high corrosion resistance and a thermodynamically stable state at physiological pH values^{[8],[9]}.

The primary goal of this study was to investigate the difference of the surfaces chemical and physical properties on the unused and the in-vitro implanted medical device by using atomic force microscopy

(AFM) to study the surface morphology and Auger electron spectroscopy (AES) to analyze the chemical composition of surface oxide layers.

EXPERIMENTAL PROCEDURE

Osteosynthetic medical implants for this study have been provided by the University Medical Centre Ljubljana. Obtained osteosynthetic material have been commercial products: compression plates LCP Locking Compression Plates, screw and Philos plate system manufactured by Synthes GmbH. Titanium based samples have been coated with TiN based hard coating with two different colours (exact preparation technique of surface coatings is unknown due to the commercial nature of obtained osteosynthetic material). Details of the implants investigated are shown in Table 1. Surface analyses were performed on the central portions of the external surfaces of implants made from AISI 316L stainless steel and Ti-based alloys.

The plate shaped implants were cut in dimensions of approximately 1×1 cm and mounted into the spectrometer. Chemical composition of the samples surfaces were characterized with AES instrument SAM, PHI Model 545A, manufactured by Physical Electronics Industries Inc. The argon pressure in the chamber during depth profiling was about 10^{-5} Pa and the base pressure was about 1.1×10^{-9} Pa. A static primary electron beam of 3 keV, 1 μ A and a diameter of approximately 40 μ m were used. The samples were sputtered using two symmetrically inclined Perkin-Elmer-

PHI Mod. 04-191 ion guns. The ion incidence angle was about 47° with respect to the normal of the sample surface. The samples were sputtered with 1 keV Ar⁺ ion beams, rastered on area of 5×5 mm. AES depth profiles of the samples were obtained by continuous ion sputtering. The sputtering rate determined on a Cr/Ni multilayer reference sample was about 4 nm/min. The sputter rate is dependent on a number of factors such as instrumental factors (adsorption from residual gas atmosphere, impurities in ion beam, etc.), sample characteristics (original surface roughness, compounds, second phases, etc.) and radiation induced effects (primary atom implantation, atomic mixing, etc.). It is well known that metallic oxides sputter at different rates, and many at rates slower than pure metal. Although the depth profiles presented in this paper and in the literature assume constant ion sputtering rates, the rates actually increase as the oxide is removed. Absolute sputter rates are unknown because the composition of the specimen is continuously changing with depth. The Auger peak-to-peak heights of P (120 eV), Mo (186 eV), K (252 eV), C (272 eV), Ca (292 eV), N (385 eV), Ti (418 eV), Cr (446 eV), O (510 eV), Fe (703 eV), Ni (848 eV) and Na (990 eV) were measured. Concentration profiles were evaluated using relative sensitivity factors from the manufacturer's handbook^[10]. The following sensitivity factors were used: P

(0.53), Mo (0.34), K (0.80), C (0.18), Ca (0.47), Ti (0.44), Cr (0.041), O (0.50), Fe (0.21), Ni (0.29), Na (0.21). The sensitivity factor of N (0.70) was determined on stoichiometric TiN thin film structure.

Surface structure was investigated with a Solver PRO-M atomic force microscope (AFM) manufactured by NT-MDT Co. in semi contact mode. The images were

recorded with a resolution of 256 points per line on a $10 \times 10 \mu\text{m}$ area using commercial Si cantilevers NSG10 series with the Au conductive coating from NT-MDT Co., with stiffness 11.5 N/m, resonant frequency 255 kHz and tip curvature 10 nm as reported by the manufacturer^[11]. The roughness amplitude Ra of medical implants surfaces was measured.

Table 1. Presentation of analyzed samples

Tabela 1. Predstavitev analiziranih vzorcev

Sample	Material	Osteosynthetic system	Exposure	Analysis method
1	AISI 316L	Compression plate	Unused	AES
2	AISI 316L	Screw	Implanted	AES
3	Ti6Al4V (golden coating)	LCP plate	Unused	AES
4	Ti6Al4V (golden coating)	LCP plate	Implanted	AES
5	Ti6Al4V (blue coating)	Philos LCP system	Implanted	AES
6	Ti6Al4V (blue coating)	Philos LCP system	Implanted	AFM
7	AISI 316L	Compression plate	Unused	AFM

RESULTS AND DISCUSSION

AES depth profiles of unused and used samples made from AISI 316L stainless steel are depicted in Figure 1a,b. Elements O, C, N, Na, Fe, Cr, Mo, and Ni have been found on an unused medical implant. Characteristic depth profile of the elements distribution is exhibited in Figure 1a, where oxygen concentrated, chromium enriched and iron impaired profiles are distinguished. The depletion of iron concentration and the enrichment of chromium on the outmost surface oxide may indicate a

selective dissolution of iron and a preferential oxidation of Cr metal in the depth of the passive film during the manufacturing of medical device where passivation (soaking in acids and heating at elevated temperatures) is process occurring after mechanical and electropolishing. Also a smaller extent of Ni is enriched in the oxide layer. Inner composition on depth profile is near bulk. Iron oxides such as Fe_3O_4 and Fe_2O_3 are normally reduced to FeO by ion bombardment^[12] and can therefore be identified even after sputtering.

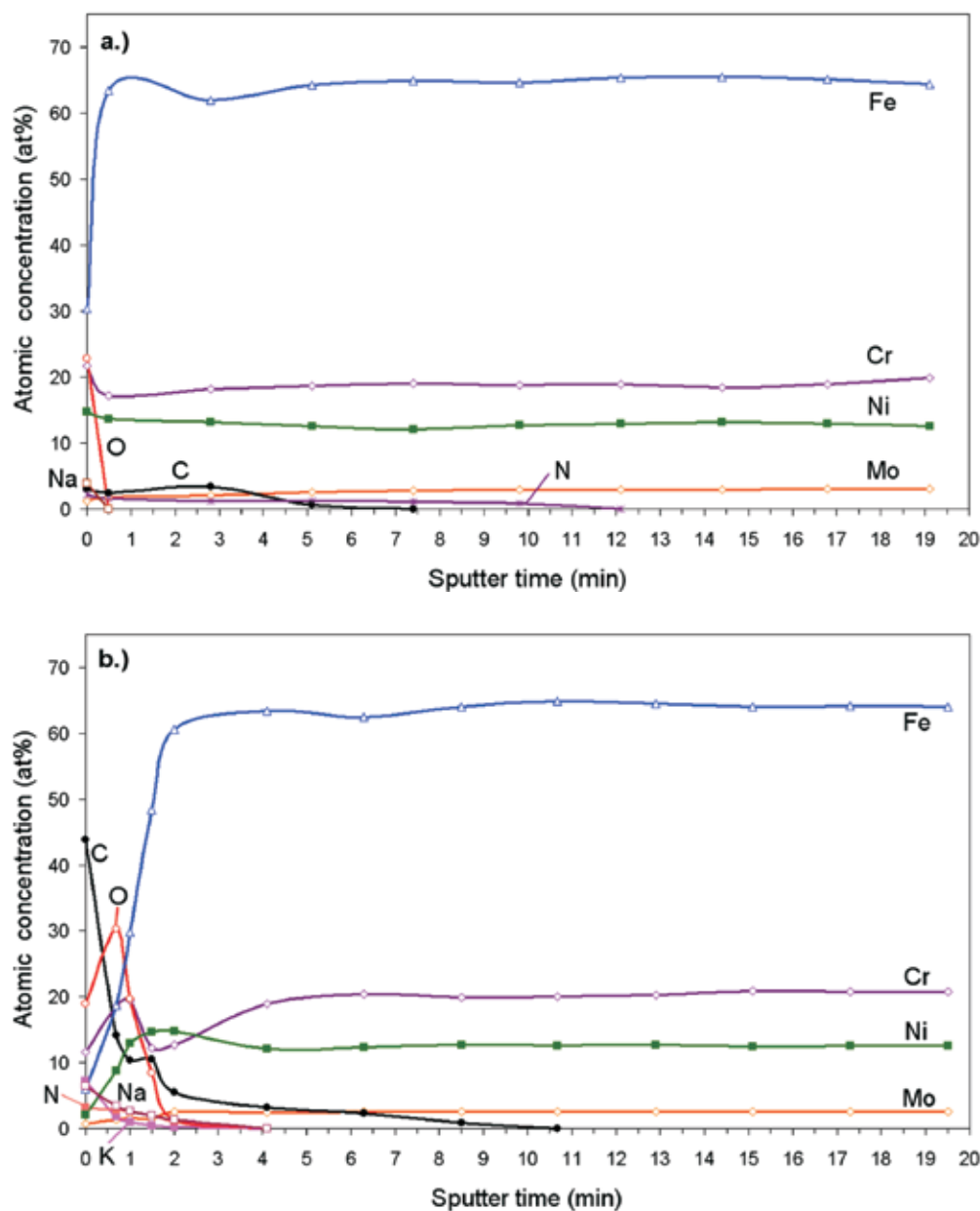


Figure 1. AES depth profile of AISI 316L sample, a.) unused medical implant, b.) used medical implant

Slika 1. AES profilna analiza vzorca iz AISI 316L, a.) neuporabljen medicinski vsadek, b.) uporabljen medicinski vsadek

Samples that have been implanted in the human body have surfaces which contain spots with layers of relatively thick organic material. In Figure 1b AES depth profile of stainless steel implant which has been in contact with living tissue is shown. The surface layer on the used implant changes compared to unimplanted sample, where on booth depth profiles inner composition is near bulk. Traces of S and K were additionally found on surface as depicted in Figure 2. Implanted sample consists of

much thicker oxide layer compared to an unimplanted sample. All metal components are diminished on the surface and organic components are enriched. Iron and Ni concentrations increase rapidly from outermost side of the surface layer to deepness in depth profile. It can also be observed from Figure 1b that concentration of Cr increases at first and then starts to sink. This can be related to oxidation of Cr in oxide layer.

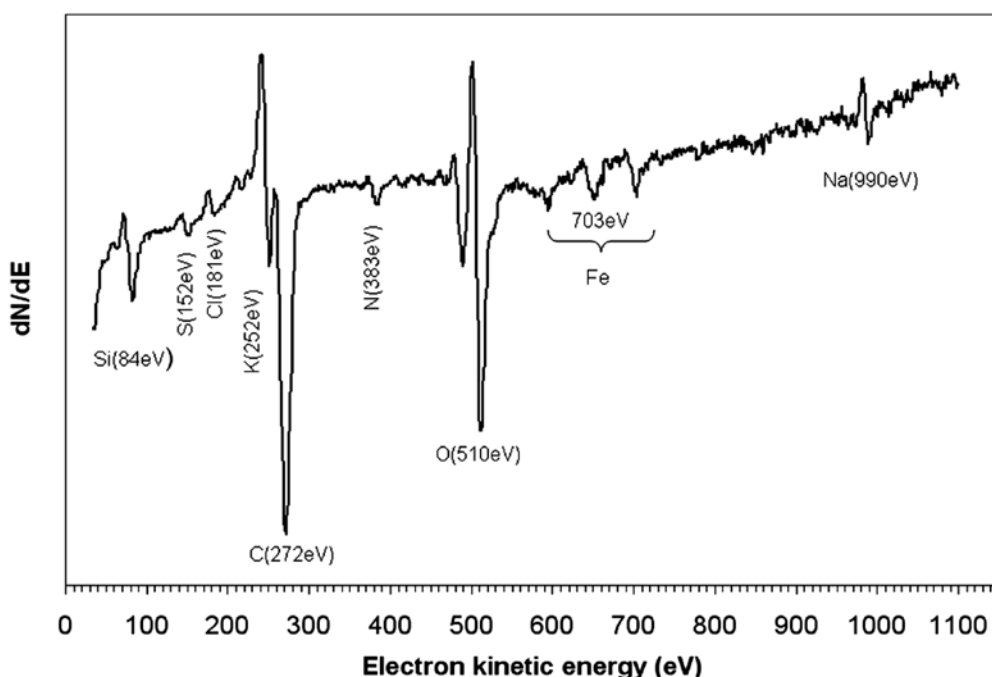


Figure 2. AES spectrum of an implanted AISI 316L sample surface

Slika 2. AES spekter na površini vsadka iz AISI 316L

According to the theory, the bipolar structure of the passive oxide film on stainless steel consists of excess metal ions or oxygen ion vacancies in the inner layer, which provide a positive fixed charge with an anion-selective property, as well as an excess oxygen ions or metal ion vacancies in the

outer layer, which result in a negative fixed charge with a cation selective property. All cells and surfaces of the body carry an electrical charge, and the majority of the particles within the blood are negatively charged^[13].

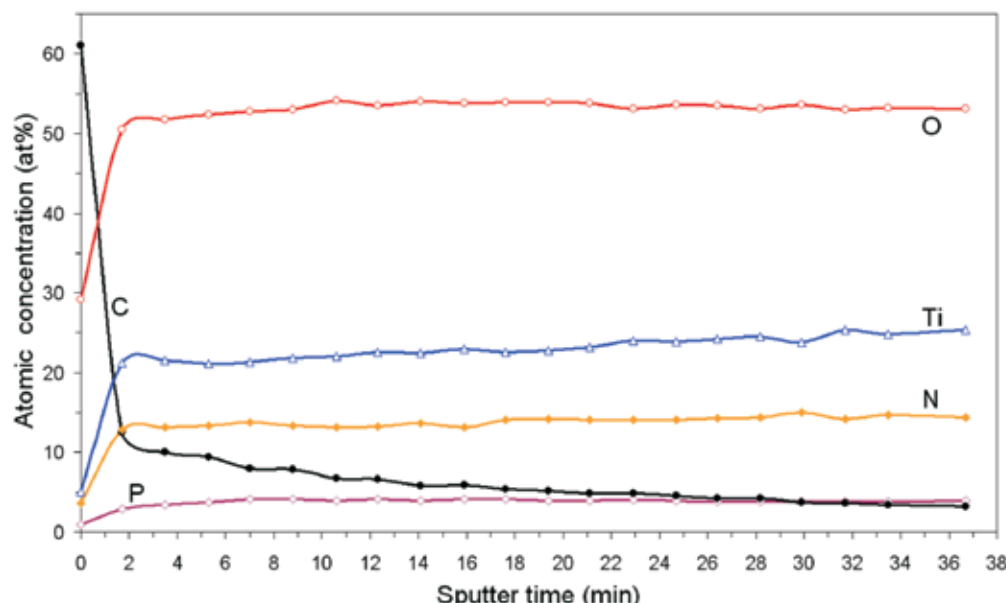


Figure 3. AES depth profile of unused titanium medical implant with golden colour protective layer

Slika 3. AES profilna analiza neuporabljenega vzorca medicinskega vsadka narejenega iz titana z zlato obarvano zaščitno prevleko

An AES depth profile of an unimplanted titanium sample with golden colour protection layer is shown in Figure 3. Elements O, Ti, N, P are compounds of an coating deposited on bulk titanium to increase biocompatibility. Carbon in the depth profile is due to surface roughness and carbon low

density. It is overestimated due to the back-scattering effect and preferential sputtering. High content of O, Ti and N is found due to the formation of protective layer and appears to consist of either mixture of TiO_2 and TiN_x or a Ti oxynitride ($\text{TiO}_{x,y}\text{N}_y$).

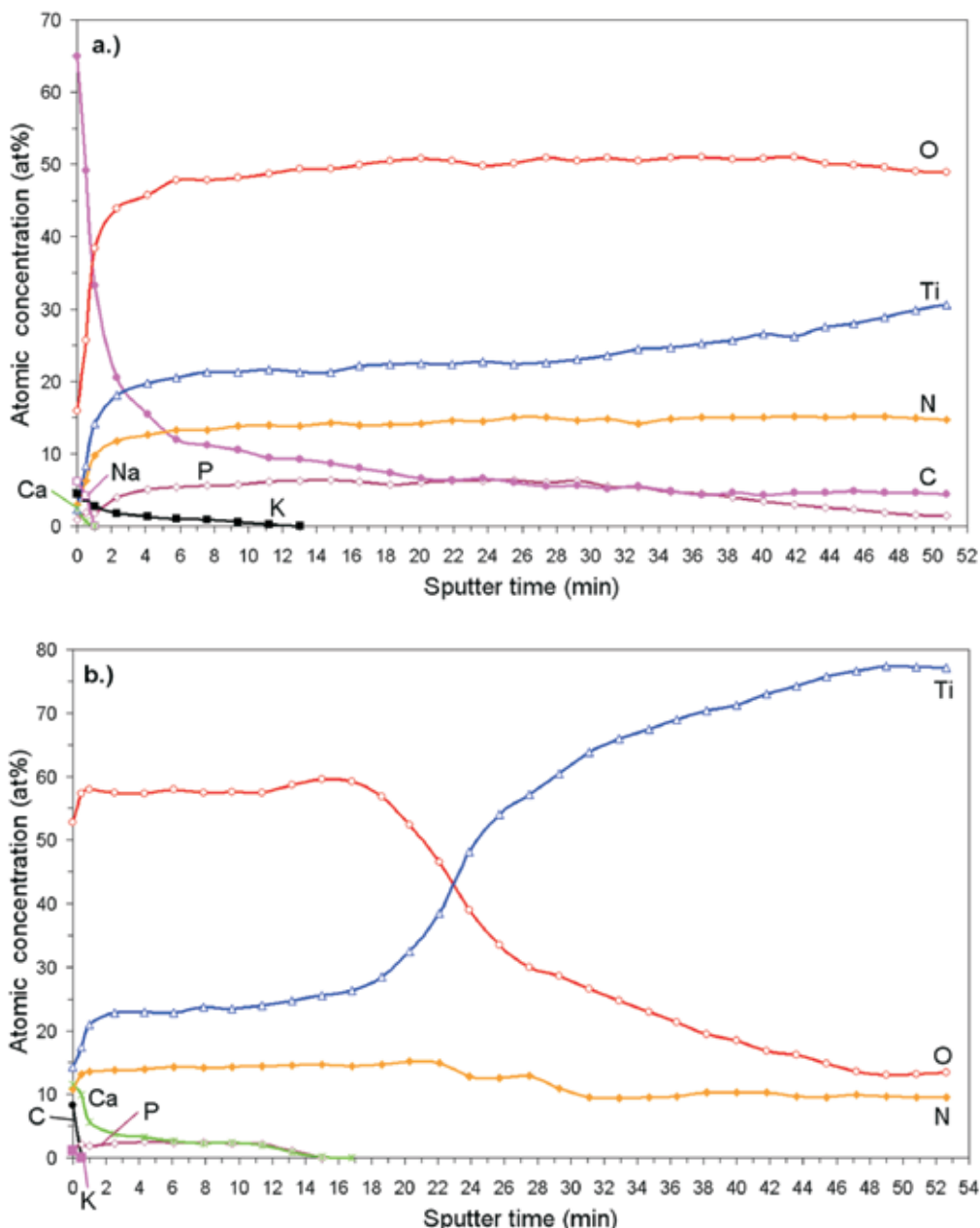


Figure 4. AES depth profile of titanium medical implants with a.) golden coloured coating, b.) blue coloured coating

Slika 4. AES profilna analiza titanovega medicinskega vsadka z a.) zlato obarvana prevleka, b.) modro obarvana prevleka

Because coating preparation technique is unknown due to commercial nature of medical products, another possible interpretation is that the surface consists of a TiO_2 layer covering the underlying Ti nitride. More detailed analysis, including angle resolved XPS, is necessary to distinguish between these interpretations. Significant change of the oxide composition in the surface region is because of contamination. Surface contamination on air-exposed samples is practically inevitable and the contamination layers on titanium oxide or oxynitride surfaces are most often dominated by oxygen and organic molecules with ingredients of Ca, Na, K and C.

Chemical properties of two used titanium medical implants with different coatings colours were examined on spectrometer by AES. Difference in the colour is due to different coating composition as can be seen in AES depth profiles of golden (sample 4) and blue (sample 5) colour coating presented in Figure 4a, and 4b, respectively. Obtained depth profiles of implanted sam-

ple 4 (Figure 4a) is significantly different compared to an unimplanted one (Figure 3). Penetration of Ca and P and also some Na was found in superficial stratum of the protective layer while K has been found relatively deeper. Sample 5 is different in composition and thickness. On its depth profile shown in Figure 4b, elements C and K were found on the surface and Ca and P in depth of the protective layer. Correlation between Ca and P can be linked to formation of calcium phosphate rich layer on its surface, very similar to hydroxyapatite which also prevents corrosion. Another advantageous property of formatted layer is that in the case of damaging the protective layer the titanium oxides and Ca-P layer regenerate^[1].

This study presents surface characterization of unused and implanted biomaterial for trauma and orthopaedic medical products. A key issue in all trauma and orthopaedic medical applications of biomaterials is how the implanted material influences, and is influenced by, the biological re-

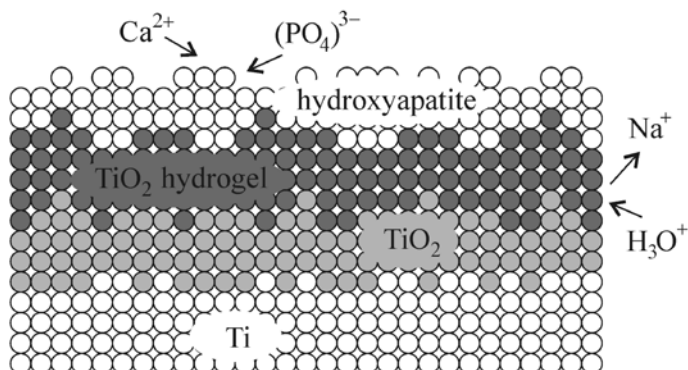


Figure 5. A formation of calcium phosphate rich layer on titanium oxide film
Slika 5. Nastanek obogatene plasti kalcijevega fosfata na substratu titanovega oksida

sponse resulting from the contact between the biological system and the biomaterial. Understanding the surface phenomena of changes when the biomaterials are used in the biosystem can improve the knowledge about material - biosystem interactions. Several scenarios have been proposed for the events that may occur when a material surface is placed in contact with a biological system. The initial events in such scenarios are adsorption of water molecules, hydrated ions, and biomolecules, which form a so-called "conditioning film" on the biomaterial surface. Cells of the host tissue interact in this hydrated biomolecule coating, therefore the original surface properties of an implanted biomaterial constitute an important starting condition for the dynamics of the interface^[14]. In Figure 5 formation of calcium phosphate rich layer similar to hidroxyapatite on hydrated surface is shown^[1].

Furthermore the titanium with different coatings and deposition techniques show a wide range of chemical and physical properties, depending on how they are prepared and handled, and by using different surface preparation methods it is possible to control and vary selected surface properties of titanium over a relatively wide range. Different chemical properties of protective layer of used titanium base implants analysed in this study show different behaviour of deposited layer. On one formation of Ca-P rich layer was found on sample 5 while on sample 4 on such layer was found.

The observed differences can be attributed mainly to the different textures of the sur-

faces, where chemical surface analyses of samples gave only a limited picture of their surface characteristics. It is equally important to characterize the structural properties also, as they influence the biological function of biomaterials as well. The topography and roughness of polished AISI 316L stainless steel (Figure 6) and blue coated titanium (Figure 7) medical implants were analyzed with AFM.

The roughness amplitude of electropolished and passivated medical implant of AISI 316L measured with AFM over area $10 \times 10 \mu\text{m}$ and the maximum Z-range of 120 nm, resulted in Ra value of 6.5 nm. Electropolishing produces surfaces which have a mirror like appearance with smooth corrugation on the scale of $10 \times 10 \mu\text{m}$ surveyed with AFM. In Figure 6 the individual granular structure is shown, with granule sizes of a few nanometres.

AFM roughness measurements on blue colour coated titanium over areas of $10 \times 10 \mu\text{m}$ give Ra values of 68.6 nm, with maximum Z-range of 400 nm respectively. Higher roughness compared to polished AISI 316L samples can be explained with implantation of molecules on coating when implant was in contact with bodily fluids. 3D topography of wavy surface of blue coloured implanted sample is depicted in Figure 7, where raised and descended regions can be seen. In comparison to topography of stainless steel sample we can see fewer apexes which are nicely rounded and measured distance from highest to lowest point is increased.



Figure 6. AFM 3D topography of unused AISI 316L medical implants ($10 \times 10 \mu\text{m}$)

Slika 6. AFM 3D prikaz topografije površine jeklenega neuporabljenega vsadka iz AISI 316L ($10 \times 10 \mu\text{m}$)

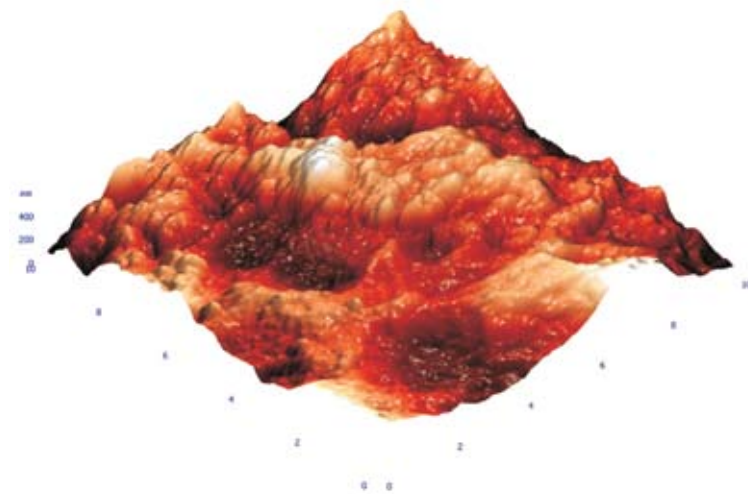


Figure 7. AFM 3D topography of used blue coated titanium trauma plate ($10 \times 10 \mu\text{m}$)

Slika 7. AFM 3D predstavitev topografije rabljene modro prevlečene titanove plošče ($10 \times 10 \mu\text{m}$)

The techniques utilised in this study were effective in the characterisation of the chemical composition, morphology and surface quality of the analysed surfaces. Analysed sample surfaces show a wide variety of structural and chemical properties. By using a combination of different experimental and analytical techniques it is possible to characterize the surface properties at a relatively high level of detail.

Further studies using carefully prepared and systematically varied samples surfaces are necessary, and are likely to lead to an increased understanding of the biocompatibility of materials in question. This development is dependent on thorough surface characterization of the materials by a broad range of surface spectroscopic and microscopic techniques.

CONCLUSIONS

Detailed information about changes in the composition of a medical implant's surface can be obtained by AES and AFM. A comparison of depth profiling results between unused and implanted commercial medical devices used for bone osteosynthesis using AES depth profiling with 3 keV Ar⁺ ion beams and physical properties examined by AFM showed that:

- Oxides grow when implant is contact with bodily fluids on both stainless steel and titanium devices.
- Type of changes in chemical composition depends on used protective coating as has

been shown on titanium implants with different coatings.

- Main factor for the colour change seems is the oxide thickness which has been confirmed by the ion sputtering of golden coated sample.
- Backscattering effect and preferential sputtering increase concentration of carbon especial on rougher titanium surfaces.
- Surfaces of stainless steel implants are much smoother, where average roughness Ra = 6.5 nm has been measured, while on coated titanium average roughness Ra was 68.6 nm, since titanium surfaces are coated with hard coatings.

POVZETKI

Karakterizacija površin medicinskih vsadkov iz titana in nerjavnih jekel

Podrobne informacije o spremembah v sestavi površine medicinskega vsadka lahko dobimo z metodama AES in AFM. Primerjava globinskih profilov novega in že uporabljenega komercialnega medicinskega vsadka za oseosintezo kostnega tkiva z

AES globinsko profilometrijo s 3 keV Ar⁺ ioni in fizikalne lastnosti preiskane z AFM so pokazale:

- Površinski oksidi rastejo pri kontaktu vsadka s telesnimi sokovi, tako na vsadkih iz nerjavnega jekla, kot tudi na vsadkih iz titana.
- Vrsta spremembe v kemijski sestavi je odvisna od vrste zaščitne prevleke, ki je bila nanesena na vsadek iz titana.
- Barva zaščitne prevleke je odvisna od re-

- ferenčne debeline oksida, kar je bilo potrjeno pri ionskem jedkanju zlato obarvane prevleke.
- Na zasenčenih površinah, ki jih pri ionskem jedkanju ne dosežemo izmerimo višjo koncentracijo ogljika, še posebej na bolj hrapavih površinah.
 - Površine vsadkov, narejenih iz nerjavnega jekla so bolj gladke, s povprečno vrednostjo $R_a = 6.5 \text{ nm}$. Na površinah titanovih vsadkov je bila izmerjena večja povprečna hrapavost $R_a = 68.6 \text{ nm}$, kar je posledica nanosa zaščitne prevleke.

Acknowledgements

The authors would like to thank to Mr. B. Pracek and dr. J. Kovac, Jozef Stefan Institute, for technical assistance.

REFERENCES

- [1] BALAZIC, M., BOMBAC, D., BROJAN, M., CARAM, R. Jr., KOSEL, F., KOPAC, J. (2007): Titanium and titanium alloy applications in medicine. *Surface Engineered Surgical Tools and Medical Devices*. Editors: J. Jackson, W. Ahmed. Springer, ISBN: 978-0-387-27026-5.
- [2] JOHNSON, SL. (2006): *Surface studies of potentially corrosion resistant thin film coatings on chromium and type 316l stainless steel: Ph.D. Thesis*. Kansas, Kansas State University, pp. 50-58.
- [3] WINDECKER, S., MAYER, I., DE PASQUALE, G., MAIER, W., DIRSCH, O., DE GROOT, P., WU, Y.P., NOLL, G., LESKOSEK, B., MEIER, B., HESS, O.M. (2001): Stent Coating With Titanium-Nitride-Oxide for Reduction of Neointimal Hyperplasia. *Circulation* 104. pp. 928.
- [4] LAUSMAA, J., KASEMO, B. (1990): Surface spectroscopic characterization of titanium implant materials. *Applied Surface Science* 44. pp. 133-146.
- [5] MACHNEE, CH., WAGNER, WC., JAARDA, MJ., LANG, BR. (1993): Identification of oxide layers of commercially pure titanium in response to cleaning procedures. *International Journal of Oral & Maxillofacial Implants* 8. pp. 529-533.
- [6] WÄLIVAARA, B., ARONSSON, BO., RODAHL, M., LAUSMAA, J., TENGVALL, P. (1994): Titanium with different oxides: in vitro studies of protein adsorption and contact activation. *Biomaterials* 9. pp. 827-834.
- [7] ZITTER, H., PLENK, H.J. (1987): The electrochemical behaviour of metallic implant materials as indicator of their biocompatibility. *Journal of Biomedical Materials Research* 21. pp. 881-896.
- [8] SOLAR, RJ., POLLACK, SR., KOROSTOFF, E. (1979): In vitro corrosion testing of titanium surgical implant alloys: an approach to understanding titanium release from implants. *Journal of Biomedical Materials Research* 13. pp. 217-250.

- [⁹] William, DF. (1976): Corrosion of implant materials. *Annual Reviews of Material Science* 6, pp. 237-265.
- [¹⁰] DAVIS, LE., MACDONALD, NC., PALMBERG, PW., RIACH, GE., WEBER RE. (1976): *Handbook of Auger electron spectroscopy 2nd ed.* Physical Electronics Industries Inc., Eden Prairie, Minnesota.
- [¹¹] NT-MDT - *Molecular devices and tools for nano technology*. Dostopno na svetovnem spletu: http://www.ntmdt-tips.com/catalog/golden/cond/non/au/products/NSG10_Au_50.html
- [¹²] SUNDGREN, J-E., BODÖ, P., LUNDSTRÖM, I. (1986): Auger electron spectroscopic studies of the interface between human tissue and implants of titanium and stainless steel. *Journal of Colloid and Interface Science* 110. pp. 9-20.
- [¹³] SHIH, CC., SHIH, CM., SU, YY., SU, LHJ., CHANG, MS. (2004): Effect of surface oxide properties on corrosion resistance of 316L stainless steel for biomedical applications. *Corrosion Science* 46. pp. 427-441.
- [¹⁴] LAUSMAA, J. (1996): Surface spectroscopic characterization of titanium implant materials. *Journal of Electron Spectroscopy and Related Phenomena* 81. pp. 343-361.

Hot forming of Zn and ZnCuTi, ZnPb alloys

Toplo preoblikovanje Zn in zlitin ZnCuTi ter ZnPb

PETER FAJFAR¹, RADOMIR TURK¹, BOJAN BRESKVAR², MILAN TERČELJ¹

¹ University of Ljubljana, Faculty of Natural Sciences and Engineering, Aškerčeva cesta 12, SI-1000 Ljubljana, Slovenia; E-mail: peter.fajfar@ntf.uni-lj.si, rado.turk@ntf.uni-lj.si, milan.tercelj@ntf.uni-lj.si

² Institute of metals and technology, Lepi pot 11, SI-1000 Ljubljana, Slovenia;
E-mail: bojan.breskvar@imt.si

Received: September 19, 2007

Accepted: October 25, 2007

Abstract: Hot compression tests of pure zinc and zinc alloyed with copper, titanium and lead have been carried out on Instron 1255. Since the testing machine was not equipped with the proper heating system, a new heating device was developed. Specimens and compression tools were heated using oil bath. Specimens were in as-cast and pre-deformed state. Tests were performed at two constant tools speeds: 0.2 and 0.01 m/s and three temperatures: 80, 150 in 210 °C. Constants for flow stress description of Hajduk-Hensel equation were determined. The comparison between measured and predicted flow stresses are in good accordance.

Izvleček: Za določitev krivulj tečenja so bili z uporabo preizkuševalne naprave Instron 1255 narejeni topli tlačni preizkusi za čist Zn in zlitini: ZnCuTi ter ZnPb. Ker preizkuševalni stroj ni bil opremljen s sistemom za ogrevanje vzorcev, smo izdelali napravo, s katero smo vzorce in tudi orodje ogrevali v oljni kopeli. Vzorci so bili tako vitem kot tudi predhodno deformirani stanju. Preizkuse smo vodili pri dveh konstantnih hitrostih pomika orodja: 0,2 in 0,01 m/s ter treh temperaturah: 80, 150 in 210 °C. Določene so bile konstante za izračun krivulj tečenja po Hajduk-Hensel. Izračunane vrednosti so v dokaj dobrem ujemanju z izmerjenimi vrednostmi.

Key words: Zn, Zn alloys, compression test, flow curves

Ključne besede: Zn, Zn zlitine, tlačni preizkusi, krivulje tečenja

INTRODUCTION

Zinc is the fourth most common metal in use. Over 7 million tons of zinc is produced annually worldwide. Only annual production of iron, aluminium and copper are major. Zinc and zinc alloys are used in the form of coatings, casting and wrought zinc products. Wrought zinc and zinc alloys may be obtained as rolled strip, sheet and foil; extruded rod and shapes; and drawn rod and wire. These metals exhibit good resistance to corrosion in many types of service. Nearly half of annual production is used for galvanizing to protect steel from corrosion. Approximately 19 % are used to produce brass and 16 % go into the production of zinc base alloys to supply e.g. the die casting industry. Significant amounts are also utilized for compounds such as zinc oxide and zinc sulphate and semi-manufactures including roofing, gutters and down-pipes. Main application areas are construction, transport, consumer goods and electrical appliances and general engineering. Wrought zinc is easily machined using standard methods and tools. However, if it is necessary to machine zinc containing exceedingly coarse grains, the metal should be heated to a temperature between 70 and 100 °C in order to avoid cleavage of crystals.

Zinc strips are usually produced from 25 to 100 mm thick slabs. Finish rolling in the temperature range 120 to 150 °C is required to obtain a bright surface and high ductility. Rolled zinc is produced as pure zinc and in seven basic alloys. Pure zinc is brittle at room temperature and at temperatures above 150 °C, being workable only in the range between 100 °C and 150 °C.

When alloyed with copper and titanium, zinc sheet is very creep resistant. This alloy is mainly used in building industry for roofing, flashing and weathering applications. In common with many other metals and alloys, wrought zinc creeps under constant loads that are substantially less than its ultimate strength; that is, wrought zinc does not have clearly defined elastic module, and hence creep data from service tests must be used in designing for strength and rigidity under conditions of continuous stress. Rolled zinc alloyed with lead is mostly used for drawn or formed articles requiring some rigidity. It must be deformed under light continuous load at elevated temperatures^{[1], [2]}.

The aim of presented work is to intensify productivity on reversing hot rolling mill with slab lengthening. Industrial measurements of loads on the mechanical side (torque on the mean shaft) and on the energetic side (current, voltage, revolutions of electromotor, etc.), and laboratory test of rolled material were carried out. Due to increasing length of the slab, the rolling time is extended. This causes the change of the slab temperature evolution and consecutive the change of rolling mill load. Because of all these changes new pass schedule must be optimized. Flow curves are very important input data for numerical modelling of rolling pass schedules. Accurate knowledge of the mechanisms acting during hot rolling is important for the manufacture of high quality products, as well as for design of optimum pass schedules.

EXPERIMENTAL

Initial state of specimens

In the present study pure zinc and two zinc alloys ZnPb (0.8 %Pb) and ZnCuTi (0.11 % Cu, 0.1 % Ti) in as-cast and deformed state were investigated. For hot compression tests cylindrical specimens with initial heights of 20 mm and initial diameters of 15.5 mm were used. For the as-cast state specimens were machined from the centre of gravity cast block of dimensions $40 \times 80 \times 1500$ mm. The bottom of the gravity die was cooled down by water that caused appearance of fine grains. In the centre part of the block the crystallization was oriented similar to macrostructure founded in plates produced in real technological process. For this reason the speci-

mens were taken from the upper two thirds of the block. Macrostructure of the transverse section in the centre of the block is presented in Figure 1. Specimens for pre-deformed state were taken from the centre of the strip which was 30 % deformed. Macrostructure of the transverse section in the centre of deformed plate shows that direction of recrystallized grains and direction of dendrite in as-cast are nearly the same (Figure 2). This effect is not presented in the specimens (Figures 3, 5 and 7) what confirmed the accurate procedure of taking specimens from plates. In deformed specimens (Figure 3b, 5b and 7b) the recrystallization of crystal grains is noticed. To clarify initial state of specimens microstructures are presented as well (Figures 4, 6 and 8) where uniformity is obvious.

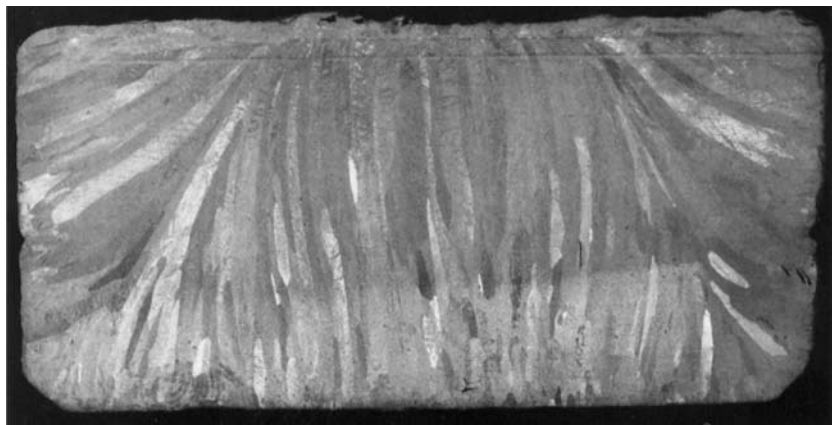


Figure 1. Transverse section of Zn cast block

Slika 1. Prečni presek ulitka iz Zn

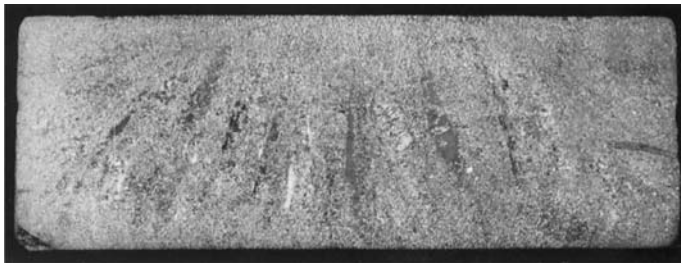


Figure 2. Transverse section of 30 % deformed Zn plate

Slika 2. Prečni presek 30 % toplo deformiranega ulitka iz Zn

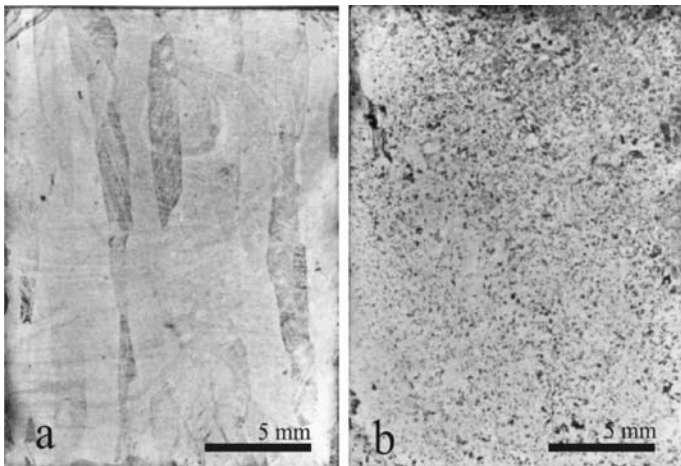


Figure 3. Macrostructure of Zn specimen: as-cast (a), deformed (b)

Slika 3. Makrostruktura Zn vzorca: ulit (a), deformiran (b)

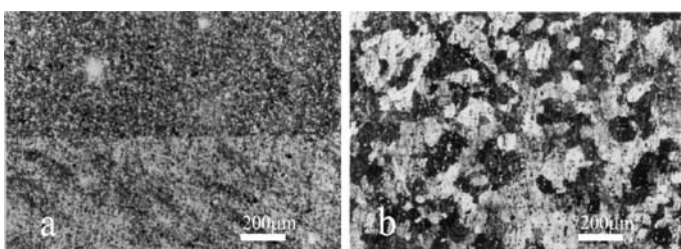


Figure 4. Microstructure of Zn specimen of as-cast (a), deformed (b)

Slika 4. Mikrostruktura Zn vzorca: ulit (a), deformiran (b)

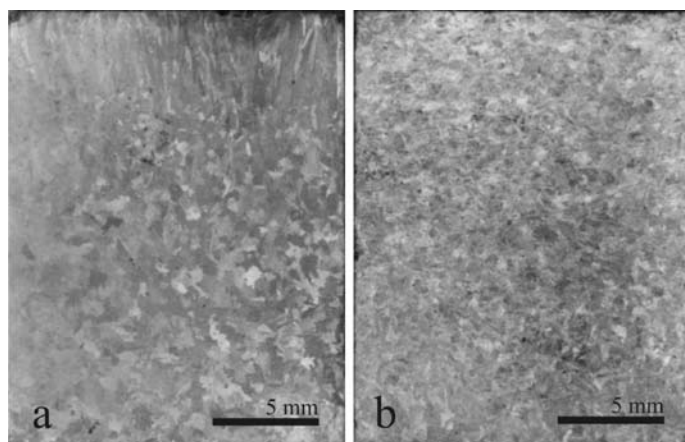


Figure 5. Macrostructure of ZnCuTi specimen: as-cast (a), deformed (b)
Slika 5. Makrostruktura ZnCuTi vzorca: ulit (a), deformiran (b)

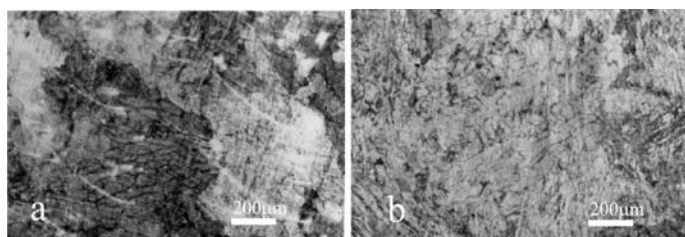


Figure 6. Microstructure of ZnCuTi specimen: as-cast (a), deformed (b)
Slika 6. Mikrostruktura ZnCuTi vzorca: ulit (a), deformiran (b)

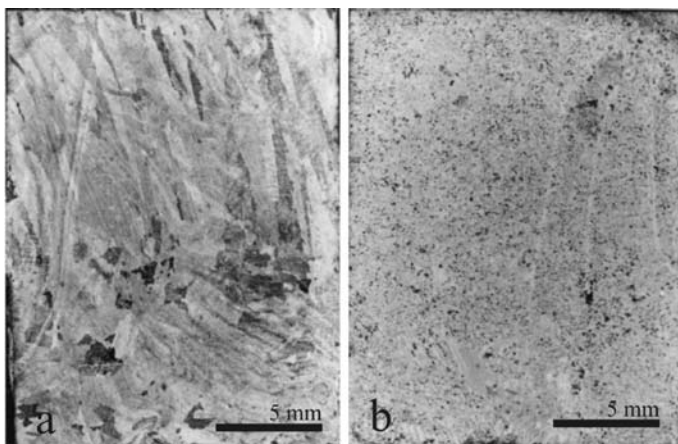


Figure 7. Macrostructure of ZnPb specimen: as-cast (a), deformed (b)
Slika 7. Makrostruktura ZnPb vzorca: ulit (a), deformiran (b)

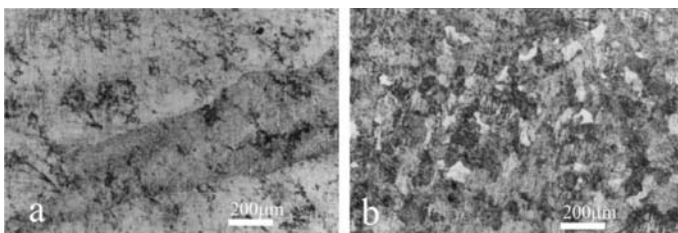


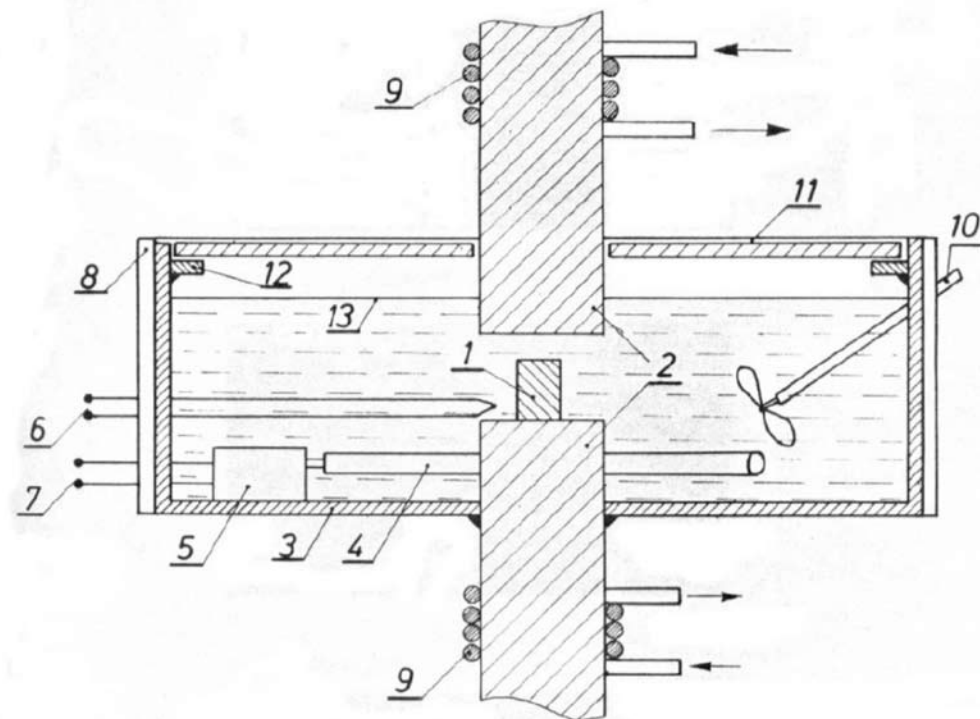
Figure 8. Microstructure of ZnPb specimen: as-cast (a), deformed (b)
Slika 8. Mikrostruktura ZnPb vzorca: ulit (a), deformiran (b)

Compression tests

A material testing machine Instron 1255 was used for compression testing. Testing was performed at two constant punch velocities: 0.01 and 0.2 m/s and three temperatures: 80, 150 in 210 °C what correspond technological condition of hot forming. Specimens were heated with use of special heating device (Figure 9). This device enables heating of specimens in the oil bath.

Oil is used as a lubricant at the contact tool-

specimen as well. In this way cooling of specimen when transported from furnace to tools was hindered. Power of a heater was 1 kW. Temperature field was homogeneous due the mechanical mixing of the oil bath. Control thermocouple was placed in the tool area. Temperature oscillation was in range of ± 2.5 °C. Jaws of the testing machine were protected against overheating with water cooling.



- | | |
|--------------------------------|-------------------------|
| 1. specimen | 8. asbestos isolation |
| 2. tool | 9. cold winding |
| 3. oil container | 10. mixer |
| 4. heater 100 W | 11. cover |
| 5. holder of the heater | 12. holder of the cover |
| 6. control thermocouple | 13. cylinder oil level |
| 7. power supply for the heater | |

Figure 9. Hot compression test device

Slika 9. Shema naprave za tlačne preizkuse v vročem

Determination of flow curves

When performing compression tests, friction between specimen and tool can result in tangential stresses at the contact surfaces, which increase the forming force. Friction has negligible influence on elastic deformation but it causes barrel-shaped specimen on plastic deformation. In extreme cases, this can lead to sticking the specimen to the tool's surface. This is why we have to determine the coefficient of friction, considering the roughness of the tool's and specimen's surface, lubrication, temperature and the strain rate. The coefficient of friction was determined using the Burgdorf's methods. This value was lower than 0,02 and was taken into account while defining hot flow curves.

Considering the coefficient of friction we calculated flow stresses for all materials at different thermo mechanical conditions and initial states from measured load and displacement of compression tool^[3].

$$\sigma_f = \frac{4 \cdot F \cdot h}{1 + \frac{\mu \cdot d_o}{3 \cdot h_o} \sqrt{\frac{h_o}{h}} \cdot d_o^2 \cdot h_o \cdot \pi} \quad (1)$$

F - force

h - instantaneous specimen height

h_o - initial specimen height

d_o - initial specimen diameter

μ - coefficient of friction

Because flow stress curves are defined at constant temperature and strain rate, thermo mechanical constants for the selected mathematical equation for flow curves were defined using experimentally acquired values with linear regression. These values are written in Table 1. Matching the measured (dashed line) and the calculated values (solid line) is shown on Figures 7, 8 and 9.

Flow curves can be written in the following form^[4]:

$$\sigma_f = \sigma_{f0} A_1 e^{-m_1 \vartheta} A_2 \varepsilon^{m_2} e^{-m_3 \dot{\varepsilon}} A_3 \dot{\varepsilon}^{m_4} \quad (2)$$

$$\varepsilon = \ln \frac{h_o}{h} \quad (3)$$

$$\dot{\varepsilon} = \frac{v}{h} \quad (4)$$

where ε is the strain, $\dot{\varepsilon}$ is the strain rate, ϑ is the temperature, $\sigma_{f0}, A_1, A_2, A_3, m_1, m_2, m_3$ are constants, h_o is the initial slab height, h is the instantaneous slab height, and v is the tool velocity.

A new constant B (Table 1) replaces product of the constants σ_{f0}, A_1, A_2 , and A_3 .

RESULTS AND DISCUSSIONS

All three materials were deformed in the temperature range between 80 and 210 °C. In this temperature range flow stresses increase with strain through work hardening up to a critical strain beyond which softening is initiated. Softening includes dynamics recovery and dynamic recrystallization where substructure rearrangements and dislocation reduction lead to decrease in flow stress. With decreasing strain rate or increasing temperature, the strain hardening effect becomes weaken, while the degree of strain softening becomes notable. This phenomena is more evident in as-cast materials. Under a constant strain rate, the peak stress and the peak strain increased with decreasing temperature (Figure 13). Under the same temperature, the peak stress and the peak strain increased with increasing strain rate.

ZnPb alloy indicated minimum values of flow stress in as-cast state at both punch velocities. At the velocity of 0.2 m/s and at the temperature of 210 °C are the values of flow stresses for pure zinc essential greater than for ZnCuTi and ZnPb alloys, at 80 °C they are all nearly the same. Flow stresses for ZnCuTi and ZnPb are similar at higher velocity while flow stresses for Zn in Zn-CuTi are similar at lower velocity.

In deformed state and at punch velocity 0.2 m/s values of flow stresses for ZnTiCu and ZnPb are similar to pure Zn with the exception of those at 210 °C where they are all very similar. At lower velocity is the value of flow stress for pure Zn lower as is case for ZnCuTi and ZnPb. At the temperature 210 °C flow stresses for Zn and ZnPb are similar, while for ZnCuTi is higher.

Table 1. The values of thermo mechanical constants

Tabela 1. Vrednosti termomehanskih konstant

Material	Initial state	B [MPa]	m_1	m_2	m_3	m_4
Zn	as-cast	545	0.00472	0.104	1.578	0.116
	deformed	694	0.00582	0.257	1.629	0.116
ZnPb	as-cast	888	0.00547	0.347	1.682	0.089
	deformed	803	0.00599	0.299	1.441	0.100
ZnCuTi	as-cast	1027	0.00460	0.407	1.890	0.061
	deformed	619	0.00531	0.210	1.085	0.085

Figures 10, 11 and 12 show the stress-strain curves of pure zinc and two alloys ZnCuTi and ZnPb under different deformation conditions. Dynamic recrystallization (DRX) is evident in all cases, even at

increasing strain rates. Although calculated flow stress curves have similar shapes as the measured ones, they cannot follow the processes of dynamic softening, present at higher temperatures.

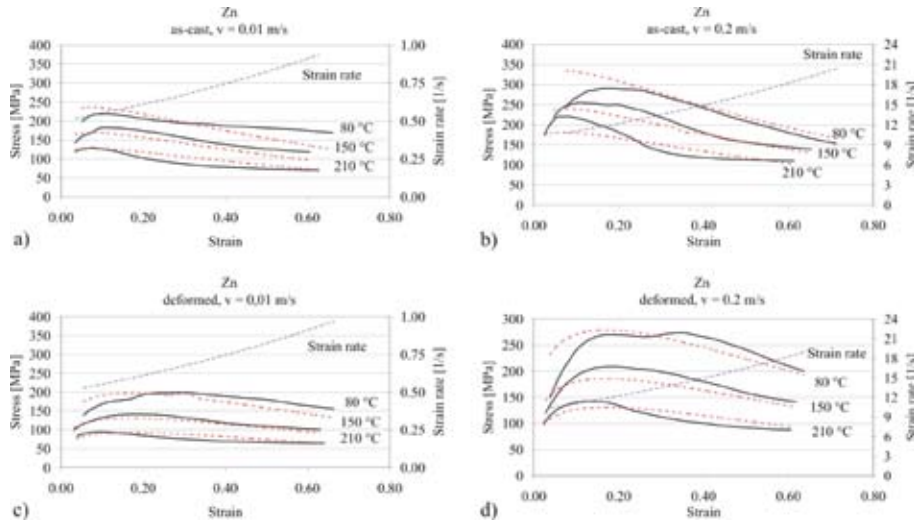


Figure 10. Flow stress curves for Zn in as-cast: $v = 0.01 \text{ m/s}$ (a), $v = 0.2 \text{ m/s}$ (b), and deformed state: $v = 0.01 \text{ m/s}$ (c), $v = 0.2 \text{ m/s}$ (d)

Slika 10. Krivulje tečenja za Zn v ulitem: $v = 0,01 \text{ m/s}$ (a), $v = 0,2 \text{ m/s}$ (b) in deformiranem stanju: $v = 0,01 \text{ m/s}$ (c), $v = 0,2 \text{ m/s}$ (d)

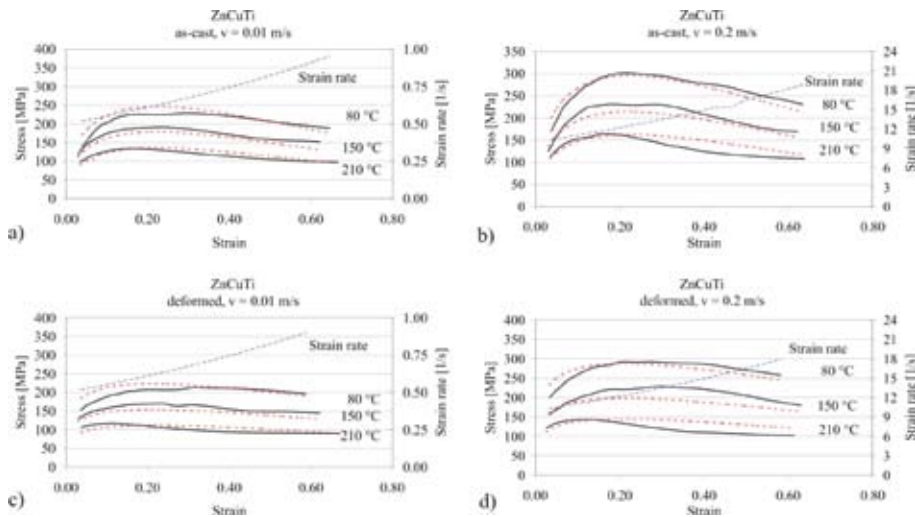


Figure 11. Flow stress curves for ZnCuTi in as-cast: $v = 0.01$ m/s (a), $v = 0.2$ m/s (b), and deformed state: $v = 0.01$ m/s (c), $v = 0.2$ m/s (d)

Slika 11. Krivulje tečenja za ZnCuTi v ulitem: $v = 0,01$ m/s (a), $v = 0,2$ m/s (b) in deformiranem stanju: $v = 0,01$ m/s (c), $v = 0,2$ m/s (d)

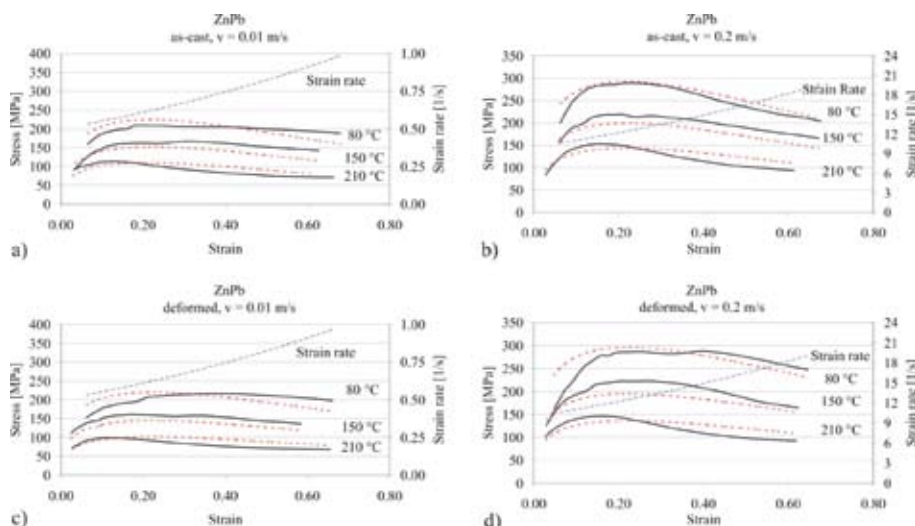


Figure 12. Flow stress curves for ZnPb in as-cast: $v = 0.01$ m/s (a), $v = 0.2$ m/s (b), and deformed state: $v = 0.01$ m/s (c), $v = 0.2$ m/s (d)

Slika 12. Krivulje tečenja za ZnPb v ulitem: $v = 0,01$ m/s (a), $v = 0,2$ m/s (b) in deformiranem stanju: $v = 0,01$ m/s (c), $v = 0,2$ m/s (d)

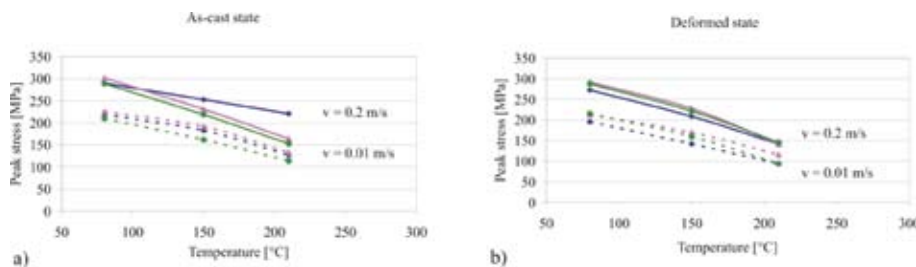


Figure 13. Peak stresses for as-cast (a) and deformed state (b)

Slika 13. Natezne trdnosti v ulitem (a) in deformiranem stanju (b)

CONCLUSIONS

- True stress-strain curves for Zn and its alloys were defined at known thermo mechanical parameters.
- Multilevel linear regression method was used to define thermo mechanical constants in dependence of initial state of material, strain, strain rate and temperature. These constants were obtained for extensive area of the thermo

mechanical parameters and therefore they render impossible to describe all fineness, which have influence to stress-strain dependences.

- For more accurate estimation of flow stress, applied mathematical expression should be improved or the area of thermo mechanical parameters should be tightened.
- In as-cast state softening process is more evident.

POVZETEK

Toplo preoblikovanje Zn in zlitin Zn-CuTi ter ZnPb

Raziskali smo tople preoblikovalnosti čistega cinka, zlitine ZnPb (0,8 %Pb) in zlitine ZnCuTi (0,11 % Cu, 0,1 % Ti) v litem in predhodno deformiranem stanju (30 %). Za določitev preoblikovalnih lastnosti smo uporabili tlačni preizkus. Preizkušanici so bili valjčki premera 15,5 mm in višine 20 mm. Za lito stanje so bili valjčki odvzeti iz sredine ulitih trakov dimenzije

40×80×1500 mm. Ker je bilo dno kokile vodno hlajeno, se je v tem področju tvorilo območje drobne kristalizacije. Srednji del traka je imel značilno območje usmerjene kristalizacije, ki je bilo primerljivo z dejansko makrostrukturo plošč izdelanih v realnih pogojih tehnološkega procesa. Tudi v deformiranih ploščah je še vedno razvidna določena usmerjenost rekristaliziranih zrn v smeri ulitih dendritskih zrn. Ta usmerjenost pa ni razvidna v makrostrukturi vzdolžnih presekov valjčkov, kar je dokaz o pravilnem odvzemu vzorcev iz plošč.

Ker preiskuševalni stroj za tlačne preizkuse ni bil opremljen s sistemom za ogrevanje vzorcev, smo izdelali napravo, s katero smo vzorce in tudi orodje ogrevali v oljni kopeli. Preizkuse smo izvajali pri dveh hitrostih pomika orodja: 0,2 in 0,01 m/s ter treh temperaturah: 80, 150 in 210 °C. Iz izmerjenih vrednosti sil in deformacij in z upoštevanjem koeficenta trenja (<0,2) smo določili preoblikovalne trdnosti.

Ker so krivulje tečenja definirane za konstantne temperature in hitrosti deformacij, smo na osnovi eksperimentalno dobljenih vrednosti z linearno regresijo določili termomehanske konstante za izbran matematičen zapis krivulj tečenja. Analitično izračunane vrednosti iz funkcionalnega izraza se z regresijsko dobljenimi konstantami za eksperimente celotnega variiranja termomehanskih parametrov bolj ali manj prilagajajo izmerjenim rezultatom. Izračunane krivulje imajo sicer podobno obliko t.j. najprej naraščajoč potem pa padajoč značaj, ne morejo pa povsem slediti procesom dinamičnega mehčanja.

Vsi preiskovani materiali so v temperaturnem območju med 80 in 210 °C nahajajo v toplem stanju, to pomeni, da začetnemu utrjevanju sledi po dosegu kritične deformacije mehčanje dinamičnega značaja. Maksimumi napetosti tečenja teh krivulj se z naraščajočo temperaturo pomikajo k nižjim deformacijam, z naraščajočo hitrostjo deformacije pa proti višjim vrednostim deformacij. Ta zakonitost je podobna za vse preiskovane materiale. Nastopajo bistvene

razlike v poteku preoblikovalnih trdnosti, če imamo za izhodišče enkrat lito drugič pa deformirano stanje. V litem stanju je intenziteta mehčanja večja, kritična napetost tečenja pa je dosežena že pri nekoliko nižjih deformacijah kot v deformiranem stanju.

V litem stanju so vrednosti preoblikovalnih trdnosti pri obeh hitrostih stiskanja najnižje za zlitino ZnPb. Pri hitrosti stiskanja 0,2 m/s in temperaturi 210 °C so vrednosti za čisti Zn bistveno večje od ostalih dveh, medtem ko so si vrednosti pri 80 °C približno enake. Pri višji hitrosti sta si preoblikovalni trdnosti za ZnCuTi in ZnPb podobni, pri nižji hitrosti pa sta si podobni preoblikovalni trdnosti za Zn in ZnCuTi.

V deformiranem stanju se pri hitrosti stiskanja 0,2 m/s vrednosti preoblikovalnih trdnosti za ZnTiCu in ZnPb bistveno ne razlikujeta in sta višji od čistega Zn razen pri temperaturi 210 °C, ko so si vrednosti enake. Tudi pri hitrosti stiskanja 0,01 m/s je preoblikovalna trdnost za Zn nižja kot pri ostalih dveh kvalitetah. Pri temperaturi 210 °C pa sta si vrednosti za Zn in ZnPb enaki, medtem, ko je preoblikovalna trdnost za ZnCuTi višja.

Zlitine se med seboj glede na legirne elemente ločijo po zahtevani napetosti tečenja in v splošnem velja brez izjem, da je proces mehčanja, ki ga pripisemo rekristalizaciji deloma pa tudi popravi, intenzivnejši pri litem stanju.

REFERENCES

- [¹] SCHWEITZER, P.A. (2003): *Metalic materials: Physical, mechanical, and corrosion properties*. New York, Basel: Marcel Dekker, Inc., 712 p.
- [²] PRASAD, Y.V.R.K., SASIDHARA, S. (1997): *Hot working guide: A compendium of processing maps*. ASM International, 543 p.
- [³] PAWELSKI, O. (1977): Theoretische Grundlagen des Freiformenschmiedens. *Stahl und Eisen* 5.
- [⁴] HENSEL, A., SPITTEL, T. (1978): *Kraft und Arbeitsbedarf Bildsamer Formgebungs-verfahren*. Leipzig, Deutscher Verlag für Grundstoffindustrie, 528 p.

Varjenje močno legiranih jekel z oplaščenimi elektrodami

Welding of high-alloy steels with covered electrodes

RAJKO KEJŽAR¹, LADO KOSEC², UROŠ KEJŽAR³

¹ Univerza v Ljubljani, Fakulteta za strojništvo, Aškerčeva cesta 6, 1000 Ljubljana;
E-mail: rajko.kejzar@fs.uni-lj.si

² Univerza v Ljubljani, Naravoslovnotehniška fakulteta, Oddelek za materiale in metalurgijo,
Aškerčeva cesta 12, 1000 Ljubljana; E-mail: kosec@ntf.uni-lj.si

³ ISKRA VARJENJE, Stegne 21c, 1000 Ljubljana; E-mail: uros.kejzar@iskra-varjenje.si

Received: April 12, 2007

Accepted: October 1, 2007

Izvleček: Oplaščene elektrode so primerne za varjenje in navarjanje močno legiranih jekel. Var lahko legiramo tako preko legirane elektrodne žice, kot tudi preko elektrodne obloge. Zgradba elektrode pomembno vpliva na njeno uporabnost, ki v največji meri zavisi od ionizacije obloka, odtaljevanja in legiranja vara. Pri varjenju z oplaščenimi elektrodami je sestava elektrodne obloge, od katere zavisi stabilnost ter produktivnost in izkoristek varjenja, odločilna za nastajanje varilne žlindre in osnovnega pomena za varilnotehnične lastnosti elektrode. Varjenje s tanko oplaščenimi močno legiranimi elektrodami (legiranje vara preko žice) je neproduktivno, ker je odtaljevanje grobo kapljičasto. Pri varjenju z debelo oplaščenimi močno legiranimi elektrodami (legiranje vara preko obloge), pa je odtaljevanje fino kapljičasto – pršeče, kar povzroči izboljšanje produktivnosti. Težave pa nastopijo pri varjenju v prisilnih legah. Zaradi visokih minimalnih izkoristkov varjenja pride do omejitev glede uporabnosti teh elektrod.

Abstract: Covered electrodes are suitable for welding and surfacing of high-alloy steels. Alloying of the weld metal can be accomplished by both an electrode wire and an electrode covering. The electrode composition has a major influence on its usability that mainly depends on arc ionisation, melting-off, and alloying of the weld metal. In welding with a covered electrode, the electrode-covering composition, on which stability, welding productivity, and efficiency depend, is a deciding factor in the formation of welding slag and of basic importance for welding characteristics of the electrode. Welding with thin-coated high-alloyed electrodes (alloying of the weld metal by the wire) is unproductive since melting proceeds in coarse drops. In welding with thick-coated high-alloyed electrodes (alloying of the weld metal by the covering), melting proceeds in fine droplets, which increases productivity. Difficulties, however, are encountered in welding out of po-

sition. Because of high minimum welding efficiencies, there are certain limitations as to the applicability of these electrodes.

Ključne besede: oplaščene elektrode, odtaljevanje, legiranje varja preko žice, legiranje varja preko obloge

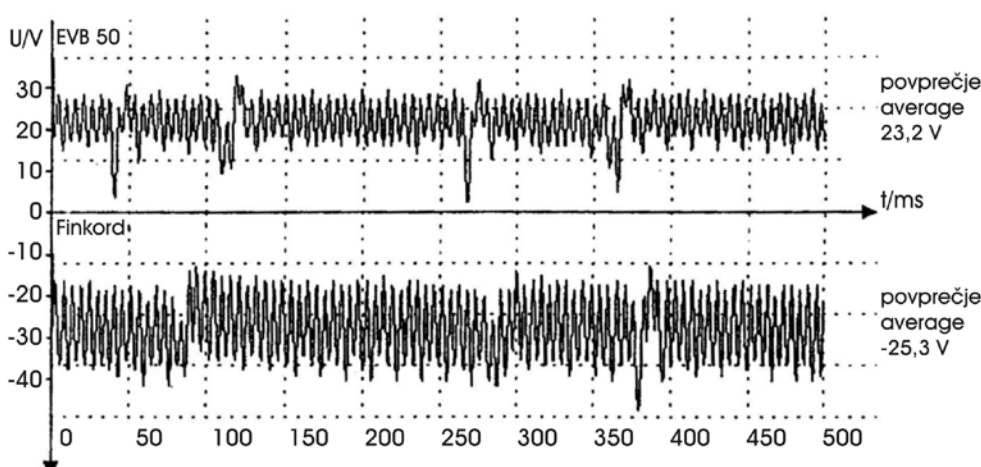
Key words: covered electrodes, melting-off, alloying of the weld metal by the wire, alloying of the weld metal by the covering

UVOD

Pri varjenju z oplaščenimi elektrodami je sestava oplaščenja bistvenega pomena za kvaliteto zvarov in navarov. Oplaščenje odločilno vpliva na stabilnost varjenja (ionizacija obloka) in odtaljevanje elektrode^[1].

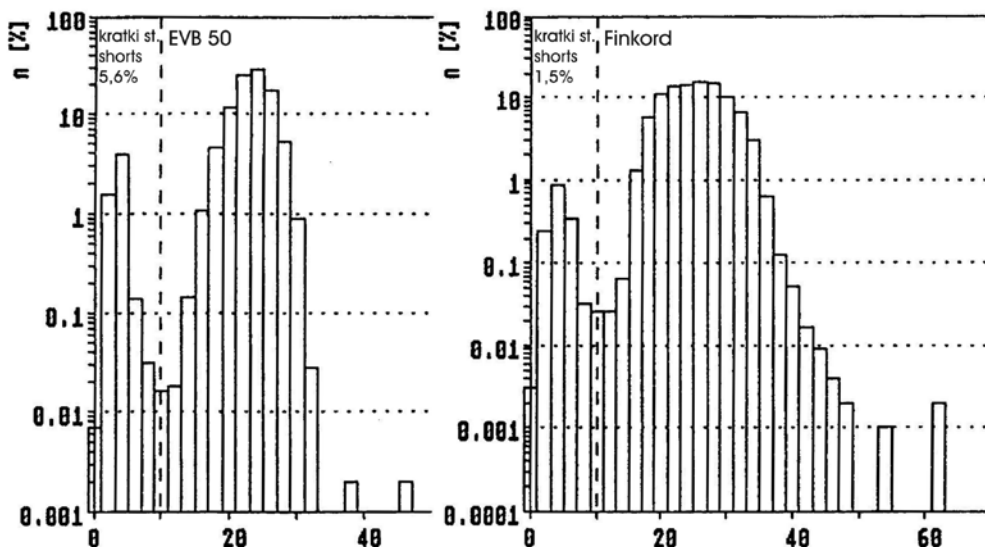
Pri varjenju z rutilno in kislo oplaščenimi elektrodami (npr. Finkord), je varjenje zelo stabilno - oblok je dobro ioniziran,

zato običajno varimo z izmeničnim ali pa enosmernim tokom na minus pol, odtaljevanje je finokapljičasto in pršeče z zelo malo kratkih stikov (glej slike 1 in 2). Pri varjenju z bazično oplaščenimi elektrodama (npr. EVB 50), pa moramo zaradi slabe ionizacije obloka variti z enosmernim tokom na plus pol, odtaljevanje je grobo kapljicasto s pogostimi kratkimi stiki (glej slike 1 in 2).



Slika 1. Časovno spremjanje varilne napetosti pri varjenju z elektrodama EVB 50 in Finkord^[2]

Figure 1. Time variation of welding voltage in welding with electrodes EVB 50 and Finkord^[2]



Slika 2. Statistična porazdelitev napetosti in ocena deleža kratkih stikov pri varjenju z elektrodama EVB 50 in Finkord^[1]

Figure 2. Statistical distribution of voltage and assessment of fraction of short circuits in welding with electrodes EVB 50 and Finkord^[1]

Preko elektrodne obloge lahko tudi legiramo navar. Tako sestava legirane varilne žice, kot tudi dezoksidanti in legirni elementi v oplaščenju, vplivajo na odtaljevanje in stabilnost varjenja. Odtaljevanje pri oplaščenih elektrodah, ki so izdelane iz močno legiranih žic, je bolj grobo kapljičasto, kot odtaljevanje pri oplaščenih elektrodah, pri katerih je legiranje in dezoksidacija preko elektrodne obloge^{[3],[4]}. Ker je oplaščenje elektrode lahko rutilno kislo ali pa bazično, poznamo najmanj štiri osnovne tipe elektrod^[4].

I. Rutilno kislo oplaščene elektrode:

- a) legiranje vara preko elektrodne žice in
- b) legiranje vara preko elektrodne obloge

II. Bazično oplaščene elektrode:

- d) legiranje vara preko elektrodne žice in
- e) legiranje vara preko elektrodne obloge

ODTALJEVANJE MOČNO LEGIRANIH ELEKTROD

Legiranje navara preko elektrodne žice

Tako rutilne kot tudi bazične elektrode so tanko oplaščene ($f.o.p.l = 1,4$). Preko oblage le dezoksidiramo in stabiliziramo navar z manganom in niobijem.

Odtaljevanje rutilno oplaščenih močno legiranih elektrod je bolj fino kapljičasto, podobno kot odtaljevanje pri varjenju s Finkord elektrodami, pri katerih zaradi oksidativnosti oblage pride do pršečega

odtaljevanja (eksplozije kapljic, zaradi nastajanja ogljikovega monoksida; $[C] + [O] = \{CO\}$). Pri bazično oplaščenih močno legiranih elektrodah pa je odtaljevanje grobo kapljičasto - celo bolj kot pri varjenju z elektrodami EVB 50. Velikost odtaženih kapljic je nad 4 mm. Pri varjenju z rutilno oplaščenimi močno legiranimi elektrodami pa se odtažujejo predvsem bolj drobne kapljice (pod 2 mm). Kemična sestava kapljic je tako pri rutilno oplaščenih elektrodah, kot tudi pri bazično oplaščenih elektrodah, zelo podobna kemični sestavi varja (tabela 1)^[5].

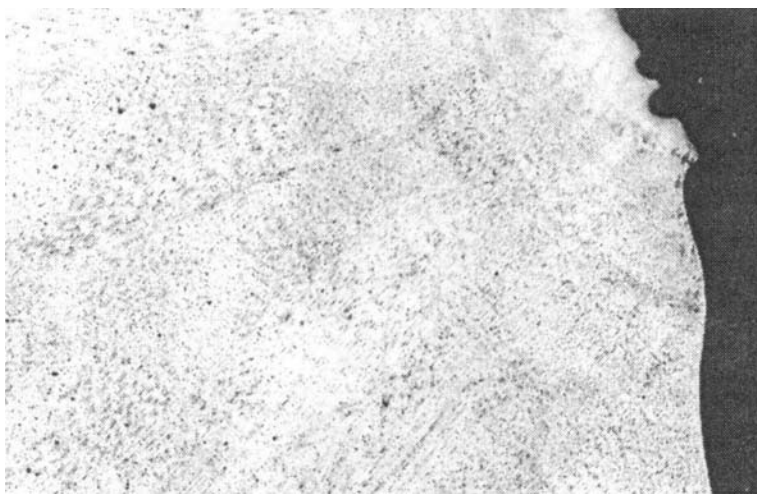
Tabela 1. Kemične sestave varov in odtaženih kapljic različne velikosti pri varjenju z močno legiranimi elektrodami (legiranje varja preko žice)

Table 1. Chemical compositions of weld metals and melted droplets of various sizes in welding with high-alloyed electrodes (weld-metal alloying by the wire)

Vzorec / Sample	Velikost kapljice / Droplet size	Kemična sestava / Chemical composition (%)			
		Si	Cr	Ni	Nb
Rutilno opl. el / Rutile:	Var / weld metal	1,38	16,6	8,5	1,41
	Nad / above 2 mm	1,80	16,9	9,1	0,75
	Nad / less than 2 mm	1,87	17,6	9,2	0,75
Bazično opl. el / Basic:	Var / weld metal	1,32	18,1	8,8	1,30
	Nad / above 4 mm	1,16	19,4	8,8	0,84

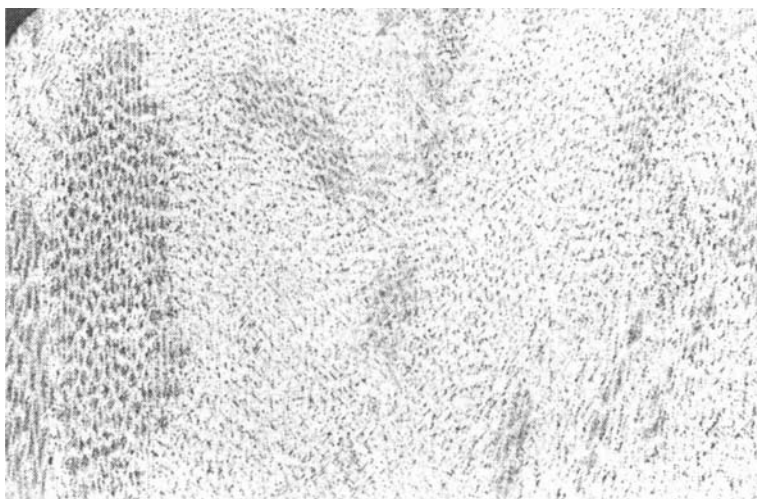
Iz rezultatov kemičnih analiz je razvidno, da so izgube legirnih elementov zaradi odgorevanja in dezoksidacije varja pri rutilno oplaščenih elektrodah večje, kot pri bazično oplaščenih. Pri bazično oplaščenih elektrodah je že na stopnji kapljice dezoksidacija zaključena. Pri rutilno oplaščenih elektrodah pa visoka vsebnost silicija v kapljici še na stopnji kopeli dezoksidira var.

Mikrostruktura kapljic, ki nastanejo pri varjenju tako z rutilno kislimi, kot tudi bazičnimi elektrodami, je ne glede na njihovo velikost podobna mikrostrukturi varja, ki je drobnozrnata avstenitna (slika 3 in 4).



Slika 3. Mikrostruktura kapljice (pod 2 mm) pri varjenju z rutilno oplaščeno elektrodo – pov. 50 x

Figure 3. Droplet microstructure (below 2 mm) in welding with rutile electrode. x50



Slika 4. Mikrostruktura kapljice (nad 4 mm) pri varjenju z bazično oplaščeno elektrodo – pov. 50 x

Figure 4. Droplet microstructure (above 4 mm) in welding with basic electrode. x50

Legiranje in dezoksidacija vara je zelo neizotermičen proces^[6]. Ravnotežje reakcij dezoksidacije in hitrost procesov se s temperaturo spreminja. Na stopnji kapljice potekajo procesi bistveno hitreje, kot v kopeli vara. Pri rutilno oplaščenih elektrodah poteka dezoksidacija in legiranje, kot je razvidno iz kemičnih sestav varu in kapljic, zelo zanimivo. Predvsem niob, ki kapljice legira preko oblage, pri visokih temperaturah obloka močno reducira SiO_2 iz oblage in s tem povzroči visok prigor Si v kapljici. Visok silicij pa pri nižji temperaturi kopeli vara reducira dezoksidacijske produkte (predvsem Nb_2O_5). Vsebnost silicija v navaru se zato zniža, nioba pa zviša. Dezoksidacija pri varjenju z rutilno kislimi elektrodami se zaključi šele v kopeli vara, pri varjenju z bazično oplaščenimi elektrodami (legiranje preko žice) pa je praktično zaključena že na stopnji kapljice.

Legiranje navara preko elektrodne oblage

Elektrode pri katerih poteka legiranje navara preko elektrodne oblage so debelo oplaščene ($f\text{-opl.} = 1,85$). Preko oblage moramo legirati navar z zadostno količino legirnih elementov. Izkoristki varjenja so zato pri teh elektrodah zelo visoki - okoli 180 %, kar je zelo neugodno pri varjenju v prisilnih legah^[4]. Tudi odtaljevanje in legiranje vara poteka nekoliko drugače, kot pri varjenju s tanko oplaščenimi elektrodami, ko legiranje navara poteka preko močno legirane elektrodne žice.

Odtaljevanje žice, ki je pri elektrodah z veliko vsebnostjo legirnih elementov in dezoksidantov v oblogi, nelegirana in običajno tudi nepomirjena, je nekoliko bolj fino kapličasto. Največja razlika pa je v prenosu

legirnih elementov iz oblage v var, ki delno poteka preko legiranja kapljic, delno pa v zelo finih kapljicah kar direktno v var. Posledica tega načina prenosa je, da imamo tudi pri varjenju z bazično oplaščenimi elektrodami (legiranje preko oblage) poleg večjih tudi drobne kapljice – podobno, kot pri varjenju z rutilno oplaščenimi elektrodami. Iz kemične analize kapljic pa je razvidno, da so drobne kapljice raztaljeni dodatki kovin in zlitin, ki so dani v oblogo za legiranje in dezoksidacijo vara (tabela 2)^[5].

Iz rezultatov kemičnih analiz čistih varov in odtaljenih kapljic je lepo vidno, da večji del procesov legiranja in dezoksidacije var poteče že na stopnji kapljice (preko 90 %). Kovinski dodatki v elektrodnih oblogah za legiranje in dezoksidacijo vara, legirajo že kapljice, ki se odtaljujejo od nelegirane žice. Sestava večjih odtaljenih kapljic je praktično enaka sestavi vara. Odstopanja so le pri legiranju in dezoksidaciji vara s silicijem in niobom pri varjenju z rutilno kislo oplaščenimi elektrodami, ker niob pri visokih temperaturah obloka reducira SiO_2 v oplaščenju ter povzroči višji prigor silicija v kapljici. Na stopnji kopeli vara pa silicij reducira nekatere dizoksidacijske produkte, kar povzroči znižanje Si in porast Nb v čistem varu, podobno kot smo ugotovili tudi pri varjenju z rutilno kislo oplaščenimi elektrodami, ko je bilo legiranje vara preko žice.

Mikrostruktura večjih kapljic je finozrnatata avstenitna in že podobna mikrostrukturi varov, le dezoksidacija še ni povsem zaključena. Pri kapljicah bazično oplaščenih elektrod (slika 5), je potekla bolj daleč, kot pri kapljicah rutilno oplaščenih elektrod

(slika 6), kar je razvidno iz bolj učinkovitega očiščenja kovine kapljice.

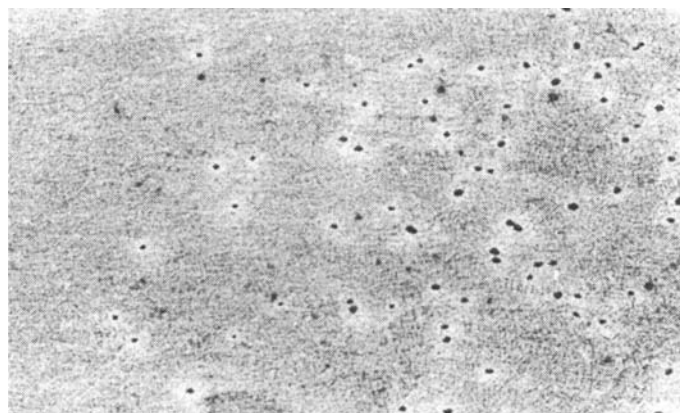
Vse zelo drobne kapljice (pod 2 mm), tako pri bazično, kot tudi rutilno kislo opla-

ščenih elektrodah (slika 7), pa so skupek dezoksidacijskih in legirnih dodatkov in so si glede mikrostrukture povsem podobne^[5].

Tabela 2. Kemične sestave čistih varov in odtaljenih kapljic različne velikosti pri varjenju z močno legiranimi elektrodami (legiranje vara preko oblage)

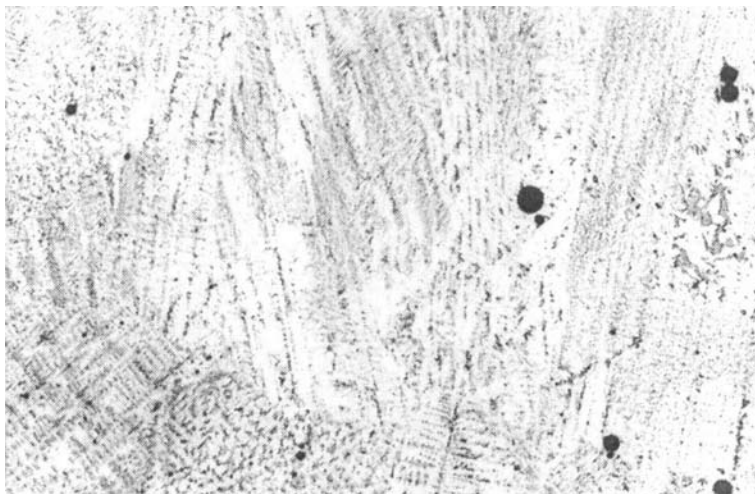
Table 2. Chemical compositions of all weld metals and melted droplets of various sizes in welding with high-alloyed electrodes (weld-metal alloying by the coating)

Vzorec / Sample		Kemična sestava (%) / chemical composition (%)			
	Velikost kapljice / droplet size	Si	Cr	Ni	Nb
Rutilno opl. el / Rutile:	Var / weld metal	1,04	20,3	8,8	0,63
	Nad / above 4 mm	1,40	20,2	9,4	0,64
	2-3 mm	1,18	23,8	9,0	0,46
	Pod / less than 2 mm	2,18	34,4	21,7	0,69
Bazično opl. el / Basic:	Var / weld metal	0,96	20,8	9,5	1,18
	Nad / above 4 mm	0,76	20,1	8,4	0,61
	2-3 mm	1,12	22,0	8,4	0,68
	Pod / less than 2 mm	2,48	40,4	15,9	3,04



Slika 5. Mikrostruktura kapljice (nad 2 mm) pri varjenju z bazično oplaščeno elektrodo; temne pike so bogate z niobom – pov. 50x

Figure 5. Droplet microstructure (above 2 mm) in welding with basic electrode; dark spots are rich in niobium. x50



Slika 6. Mikrostruktura kapljice (pod 2 mm) pri varjenju z rutilno kislo oplasčeno elektrodo; temne pike so dezoksidacijski vključki – pov. 50x.

Figure 6. Droplet microstructure (below 2 mm) in welding with rutile-acid electrode; dark spots are deoxidation inclusions. x50



Slika 7. Mikrostruktura zelo drobne kapljice (pod 2 mm) pri varjenju z rutilno kislo oplasčeno elektrodo; svetla polja so bogata s kromom, temnejša pa z nikljem – pov. 50x.

Figure 7. Microstructure of very fine droplet (below 2 mm) in welding with rutile-acid electrode; light spots are rich in chromium and darker spots in nickel. x50

SKLEPI

Pri varjenju z oplaščenimi elektrodami sestava elektrodne obloge odločilno vpliva na varilno tehnične lastnosti elektrode. Z rutilno kislimi elektrodami lahko varimo z izmeničnim tokom in enosmernim tokom na minus pol. Oblok je zelo dobro ioniziran, zato je varjenje stabilno, odtaljevanje kapljic pa fino kapljičasto z zelo malo kratkih stikov (pod 2 %). Pri bazično oplaščenih elektrodah pa je oblok slabše ioniziran, zato moramo z njimi variti z enosmernim tokom na plus pod. Odtaljevanje kapljic pa je grobo kapljičasto s pogostimi kratkimi stiki (preko 5 %).

Preko elektrodne obloge pa lahko tudi legiramo in dezoksidiramo navar. Pri močno legiranih oplaščenih elektrodah je odtaljevanje bolj grobo kapljičasto, še posebno, če je oplaščenje elektrode bazično. Zanimivo je, da legirni in dezoksidacijski kovinski dodatki v elektrodni oblogi legirajo in dezoksidirajo že kapljice, ki se odtaljujejo od nelegirane žice. To pomeni, da večji del procesov legiranja in dezoksidacije

med varjenjem poteče že na stopnji kapljice (preko 90 %). Odstopanja so le pri legiranju in dezoksidaciji vara s silicijem in niobom pri varjenju z rutilno kislo oplaščenimi elektrodami, ker niob pri visokih temperaturah obloka močno reducira SiO_2 v oplaščenju ter povzroči visok prigor Si v kapljici. Na stopnji kopeli vara pa silicij reducira produkte dezoksidacije (predvsem Nb_2O_5), kar ima za posledico znižanje siličija in zvišanje nioba v navaru.

Manjši del legirnih in dezoksidacijskih dodatkov pa legira navar preko zelo drobnih kapljic, ki nastajajo z zlivanjem. Zelo drobne kapljice so zato močno legirane in nehomogene, velike kapljice pa tako po mikrostrukturi, kot tudi kemični sestavi podobne sestavi varov.

Prednost bazičnega oplaščenja je intenzivnejše legiranje in dezoksidacija vara. Izgube legirnih dodatkov so manjše. Hiba pa je slabša ionizacija obloka, zato z njimi lahko kvalitetno varimo le z enosmernim tokom na plus pol.

SUMMARY

Welding of high-alloy steels with covered electrodes

In welding with covered electrodes, the composition of an electrode coating has a decisive influence on technical features of the electrode. Rutile-acid electrodes permit welding with alternating current and direct current negative. The arc obtained is well ionised; therefore, welding is sta-

ble and melting-off proceeds in fine droplets with very few short circuits (below 2 %). With basic covered electrodes the ionization of the arc is poorer; therefore, welding should be carried out with direct current positive. Melting-off proceeds in coarse drops with frequent short circuits (above 5 %), (see Figures 1 and 2).

By means of the electrode coating a surfacing weld may be alloyed and deoxidized. With high-alloy covered electrodes

melting-off proceeds in coarse drops, particularly if the electrode coating is basic. It is interesting that alloying and deoxidizing metal additions to the electrode coating produce alloying and deoxidization of the droplets melting off from an unalloyed wire. This means that the major part of alloying and deoxidation processes during welding occur at the stage of droplets (over 90 %) (see Tables 1 and 2, and Figures 3 through 6). There are some deviations only in case of alloying and deoxidation of a weld metal with silicon and niobium in welding with a rutile-acid electrodes because niobium at high arc temperatures strongly reduces SiO_2 in the coating and produces a high pick-up of Si in a droplet. At the stage of a weld pool, silicon, however, will reduce products of deoxidation (particularly Nb_2O_5), which will result in silicon reduction and an increase in nio-

bium in the surfacing weld (see Tables 1 and 2).

A minor portion of the alloying and deoxidizing additions, however, will alloy the surfacing weld via very fine droplets produced by fusion (see Figure 7). Consequently, the fine droplets are strongly alloyed and non-homogeneous whereas coarser droplets are similar, in terms of microstructure and chemical composition, to the weld metal (see Figures 3 through 6, Tables 1 and 2).

An advantage of the basic coating consists in more intense alloying and deoxidation of the weld metal. Losses of the alloying additions are small. Its disadvantage, however, is poorer ionization. Consequently, quality welding requires the use of direct current positive.

VIRI

- [¹] KEJŽAR, R., KRALJ, V., REHFELDT, D. (1991): Analiza obloka z analizatorjem, Hanover AH-7. *Poročilo ZRMK*. Ljubljana, 1991.
- [²] KEJŽAR, U., KEJŽAR, R. (2001): Izpopolnjevanje programske opreme za opazovanje električnih parametrov varjenja. *Poročilo o delu*. Fakulteta za strojništvo Univerze v Ljubljani, Ljubljana, 2001.
- [³] BECKEN (1970): Werkstoffübergang bei Schweißelektroden. *Schweissen und Schneiden* 22. Düsseldorf, 11, str. 478/479.
- [⁴] KEJŽAR, R. (1975): Vpliv dezoksidantov na vsebnost kisika v čistem varu in izkoristek Cr iz plašča pri elektroobločnem varjenju. *Železarski zbornik* 9. Jesenice, 1, str. 19/27.
- [⁵] KOSEC, L., KEJŽAR, R., RALIČ, B. (1974): Mehanizem legiranja varov – analiza produktov varjenja. *Poročilo Metalurškega inštituta*. Ljubljana, 1974.
- [⁶] EVOHIN, A.A. (1965): *Kinetika metallurgičeskikh processov dugovoj svarki*. Mašinostroenie, Moskva.

Določitev meje T/J z analizo stabilnih izotopov $\delta^{13}\text{C}$ in $\delta^{18}\text{O}$ (Krim, Slovenija)

Determination of T/J boundary by $\delta^{13}\text{C}$ and $\delta^{18}\text{O}$ stable isotope analysis (Krim Mountain, Slovenia)

MILOŠ MILER¹, JERNEJ PAVŠIC², MATEJ DOLENEC³

¹ Hribi 2, 1291 Škofljica, Slovenija; E-mail: mmiler@email.si

² Univerza v Ljubljani, Naravoslovnotehniška fakulteta, Oddelek za geologijo, Privoz 11,
1000 Ljubljana, Slovenija; E-mail: jernej.pavsic@ntf.uni-lj.si

³ Univerza v Ljubljani, Naravoslovnotehniška fakulteta, Oddelek za geologijo,
Aškerčeva cesta 12, 1000 Ljubljana, Slovenija; E-mail: matej.dolenec@s5.net

Received: June 21, 2007

Accepted: October 23, 2007

Izvleček: Izotopske analize ogljika in kisika v dolomitih triasne in jurske starosti iz profilov Žvencelj-Novi zavodi in Tresenk-Rupendol na območju Krimskega hribovja, so bile preliminarne, izvedene z namenom določitve meje med triasom in juro. Zaradi neprekinjene sedimentacije karbonatov na prehodu iz triasa v juro in pomanjkanja fosilnih ostankov meja ni bila natančno določena. Predpostavljena je bila tam, kjer med zrnatim dolomitom glavnega dolomita v loferskem razvoju ni več laminiranega dolomita. Za prehod iz triasa v juro je značilna negativna ogljikova anomalija. Ta je verjetno posledica zgornjetriasne regresije morja. Na zgornjetriasno regresijo kažejo tudi vedno pogosteje dolomitne breče v zgornjem delu zgornjetriasnih plasti. Za spodnjeliasne plasti so značilne povisane vrednosti $\delta^{13}\text{C}$, ki sovpadajo z nenadno transgresijo morja. Na podlagi rezultatov izotopskih analiz ogljika in kisika je bila meja med triasom in juro natančneje postavljena med črnimi dolomitnimi brečami zgornjetriasne starosti in svetlosivimi zmatimi dolomiti spodnjeliasne starosti.

Abstract: Carbon and oxygen stable isotope analyses of Triassic and Jurassic dolomites from Žvencelj-Novi zavodi and Tresenk-Rupendol sections on Krim Mountain area, were preliminary and were carried out with the purpose of determining T/J boundary. Due to lack of fossil remains and continuous carbonate sedimentation during T/J transition, the exact position of T/J boundary has not been defined yet. It was presumed in coarse-grained Main dolomite in which intermediate beds of laminated dolomites are no longer present. The T/J transition is characterised by negative excursion in $\delta^{13}\text{C}$. The carbon isotope variability is probably a consequence of Upper Triassic marine regression which is also indicated by more frequently appearing beds of dolomitic breccias in the upper part of Upper Triassic. Fol-

lowing positive shift in $\delta^{13}\text{C}$ values is characteristic of Lower Liassic beds and is consistent with sudden marine transgression. Based on results of carbon and oxygen isotope analyses the T/J boundary was more accurately placed between Upper Triassic black dolomitic breccias and Lower Liassic light grey coarse-grained dolomites.

Ključne besede: meja T/J, dolomiti, stabilni izotopi ogljika in kisika, Dinarska karbonatna platforma, Krim

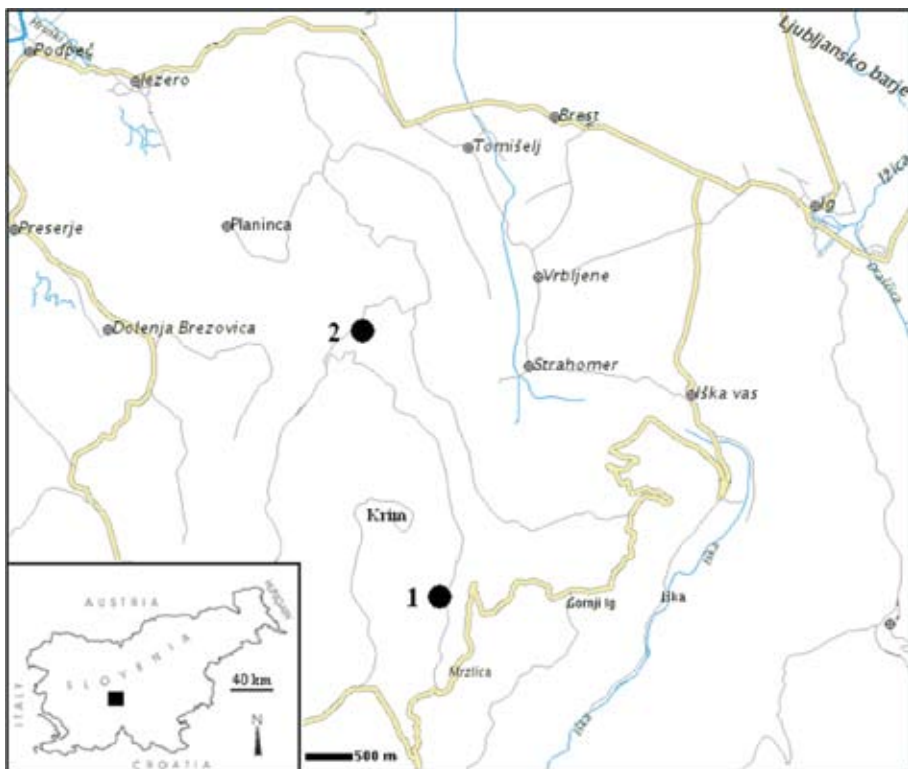
Key words: T/J boundary, dolomites, carbon and oxygen stable isotopes, Dinaric Carbonate Platform, Krim Mountain

Uvod

Konec triasa je prišlo do enega največjih množičnih izumrtij, ki po svojem obsegu preseže celo izumrtje ob koncu krede (McROBERTS ET AL., 1997). Pri tem je izumrlo nekaj več kot polovica vseh rodov morskih organizmov. Različni avtorji navajajo različne razloge za izumrtje, kot so zmanjšana bioprodukcija in akumulacija C^{12} v rezervoarju ogljika (KUMP & ARTHUR, 1999), povečanje količine CO_2 v atmosferi zaradi vulkanizma (KUMP & ARTHUR, 1999), sproščanje metana iz metanovih hidratov kot posledica vulkanizma in sledeče spremembe okolja, ki so vplivale na organizme (PALFY ET AL., 2001), zmanjšanje morskih habitatov zaradi regresije morja in širjenje anoksične vode med sledečo transgresijo (HALLAM, 1981) ter prekinitev morske in kopenske prehranjevalne verige zaradi znižanja primarne produkcije (McROBERTS ET AL., 1995). Verjetno pa je šlo za kombinacijo naštetih dogodkov.

Raziskave meje T/J na območju avstrijskih Severnih apneniških Alp (McROBERTS ET AL., 1997; KRYSTYN ET AL., 2005) in Csővar na Madžarskem (PALFY ET AL., 2001) kažejo, da je za prehod iz triasa v juro značilna negativna $\delta^{13}\text{C}$ anomalija anorganskega in organskega ogljika. Veliko množičnih izumrtij je povezanih z negativno $\delta^{13}\text{C}$ anomalijo in bolj ali manj vzporedno anomalijo $\delta^{18}\text{O}$. To pomeni, da so povezana tudi s spremembami v globalnem ogljikovem ciklu (PALFY ET AL., 2001).

Negativna $\delta^{13}\text{C}$ anomalija je posledica zgornjetriaspne regresije morja, pri kateri je prišlo do povečanega dotoka meteorne vode in oksidacije organske snovi v morju (McROBERTS ET AL., 1997; PALFY ET AL., 2001). Izotopska sestava kisika v diagenetsko nespremenjenih karbonatih pa lahko odraža izotopsko sestavo in temperaturo morske vode (SCHRAG ET AL., 1995).



Slika 1. Geografski položaj profilov Žvencelj-Novi zavodi (1) in Tresenk-Rupendol (2) na območju Krima

Figure 1. Geographic location of Žvencelj-Novi zavodi (1) and Tresenk-Rupendol (2) sections (Krim Mountain, Slovenia)

GEOLOŠKA ZGRADBA IN PALEOGEOGRAFIJA

Za potrebe analize izotopske sestave kisika in ogljika v karbonatih na meji T/J so bile vzorčevane kamnine v profilih Žvencelj-Novi zavodi in Tresenk-Rupendol. Profila sta na območju Kirmskega hribovja in sicer vzhodno ter severozahodno od Krima (slika 1). Kirmsko hribovje leži v severnem delu Zunanjih Dinaridov, ki so v triasu in juri pripadali Dinarski karbonatni platformi.

Na območju Kirmskega hribovja je na prehodu iz triasa v juro potekala neprekinitnjena karbonatna sedimentacija (PLENIČAR, 1970). Zaradi postopne lithostratigrafske meje in odsotnosti fosilnih ostankov meja med zgornjetriasmimi in spodnjelasnimi plastmi ni bila biostratigrafsko določena. Po Pleničarju (1970) in Buserju (1986) je meja postavljena tam, kjer med zrnatim dolomitom ni več laminiranega dolomita ozziroma tam, kjer se pojavlja sive dolomitne breče z zrnatim dolomitnim vezi-

vom in ostrorobimi klasti laminiranega dolomita. Po Novaku (2003) pa je meja T/J v litološkem pogledu postavljena v pas, kjer se zaključi loferska sedimentacija, paleontološko pa po izumrtju megalodontid.

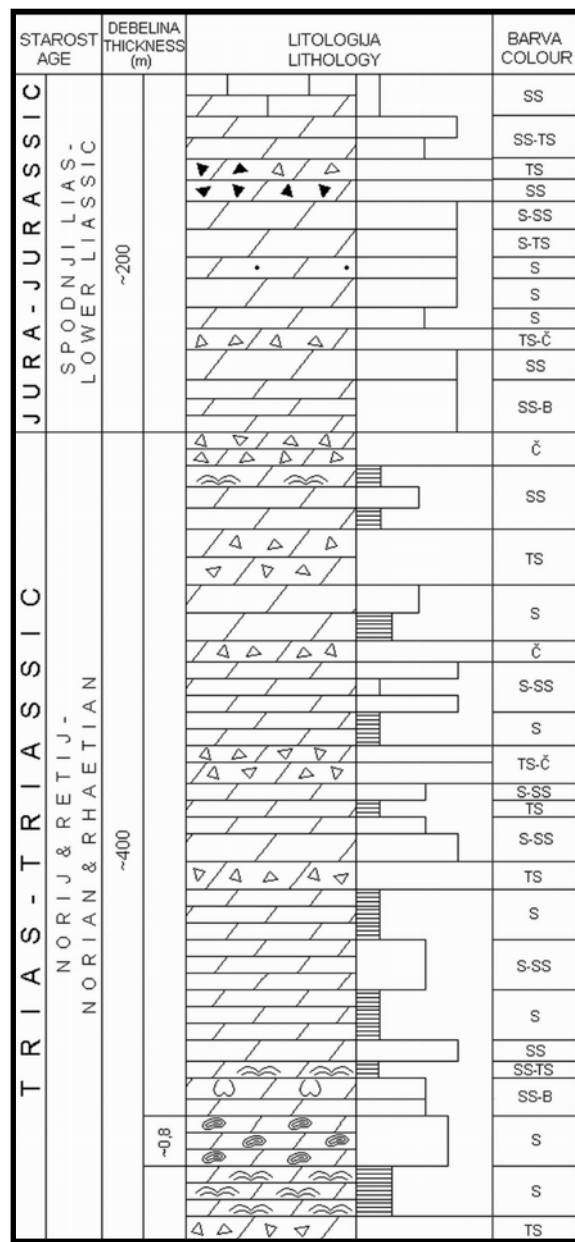
Zgornjetrijsne plasti predstavlja glavni dolomit v loferskem razvoju (slika 2). Gre za menjavanje sivega do svetlosivega zrnatega dolomita, sivega do temnosivega stromatolitnega dolomikrita, ki ponekod navzgor prehaja v siv onkodolomikrosparit in temnosivih do črnih dolomitnih breč s svetlosivimi klasti. Siv in svetlosiv zrnat dolomit, ki ponekod vsebuje megalodontidne školjke, predstavlja člen C loferske cikloteme in je nastal v podplimskem okolju. Siv in temnosiv stromatoliten dolomikrit s horizontom sivega onkodolomikrosparita, ki ga tvorijo ostanki onkoidov tipa »*Sphaerocodium bornemannii*«, predstavlja člen B, ki je nastal v medplimskem okolju. Temnosive do črne dolomitne breče pa so nastale v nadplimskem okolju in predstavljajo člen A. Menjanje teh členov je posledica pogrezanja šelfa, evstazije in produkcije karbonata. Dolomitnih breč člena A je navzgor vedno več, kar kaže na postopno regresijo morja (McROBERTS ET AL., 1997; KRYSSTYN ET AL., 2005). Večje debeline breč v skrajnjem zgornjem delu zgornjega triasa so lahko tudi posledica močnejše sinsedimentne tektonike.

V spodnjem delu spodnjeliasnih plasti je menjavanje sive do črne dolomitne breče s klasti zrnatega in laminiranega dolomita, s sivim do svetlosivim zrnatim dolomitom. Sive do črne dolomitne breče so verjetno nastale še v plitvem okolju pod vplivom sinsedimentne tektonike (McROBERTS ET AL., 1997). Zaradi poglabljanja morja oz. spodnjeliasne transgresije (HALLAM, 1997) stromatolitne lamine niso več nastajale in so zato v sivem zrnatem dolomitu odsotne. V zgornjem delu spodnjeliasnih plasti pa se že pojavlja svetlosiv mikriten apnenec.

MATERIALI IN METODE

Analiziranih je bilo 16 vzorcev iz profilov Žvencelj-Novi zavodi in Tresenk-Rupendol. Uporabljeni so bili sveži neprepereli vzorci dolomitov. Vzorci dolomitov so bili zmleti v homogen prah. Vsak izmed 16 vzorcev je bil razdeljen na 4 manjše 8 miligramske vzorce, ki so bili odtehtani s tehnico Mettler Toledo AE240.

Pri reakciji 100 % fosforne kisline (H_3PO_4) s karbonatom pri 50 °C se je tvoril plin CO_2 , ki je bil nato analiziran z masnim spektrometrom Varian MAT 250. Vrednosti razultatov so bile normalizirane glede na standarda IAEA-CO-1 (8× po 4 mg) z $\delta^{13}C$ vrednostjo +2,48 ‰ in $\delta^{18}O_{VPDB}$ vrednostjo -2,44 ‰ ter NBS-19 (8× po 4 mg) z $\delta^{13}C$ vrednostjo +1,95 ‰ in $\delta^{18}O_{VPDB}$ vrednostjo -2,20 ‰. Vsi vzorci so bili analizirani na Inštitutu Jožef Štefan v Ljubljani.



Slika 2. Litostratigrafski stolpec zgornjetriasnih in spodnjeliasnih plasti na območju Krima

Figure 2. Lithostratigraphic column of Upper Triassic and Lower Liassic beds in Krim Mountain area

REZULTATI RAZISKAV

Izotopske analize ogljika in kisika so bile preliminarne, opravljene z namenom natančnejše določitve postopne meje med triasom in juro zaradi pomanjkanja fosilnih ostankov v dolomitih. Izotopske sestave ogljika in kisika iz profilov Žvencelj-Novih zavodov in Tresenk-Rupendol so navedene v tabeli 1 in 2 ter grafično prikazane na sliki 3.

Vrednosti $\delta^{13}\text{C}$ v profilu Žvencelj-Novih zavodov (tabela 1) se gibljejo med +0,62 ‰ in

+1,82 ‰, vrednosti $\delta^{18}\text{O}$ pa med -4,15 ‰ in +0,67 ‰. V profilu Tresenk-Rupendol (tabela 2) pa so vrednosti $\delta^{13}\text{C}$ med +1,04 ‰ in +2,72 ‰ ter $\delta^{18}\text{O}$ med -5,28 ‰ in +0,64 ‰.

Najvišja vrednost $\delta^{13}\text{C}$ je v obeh profilih dosežena v zgornjetriasmem sivem stromatolitnem in svetlosivem drobno in srednjezrnatem dolomitu (vzorci IA0, IA16-2 in IA16-1), ki se pojavlja med stromatolitnim. Minimalna vrednost je pri obeh profilih dosežena v debeli črni in temnosivi

Tabela 1. Izotopska sestava ogljika in kisika v dolomitih iz profila Žvencelj-Novih zavodov

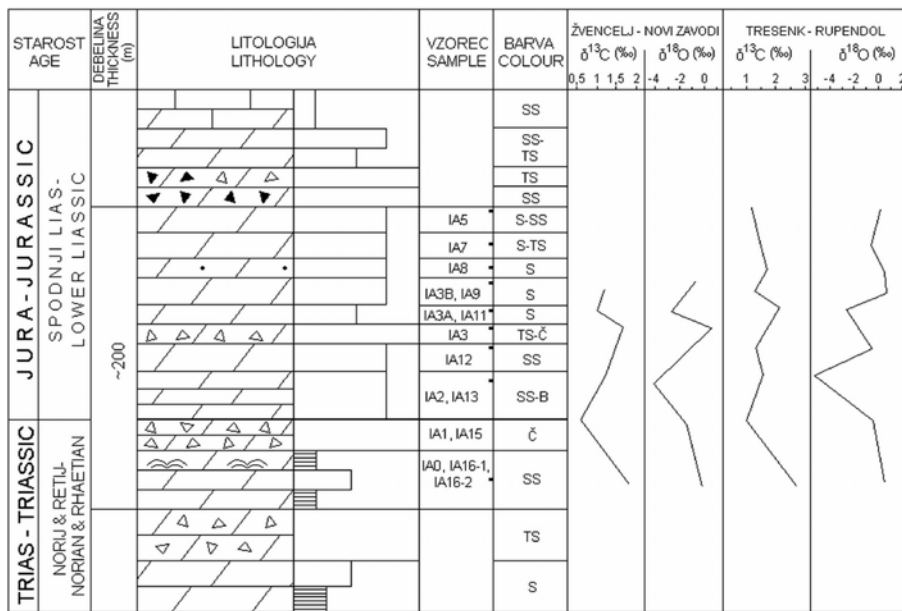
Table 1. Isotopic composition of carbon and oxygen in dolomites from Žvencelj-Novih zavodov section

Vzorec-Sample	$\delta^{18}\text{O}$	std.	$\delta^{13}\text{C}$	std.
IA0	-0,16	0,00	1,82	0,04
IA1	-1,36	0,03	0,62	0,08
IA2	-4,15	0,06	1,22	0,03
IA3	0,67	0,07	1,75	0,07
IA3a	-2,70	0,06	1,00	0,08
IA3b	-0,68	0,03	1,19	0,01

Tabela 2. Izotopska sestava ogljika in kisika v dolomitih iz profila Tresenk-Rupendol

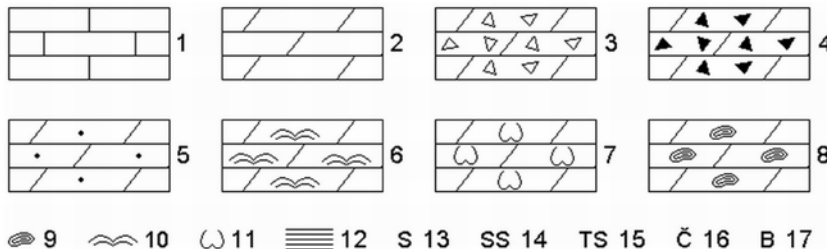
Table 2. Isotopic composition of carbon and oxygen in dolomites from Tresenk-Rupendol section

Vzorec-Sample	$\delta^{18}\text{O}$	std.	$\delta^{13}\text{C}$	std.
IA16-2, IA16-1	0,45	0,12	2,72	0,09
IA15	-0,40	0,15	1,04	0,14
IA13	-5,28	0,04	1,55	0,07
IA12	-0,46	0,08	1,36	0,12
IA11	-2,63	0,01	2,12	0,04
IA9	0,64	0,04	1,30	0,05
IA8	0,53	0,02	1,72	0,05
IA7	-0,57	0,14	1,48	0,13
IA5	0,20	0,03	1,21	0,05



Slika 3. Litostratigrafski stolpec in izotopska sestava ogljika in kisika v dolomitih raziskanih profilov

Figure 3. Lithostratigraphic column and isotopic composition of carbon and oxygen in dolomites from studied sections



Legenda k sliki 2 in 3

1 - apnenec, 2 - dolomit, 3 - dolomitna breča s svetlosivimi klasti, 4 - dolomitna breča s černimi klasti, 5 - bituminozni dolomit, 6 - stromatolitni dolomit, 7 - dolomit z megalodontidami, 8 - onkoidni dolomit, 9 - onkoidi, 10 - stromatoliti, 11 - megalodontidne školjke, 12 - vzporedna laminacija, 13 - siva, 14 - svetlo siva, 15 - temno siva, 16 - črna, 17 - bela

Explanation of Figure 2 and 3

Explanation of Figure 2 and 3
1 - limestone, 2 - dolomite, 3 - dolomitic breccia with light grey clasts, 4 - dolomitic breccia with black clasts, 5 - bituminous dolomite, 6 - stromatolitic dolomite, 7 - dolomite with Megalodontids, 8 - oncoidal dolomite, 9 - oncoids, 10 - stromatolites, 11 - Megalodontids, 12 - parallel lamination, 13 - grey, 14 - light grey, 15 - dark grey, 16 - black, 17 - white

dolomitni breči (vzorca IA1 in IA15), ki predstavlja skrajni zgornji del zgornjega triasa in je verjetno nastala v času viška zgornjetriaspne regresije morja. Prvo zvišanje vrednosti $\delta^{13}\text{C}$ v svetlosivih zrnatih dolomitih (vzorca IA2 in IA13) sovpada z začetkom spodnjeliasnega zvišanja gladine morja oziroma transgresije. Meja med triasom in juro je bila tako postavljena med črnimi dolomitnimi brečami in svetlosivim zrnatim dolomitom (slika 3).

Vrednost $\delta^{18}\text{O}$ v vzorcih IA1 in IA15, vzporedna minimalni vrednosti $\delta^{13}\text{C}$, je relativno visoka in bi lahko sovpadala s povišano temperaturo v času viška regresije. Minimalna vrednost $\delta^{18}\text{O}$ v vzorcih IA2 in

IA13 pa poteka vzporedno s prvim povišanjem vrednosti $\delta^{13}\text{C}$ in sovpada z znižanjem temperature oziroma spremembo kemizma morske vode (pornih voda) pri spodnjeliasni transgresiji morja. Nadaljnja nihanja vrednosti $\delta^{13}\text{C}$ in $\delta^{18}\text{O}$ predstavlja manjša nihanja gladine morja med napredujočo spodnjeliasno transgresijo.

Med analiziranimi različki dolomitov prevladujejo zrnati dolomiti in vezivo dolomitnih breč ter redki mikritni in laminirani mikritni dolomiti. Zrnati dolomiti so nastali s pozognadiagenetsko dolomitizacijo, laminirani mikritni dolomiti pa imajo ohranljeno prvotno strukturo kamnine in so nastali z zgodnjedadiagenetsko dolomitizacijo.

RAZPRAVA

Rezultati izotopskih analiz ogljika in litoloških raziskav kažejo, da je debela črna in temnosiva dolomitna breča nastala pod vplivom močne sinsedimentne tektonike verjetno v času viška zgornjetriaspne regresije morja, ob kateri je prišlo do povečanega dotoka meteornih voda, in predstavlja skrajni zgornji del zgornjega triasa. Svetlosivi zrnati dolomiti nad brečo so nastali v nekoliko globlji vodi med začetkom spodnjeliasne transgresije morja.

Podatki o izotopski sestavi kisika kažejo, da je bila v zgornjem delu zgornjega triasa, v času viška regresije, temperatura vode verjetno nekoliko povišana. Nasprotno se je v spodnjem delu spodnjega liasa, zaradi napredujoče transgresije, temperatura vode znižala oziroma je prišlo do spremembe kemizma morske vode (pornih voda).

Za mejo T/J je značilna negativna $\delta^{13}\text{C}$ anomalija, ki je posledica povečanega doleta meteorne vode in oksidacije morske organske snovi med zgornjetriaspno regresijo morja. Zaradi regresije je prišlo do subaerske oksidacije organske snovi, pri čemer se je C¹² vezal v CO₂ in se uravnotežil z oceansko vodo. Pri tem se je rezervoar ogljika v oceanski vodi obogatil z lažjim izotopom ogljika (DOLENEC ET AL., 1998; PALFY ET AL., 2001). Pri transgresiji morja pa se je zgodilo ravno obratno. Oceanska voda se je relativno obogatila s težjim ogljikovim izotopom. Poleg tega pa zaradi poglabljanja morja stromatolitne lamine med spodnjeliasnimi zrnatimi dolomiti niso več nastajale.

Zaradi pomanjkanja oziroma odsotnosti fosilnih ostankov meja med triasom in juro ni bila paleontološko utemeljena. Naše

raziskave so izhajale iz stare predpostavke, da je meja med triasom in juro postavljena tam, kjer se med zrnatim dolomitom laminiran dolomit ne pojavlja več (PLENIČAR, 1970; BUSER, 1986). V litološkem pogledu je meja T/J postavljena v pas, kjer se zaključi loferska sedimentacija, paleontoško pa po izumrtju megalodontid (NOVAK, 2003). Samo na podlagi litoloških in sedimentoloških značilnosti ne moremo določiti natančnega položaja meje, lahko pa vsaj približno opredelimo interval, v katerem se meja nahaja. Vzorci so bili odvzeti v intervalu od zrnatega dolomita, ki leži pod laminiranim dolomitom do prvega pojava mikritnega apnенca, nad katerim leži ooidni apnenec, ki je biostratigrafsko dokazano srednjeliasne starosti. Obravnavano zaporedje kamnin tako skoraj zagotovo obsega skrajni zgornji del retija in spodnji del spodnjega liasa ter s tem tudi mejo T/J.

Primerjava obravnavanih plasti z zgornjetriasmimi in spodnjeliasnimi plastmi Severnih Apneniških Alp (MCROBERTS ET AL., 1997; KRYSTYN ET AL., 2005) je pokazala, da so v Severnih Apneniških Alpah v noriju nastajali glavni dolomiti in dachsteinski apnenci v laguni, ki so jo pričeli v zgornjem retiju prekrivati bioklastični apnenci in laporovci, medtem ko se je na obravnavanem ozemlju sedimentacija glavnega dolomita zaključila s temnosivimi do črnimi sin-sedimentnimi brečami večjih debelin. Zaradi napredujoče sedimentacije klastičnih kamnin se je karbonatna platforma skrčila in delno okopnila. Sedimentacija pa se je nadaljevala v bazenskih predelih, kjer so nastala t.i. »znotrajplatformska« medplimska okolja z značilno favno megalodontidnih školjk in loferskim faciesom (MCROBERTS

ET AL., 1997). Med retijem in spodnjim liasom so se ob začetku transgresije odložile klastične in karbonatno klastične kamnine mejnih plasti (muljevci, meljevci in laporati apnenci) brez značilnih fosilov. Nad mejnimi plasti je več horizontov z zaobljenimi klasti apnencev, ki vsebujejo zgornjetriasne foraminifere (MCROBERTS ET AL., 1997). Te horizonte bi lahko primerjali s temnosivimi do črnimi dolomitnimi brečami obravnavanega ozemlja, ki vsebujejo klaste zrnatega in laminiranega zgornjetriasnega dolomita. V plitvem podplimskem okolju pa so nastali ooidni apnenci z amoniti, ki kažejo na hettangijsko starost.

Ker so bili vzorčevani predvsem pozno-diagenetski dolomiti, obstaja verjetnost, da so primarni izotopski signal zabrisale poznodiagenetske spremembe. Dobljeni izotopski signal je tako lahko posledica izmenjave z izotopsko lažjo porno vodo pri poznodiagenetskih procesih. Poznodiagenetski dolomiti so glede na zgodnjediagenetske običajno obogateni z lakkima izotopoma ogljika in kisika, vendar pa imajo nekateri norijsko-retijski poznodiagenetski dolomiti podobno izotopsko sestavo kot zgodnjediagenetski, kar pomeni, da se temperatura in izotopska sestava raztopin, ki so povzročile poznodiagenetsko dolomitizacijo, nista bistveno razlikovali od morske vode, v kateri je nastal zgodnjediagenetski dolomit (OGORELEC ET AL., 1999). Ker je do poznodiagenetske dolomitizacije glavnega dolomita prišlo še v času norija in retija (OGORELEC & ROTHE, 1993) in se je poznodiagenetska dolomitizacija spodnjeliasnih dolomitov izvršila v spodnjem liasu, so imele porne raztopine, ki so časovno različni dolomitizaciji povzročile, verjetno različno izotopsko sestavo. Zato

je primerjava rezultatov izotopskih analiz poznodiagenetskih dolomitov zgornjetriassne in spodnjeliasne starosti smiselna. Da je prišlo do popolne dolomitizacije glavnega dolomita v času zgornjega triasa, dokazujejo tudi klasti zrnatih in laminiranih dolomitov v liasnih brečah.

Za kvalitetnejšo interpretacijo rezultatov izotopske analize bi bilo potrebno analizirati večje število vzorcev, odvzetih v manjših medsebojnih intervalih in obravnavati večji profil.

SKLEPI

Na območju Kirmskega hribovja so v času zgornjega triasa na Dinarski karbonatni platformi nastajali glavni dolomiti v loferskem razvoju z redkimi ohranjenimi fosilnimi ostanki. V nadplimskem okolju so nastale dolomitne breče, v medplimskem okolju zgodnjediagenetski stromatolitni dolomiti in v podplimskem okolju zrnati dolomiti, ki so nastali s poznodiagenetsko dolomitizacijo. V času spodnjega liasa pa so nastajale črne in svetlosive dolomitne breče ter sivi zrnati dolomiti brez vmesnih plasti laminiranih dolomitov.

Litološka in izotopska analiza zgornjetriassnih kamnin sta pokazali, da je v času zgornjega triasa prišlo do napredajoče regresije morja, ki je dosegla svoj višek konec zgornjega triasa. Z začetkom spodnjega liasa pa se je pričelo poglabljanje morja ozziroma transgresija, na kar kaže tudi odsotnost stromatolitnih dolomitov med zrnatimi dolomiti.

Na podlagi litoloških značilnosti in rezultatov izotopskih analiz smo sklepali, da poteka meja T/J, na območju Krima, med črnimi dolomitnimi brečami (zgornjetri-

asna starost) in svetlosivimi zrnatimi dolomiti (spodnjeliasna starost). Za natančejšo in bolj zanesljivo določitev meje pa bi bile vsekakor potrebne podrobnejše in obširnejše izotopske analize s pogostejšim vzorčevanjem.

Na vrednosti $\delta^{13}\text{C}$ in $\delta^{18}\text{O}$ v karbonatih vpliva izotopska sestava organske snovi v morju med sedimentacijo in kasnejše diagenetske spremembe (PEZDIČ, 1999). Diagenetske spremembe, ki lahko povzročijo vzporedne negativne anomalije $\delta^{18}\text{O}$ in $\delta^{13}\text{C}$, vplivajo predvsem na vrednosti $\delta^{13}\text{C}_{\text{karbonatni}}$ (PALFY ET AL., 2001).

Pri pozodiagenetskih dolomitih, ki imajo podobno izotopsko sestavo kot zgodnjediagenetski, je bila izotopska sestava raztopin, ki so povzročile poznodiagenetsko dolomitizacijo, verjetno podobna izotopski sestavi morske vode. Poleg tega je do popolne dolomitizacije glavnega dolomita prišlo še v času norija in retija (OGORELEC & ROTHE, 1993; NOVAK, 2003), zato lahko s primerjavo izotopske sestave ogljika in kisika v pozodiagenetskih dolomitih zgornjetriassne in spodnjeliasne starosti dobimo zadovoljive rezultate, ki so uporabni pri določitvi meje T/J.

SUMMARY

Determination of T/J boundary by $\delta^{13}\text{C}$ and $\delta^{18}\text{O}$ stable isotope analysis (Krim Mountain, Slovenia)

One of the most extensive mass extinctions, which caused extinction of more than 50 % of marine genera (McROBERTS ET AL., 1997), took place at the end of Triassic period. There are different hypotheses explaining this extinction, but the most possible reason is a decrease in primary productivity and a reduction of marine habitats due to marine regression.

Dolomites from two locations on Krim Mountain area (Figure 1) were sampled to define Triassic-Jurassic boundary. Krim Mountain area belongs to northern part of External Dinarides. During Triassic and Jurassic period carbonates of External Dinarides were deposited on Dinaric Carbonate Platform. The transition from Triassic to Jurassic was characterized by continuous carbonate sedimentation. Dolomites that exhibit cyclic bedded, supratidal "Lofer facies" (Main dolomite) were deposited during Upper Triassic. Characteristic of Upper Triassic beds is an alternation of grey to light grey coarse-grained dolomites with rare megalodontid bivalves, grey and dark grey stromatolitic dolomicrite, grey oncocolomicrosparite with *Sphaerocodium bornemanni* and dark grey to black dolomitic breccias (Figure 2). Beds of supratidal dolomitic breccias appear more and more frequently upwards in the upper part of Upper Triassic, which indicates gradual sea-level fall (McROBERTS ET AL., 1997; KRYSTYN ET AL., 2005). Alternation of grey to black dolomitic bre-

ccias that contain clasts of coarse-grained and laminated dolomites with grey to light grey coarse-grained dolomites without intermediate stromatolitic laminae, in the lower part of Lower Liassic beds, indicates sea-level rise. Coarse-grained dolomites and dolomitic breccias are overlain by light grey micritic limestones in the upper part of Lower Liassic beds.

16 samples of non-degraded dolomites from Žvencelj-Novi zavodi and Tresen-Rupendol sections were analysed. Samples were powdered and homogenized and treated with phosphoric acid. Isotopic composition of obtained CO_2 was measured on Varian MAT 250 mass spectrometer. Data were normalized according to international standards. Oxygen and carbon isotope compositions are presented in Tables 1 and 2 and shown in Figure 3.

Stable isotope studies of Triassic-Jurassic boundary in the Northern Calcareous Alps, Austria (McROBERTS ET AL., 1997; KRYSTYN ET AL., 2005) and Csővar section, Hungary (PALFY ET AL., 2001), show negative $\delta^{13}\text{C}$ anomaly in boundary beds as a consequence of meteoric water influx and oxidation of organic matter during Upper Triassic marine regression (McROBERTS ET AL., 1997; PALFY ET AL., 2001).

$\delta^{13}\text{C}$ values in dolomites from sections Žvencelj-Novi zavodi and Tresen-Rupendol range from +0,62 ‰ to +2,72 ‰ and $\delta^{18}\text{O}$ from -5,28 ‰ to +0,67 ‰. Positive excursion in $\delta^{13}\text{C}$ was recorded in Upper Triassic grey stromatolitic and light grey grainy dolomites. It is followed by pronounced negative $\delta^{13}\text{C}$ anomaly in black and dark grey dolomitic breccias, coinciding

with sea-level fall. Following positive $\delta^{13}\text{C}$ anomaly within light grey coarse-grained dolomites may reflect the beginning of the Lower Liassic sea-level rise. Based on lithologic features and results of oxygen and carbon isotope analyses, the Triassic-Jurassic boundary was more accurately defined between black dolomitic breccias and light grey coarse-grained dolomites (Figure 3). The $\delta^{18}\text{O}$ variability could reflect temperature changes and changes in isotopic composition of seawater or pore fluids during sea-level fluctuations.

Due to lack of fossil remains, the Triassic-Jurassic boundary was not paleontologically documented. Thus, our researches were based on old presumption that Triassic-Jurassic boundary lies within coarse-grained dolomite in which intermediate beds of laminated dolomites are no longer present (PLENIČAR, 1970; BUSER, 1986).

The analysed dolomites were mostly late diagenetic therefore the diagenetic alterations could have significant influence on $\delta^{13}\text{C}$ and $\delta^{18}\text{O}$ values. Late diagenetic dolomites are usually depleted in heavy carbon and oxygen isotopes compared to early diagenetic dolomites. However, some late diagenetic dolomites have isotopic com-

position similar to that of early diagenetic dolomites, which means that temperature and isotopic composition of pore fluids, that caused late diagenetic dolomitization were similar to those of sea-water, in which early diagenetic dolomites were deposited (OGORELEC ET AL., 1999).

Upper Triassic carbonates were completely dolomitized by the end of Triassic (OGORELEC & ROTHE, 1993), which is proved by Liassic breccias containing clasts of coarse-grained and laminated dolomites, and late diagenetic dolomitization of Lower Liassic carbonates occurred within Lower Liassic, it can be assumed that isotopic composition of pore fluids that caused dolomitization of Upper Triassic carbonates probably differs from isotopic composition of pore fluids that caused dolomitization of Lower Liassic carbonates. Thus, it can be concluded that results of isotopic analyses of late diagenetic dolomites can be used for determination of Triassic-Jurassic boundary.

For more precise determination of the Triassic-Jurassic boundary, more detailed isotopic and lithologic analyses with more frequent sampling should be carried out

Zahvala

Avtorji se zahvaljujemo Institutu Jožef Stefan, predvsem dr. Sonji Lojen, za opravljene izotopske analize ter tehničnim sodelavcem Oddelka za geologijo Naravoslovno-tehniške fakultete za pomoč pri pripravi vzorcev.

VIRI

- BUSER, S. (1986): *Osnovna geološka karta SFRJ 1:100.000. Tolmač listov Tolmin in Viđem.* Zvezni geološki zavod, Beograd, pp. 1-103.
- DOLENEC, T., BUSER, S., DOLENEC, M. (1998): The Permian-Triassic boundary in the Karavanke Mountains (Slovenia): Stable isotope variations in the boundary carbonate rocks of the Košutnik Creek and Brsnina section = Perm-sko-triasna meja v Karavankah: variabilnost izotopske sestave v karbonatih Košutnikovega potoka in Brsnine. *Geologija.*; Vol. 41, pp. 17-27.
- HALLAM, A. (1981): The end-Triassic bivalve extinction event. *Palaeogeography, Palaeoclimatology, Palaeoecology.*; Vol. 35, pp. 1-44.
- HALLAM, A. (1997): Estimates of the amount and rate of sea-level change across the Rhaetian-Hettangian and Pliensbachian-Toarcian boundaries (latest Triassic to early Jurassic). *Journal of the Geological Society.*; Vol. 154, pp. 733-779.
- KRYSTYN, L., BOHM, F., KURSCHNER, W., DELECAT, S. (2005): The Triassic-Jurassic boundary in the Northern Calcareous Alps. *Field guide.*; pp. 1-14.
- KUMP, L. R., ARTHUR, M. A. (1999): Interpreting carbon-isotope excursions: Carbonates and organic matter. *Chemical Geology.*; Vol. 161, pp. 181-198.
- MICROBERTS, C. A., NEWTON, C. R. (1995): Selective extinction among end-Triassic European bivalves. *Geology.*; Vol. 23, pp. 102-104.
- MICROBERTS, C. A., FURRER, H., JONES, D. S. (1997): Palaeoenvironmental interpretation of a Triassic-Jurassic boundary section from Western Austria based on palaeoecological and geochemical data. *Palaeogeography, Palaeoclimatology, Palaeoecology.*; Vol. 136, pp. 79-95.
- NOVAK, M. (2003): Zgornjjetriaspne in spodnjegurske plasti na območju Podutika pri Ljubljani = Upper Triassic and Lower Jurassic beds in the Podutik area near Ljubljana (Slovenia). *Geologija.*; Vol. 46/1, str. 65-74.
- OGORELEC, B., ROTHE, P. (1993): Mikrofazies, Diagenese und Geochemie des Dachsteinkalkes und Hauptdolomits in Süd-West-Slowenien. *Geologija.*; Vol. 35, pp. 81-181.
- OGORELEC, B., DOLENEC, T., PEZDIČ, J. (1999): Izotopska sestava O in C v mezozojskih karbonatnih kamninah Slovenije – vpliv facies in diageneze = Isotope composition of O and C in Mesozoic carbonate rocks of Slovenia – effect of facies and diagenesis. *Geologija.*; Vol. 42, pp. 171-205.
- PALFY, J., DEMENY, A., HAAS, J., HETENYI, M., ORCHARD, M. J., VETO, I. (2001): Carbon isotope anomaly and other geochemical changes at the Triassic-Jurassic boundary from a marine section in Hungary. *Geology.*; Vol. 29/11, pp. 1047-1050.
- PEZDIČ, J. (1999): *Izotopi in geokemijski procesi.* Naravoslovnotehniška fakulteta, Oddelek za geologijo, Ljubljana, 281 str.
- PLENIČAR, M. (1970): *Osnovna geološka karta SFRJ 1:100.000. Tolmač lista Postojna.* Zvezni geološki zavod, Beograd, str. 62.
- SCHRAG, D. P., DEPAOLO, D. J., RICHTER, F. M. (1995): Reconstructing past sea surface temperatures: Correcting for diagenesis of bulk marine carbonates. *Geochimica et Cosmochimica Acta.*; Vol. 59, pp. 2265-2278.

Foraminiferal suborder Robertinina from the Badenian of Kozjansko (Eastern Slovenia)

Foraminiferni podred Robertinina iz badenija na Kozjanskem (vzhodna Slovenija)

KATARINA OBLAK¹

¹ University of Ljubljana, Faculty of Natural Sciences and Engineering, Department of Geology, Privoz 11, SI-1000 Ljubljana, Slovenia; E-mail: katarina.oblak@ntf.uni-lj.si

Received: September 5, 2007

Accepted: October 18, 2007

Abstract: In this study, two Badenian foraminiferal species of the suborder Robertinina from Kozjansko (Eastern Slovenia) are presented. Both species *Ceratobulimina contraria* (Reuss) and *Hoeglundina elegans* (d'Orbigny) occur frequently in samples from the Lower to Upper Badenian (Middle Miocene). The occurrence of *C. contraria* in the Upper Badenian indicates a wider stratigraphic range for the Central Paratethys than was previously recognized. This species has not been determined from Middle Miocene strata of Slovenia before this work. *H. elegans* is already known from the Middle Miocene of Slovenia, but in this paper specimens are described, imaged and classified for the first time.

Povzetek: V prispevku sta predstavljeni dve badenijski foraminiferni vrsti iz podreda Robertinina s Kozjanskega (vzhodna Slovenija). Obe vrsti, *Ceratobulimina contraria* (Reuss) in *Hoeglundina elegans* (d'Orbigny), sta številčno zastopani v vzorcih od spodnjega do zgornjega badenija (srednji miocen). Pojav vrste *C. contraria* v zgornjebadenijskih plasteh kaže na njen širši stratigrafski razpon kot je bil za območje Centralne Paratetide poznan doslej. V srednjemiocenskih sedimentih Slovenije vrsta še ni bila določena. Vrsta *H. elegans* je iz srednjega miocena Slovenije sicer že poznana, vendar je v prispevku prvič opisana, upodobljena in uvrščena v sistem.

Key words: Foraminifera, Robertinina, Badenian, Miocene, Central Paratethys

Ključne besede: foraminifere, Robertinina, badenij, miocen, Centralna Paratetida

INTRODUCTION

The suborder Robertinina LOEBLICH & TAPPAN, 1984 is the last of twelve suborders described in the foraminiferal classification of LOEBLICH & TAPPAN (1987). The suborder is defined by the following characteristics; planispirally to trochospirally-enrolled tests, chambers commonly with internal partition and hyaline perforate wall composed of ultrastructurally and optically radiate aragonite (LOEBLICH & TAPPAN, 1984). With the exception of the extinct suborder Involutinina, which died out during the Mesozoic, all other hyaline foraminifera have tests formed of calcite. According to the foraminiferal classification of LOEBLICH AND TAPPAN (1987), the suborder Robertinina includes 48 genera, ranging from the Upper Triassic to Holocene. From the Middle Miocene, six genera are recognized globally, and only four have been noted in European sediments: *Ceratobulimina* Toula, 1915, *Lamarckina* (Berthelin, 1881), *Hoeglundina* Brotzen, 1948 and *Robertina* d'Orbigny, 1846. Due to its relatively low species diversity in the Middle Miocene deposits, the suborder Robertinina represents a less frequent mentioned foraminiferal taxon in the literature.

MATERIAL AND METHODS

Robertininas of Kozjansko were studied from six sections of the Planina syncline; Imenska Gorca, Plohov breg, Javoršica, Sveta Ana and Trobni Dol on the northern flank and Drensko Rebro on the south-

In Slovenia, foraminifera of the suborder Robertinina are poorly represented in sedimentary sequences. In Miocene sediments, only the species *Hoeglundina elegans* has been identified. It is noted as *Hoeglundina elegans* or *Epistomina elegans* from the Lower Egerian of the Laško syncline (DOZET ET AL., 1999), from the Upper Egerian of the Laško syncline (DOZET ET AL., 1999) and Planina syncline (PETRICA ET AL., 1995, DOZET ET AL., 1999), from the Lower Badenian of Dravinske gorice (RIJAVEC, 1975), from the Middle Badenian of the Laško syncline (RIJAVEC, 1976 in 1984) and Planina syncline (RIJAVEC, 1977), and from the Upper Badenian of the Laško syncline (RIJAVEC, 1976 in 1984). The species hasn't been described, imaged and classified further in a system previously. The species *Ceratobulimina contraria* hasn't been determined in any other previous research in Slovenia.

In Kozjansko, robertininas were studied from six sections. The investigated area belongs to the Planina syncline, the westernmost margin of the Central Paratethys (BUSER, 1977, 1979, ANIČIĆ & JURIŠA 1984, ANIČIĆ & JURIŠA 1985, ANIČIĆ ET AL., 2004).

ern flank (OBLAK, 2006). One hundred and twenty-eight samples of Badenian marl and marly calcarenite were studied. Samples range from the Lower Badenian Lower Lagenidae Zone to the Upper Badenian *Virgulinella pertusa* Zone (Figure 1, OBLAK, 2006). 187 species were deter-

mined and classified into seven foraminiferal suborders. The suborder Robertinina is represented by two species: *Ceratobulimina contraria* (Reuss) and *Hoeglundina elegans* (d'Orbigny). Although the preser-

vation is poor due to aragonitic composition, the characteristic appearance of both species allows accurate identification of specimens.

RESULTS AND DISCUSSION

Taxonomy of Foraminifera

(according to LOEBLICH & TAPPAN, 1987)

Ordo Foraminiferida Eichwald, 1830

Subordo Robertinina Loeblich & Tappan, 1984

Superfamilia Ceratobuliminacea Cushman, 1927

Familia Ceratobuliminidae Cushman, 1927

Subfamilia Ceratobulimininae Cushman, 1927

Genus *Ceratobulimina* Toula, 1915

Ceratobulimina contraria (Reuss, 1851)

(Plate 1, figs. 1-8)

1851 *Rotalina contraria* - REUSS, 76, Taf. V, Fig. 37a-c.

1969 *Ceratobulimina (Ceratobulimina) contraria* (Reuss) - LANGER, 62, Abb. 12b-c, Taf. 3, Fig. 15.

1975 *Ceratobulimina contraria* (Reuss) - POPESCU, 105, pl. XC, Figs. 2a-b.

1982 *Ceratobulimina contraria* (Reuss) - DONDI & BARBIERI, tav. XLIII, Fig. 2.

1987 *Ceratobulimina contraria* (Reuss) - LOEBLICH & TAPPAN, pl. 473, Figs. 9-13.

1995 *Ceratobulimina contraria* (Reuss) - YASSINI & JONES, 142, Figs. 960-961.

1998 *Ceratobulimina contraria* (Reuss) - CICHA ET AL., 89, pl. 29, Figs. 9-10.

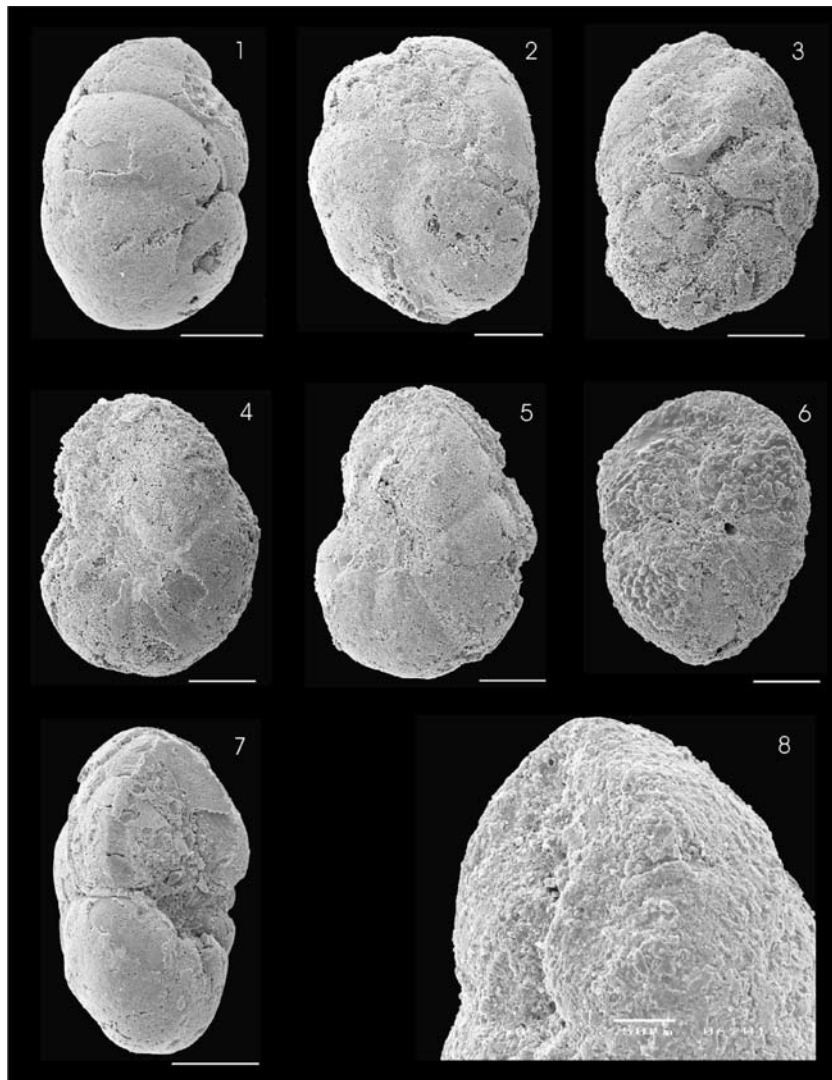


Plate 1. *Ceratobulimina contraria* (Reuss, 1851). Fig. 1: Spiral side; J 33, Fig. 2: Spiral side; J 33, Fig. 3: Spiral side; J 33, Fig. 4: Umbilical side; J 33, Fig. 5: Umbilical side; J 33, Fig. 6: Umbilical side; J 27, Fig. 7: Side view; J 33, Fig. 8: Aperture; J 32. Scale bar represents 100 µm.

Tabla 1. *Ceratobulimina contraria* (Reuss, 1851). Sl. 1: Spiralna stran; J 33, Sl. 2: Spiralna stran; J 33, Sl. 3: Spiralna stran; J 33, Sl. 4: Umbilikalna stran; J 33, Sl. 5: Umbilikalna stran; J 33, Sl. 6: Umbilikalna stran; J 27, Sl. 7: Pogled s strani; J 33, Sl. 8: Ustje; J 32. Merilce predstavlja 100 µm.

Material: Rare to numerous tests from 15 samples (Figure 1).

Description: Test consists of trochospirally arranged chambers. It is ovate in outline. Spiral side is slightly convex. Sutures are curved on the spiral side and straight on the umbilical side. Umbilicus is deep. Periphery is broadly rounded. Surface is very smooth and finely perforate. Aperture is in a shape of a narrow loop, running vertically along the apertural face. Wall is aragonitic (LOEBLICH & TAPPAN, 1987).

Remark: Preservation of tests is poor. In the study of GRÜNING (1985), specimens are similar to mine by shape but differ in low slitlike aperture that characterize the genus *Ceratocancris*. Considering this, the species is cited as *Ceratocancris contraria*.

Size: Test height is 0.38 - 0.45 mm, broadness 0.27 - 0.34 mm and thickness 0.2 mm.

Occurrence: The species was first described from the Oligocene of Germany

(remark: in 1851, the geological period Oligocene hasn't been assigned yet so these strata were determined as of Eocene age). In Germany, it is known from the Oligocene (LOEBLICH & TAPPAN, 1987) and the Middle Miocene (LANGER, 1969), in Denmark from the Oligocene (LOEBLICH & TAPPAN, 1987) and in Italy from the Upper Oligocene to the Serravallian, maybe also to the Tortonian; it is most common in the Serravallian (DONDI & BARBIERI, 1982: identified from samples collected in the Po Valley).

The species is extant; it is noted from the South Pacific (YASSINI & JONES, 1995). In the Central Paratethys, it appears from the Upper Eocene to the end of the Middle Badenian, its appearance in the Ottnangian and Karpatian is not certain (CICHA ET AL., 1998). In Hungary, it is known from the Lower Egerian (SZTRÁKOS, 1979) and in Romania from the Miocene (POPESCU, 1975).

Familia Epistominidae Wedekind, 1937
Subfamilia Epistomininae Wedekind, 1937
Genus *Hoeglundina* Brotzen, 1948

Hoeglundina elegans (d'Orbigny, 1826)
(Plate 2, Figs. 1-5)

- 1826 *Rotalia (Turbinulina) elegans* - d'ORBIGNY, 110.
- 1959 *Epistomina elegans* (d'Orbigny) - DIECI, 81, tav. VI, Fig. 31.
- 1960 *Hoeglundina elegans* (d'Orbigny) - BARKER, 216, pl. 105, Figs. 3-6.
- 1975 *Hoeglundina elegans* (d'Orbigny) - POPESCU, 106, pl. XC, Figs. 3a-c.
- 1982 *Hoeglundina elegans* (d'Orbigny) - DONDI & BARBIERI, tav. XLI, Fig. 10.
- 1985 *Hoeglundina elegans* (d'Orbigny) - PAPP & SCHMID, 59, Taf. 49, Fig. 1-6.
- 1991 *Hoeglundina elegans* (d'Orbigny) - CIMERMAN & LANGER, 56, pl. 59, Figs. 10-12.
- 1998 *Hoeglundina elegans* (d'Orbigny) - CICHA ET AL., 108, pl. 29, Figs. 19-21.
- 1998 *Hoeglundina elegans* (d'Orbigny) - ROBERTSON, 114, pl. 44, Figs. 2a-e.

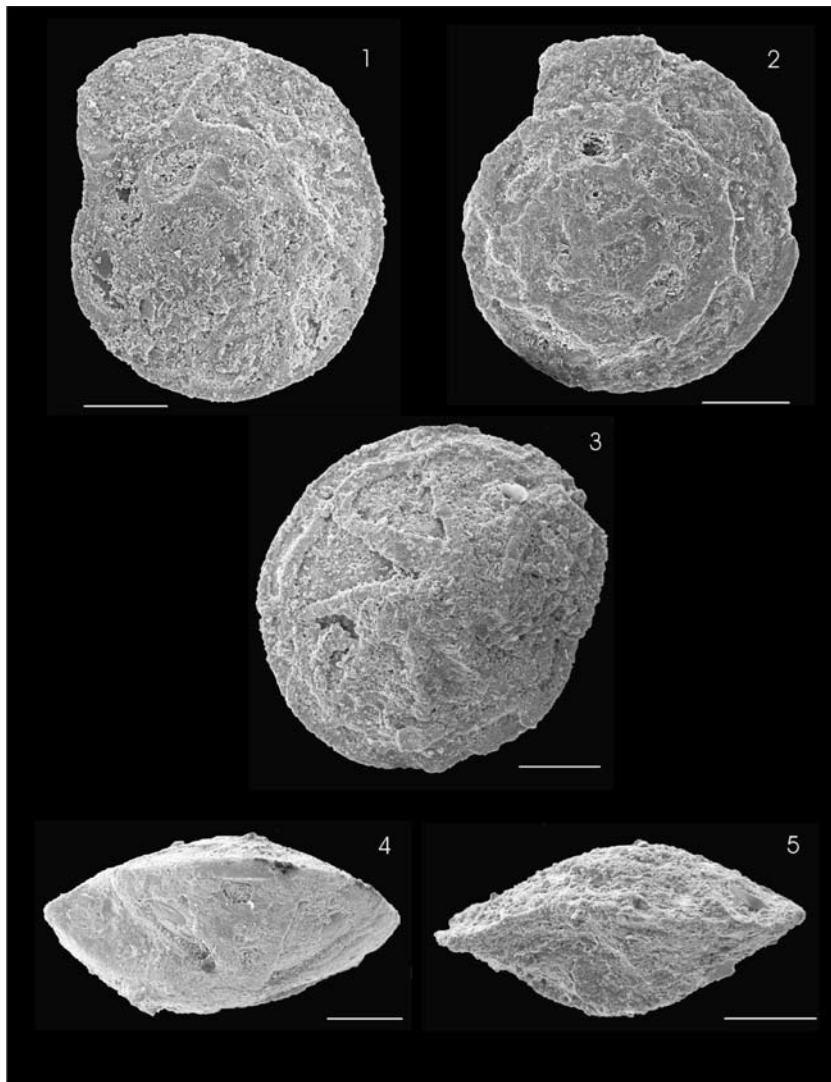


Plate 2. *Hoeglundina elegans* (d'Orbigny, 1826). Fig. 1: Spiral side; Dr 17, Fig. 2: Spiral side; J 32, Fig. 3: Umbilical side; Dr 17, Fig. 4: Side view; Dr 17, Fig. 5: Side view; J 32. Scale bar represents 100 µm.

Tabla 2. *Hoeglundina elegans* (d'Orbigny, 1826). Sl. 1: Spiralna stran; Dr 17, Sl. 2: Spiralna stran; J 32, Sl. 3: Umbilikalna stran; Dr 17, Sl. 4: Pogled s strani; Dr 17, Sl. 5: Pogled s strani; J 32. Merilce predstavlja 100 µm.

Material: Rare to numerous tests from 16 samples (Figure 1).

Description: Test is trochospiral and bi-convex. Sutures are thickened. They are curved backward on the spiral side, and straight and oblique on the umbilical side. Periphery is subacute. Surface is smooth and finely perforate. Slitlike aperture is lat-eromarginal. Wall is aragonitic (LOEBLICH & TAPPAN, 1987).

Size: Test diameter is 0.42 - 0.52 mm and thickness 0.25 mm.

Remark: Preservation of tests is poor.

Occurrence: There are no data about the type locality and type level by the first description (D'ORBIGNY, 1826). In Italy, the species is known from the Middle Eocene to Pleistocene, it is very frequent in the Upper Pliocene (DONDI & BARBIERI, 1982: Po Valley, DIECI, 1959: Tortonian, Pliocene). In Middle America, it is known from the Upper Eocene (BOLLI ET AL., 1994), Miocene and Pliocene (ROBERTSON, 1998), in California, from the Pleistocene (ROBERTSON, 1998), in Australia, from the Upper Oligocene and Lower Miocene (LI & McGOWRAN, 2000), in the India Ocean from the Pliocene and Pleistocene (BASOV & KRASHENINNIKOV, 1995), and in the Atlantic from the Pleistocene (LÉVY ET AL., 1998).

The species is extant; it is known from the Atlantic (BARKER, 1960), Pacific (DIECI, 1959, YASSINI & JONES, 1995) and Mediterranean (DIECI, 1959, CIMERMAN & LANGER, 1991, SGARRELLA & MONCHARMONT ZEI, 1993).

In the Central Paratethys, it appears from the Upper Eocene to the end of the Bade-

nian (CICHA ET AL., 1998). It is most frequent in the Karpatian and Badenian (CICHA ET AL., 1971). In Austria, it is known from the Upper Eocene (GOHRBANDT, 1961) and Karpatian (RÖGL, 1969), and in Bavaria, from the Kiscellian to Ottangian (REISER, 1987: Lower Rupelian - Lower Egerian, WENGER, 1987: Upper Egerian - Lower Ottangian).

Remark: In the literature that discusses Paleogene sedimentary sequences (Eocene of Italy: GRÜNIG (1985), Eocene of Slovenia: CIMERMAN ET AL. (2006), Lower Egerian of Hungary: SZTRÁKOS (1979)), morphologically similar tests have been determined as the species *Hoeglundina eocenica* (Cushman & Hanna). In the study of BRAGA & GRÜNIG (1975), the specimens noted as *H. elegans* from the Oligocene of Belgium are identified in the synonymy of the species *H. eocenica* from the Eocene of Italy. There are three possible interpretations of the cited literature above. That the species *H. elegans* ranges from the Eocene to Holocene, while the morphologically similar *H. eocenica* is restricted to the Paleogene only, where the two very similar species were coexistent. Alternatively, *H. eocenica* (Paleogene) and *H. elegans* (Neogene) may be chronologically distinct species; in this case identification of *H. elegans* in Paleogene strata would represent a false identification of *H. eocenica*. It is also possible that both names are only synonyms of one species, ranging from the Eocene to Holocene. Further comparative study of specimens from the Paleogene and Neogene is required to determine the relationship between both species.

Distribution of robertininas in sections

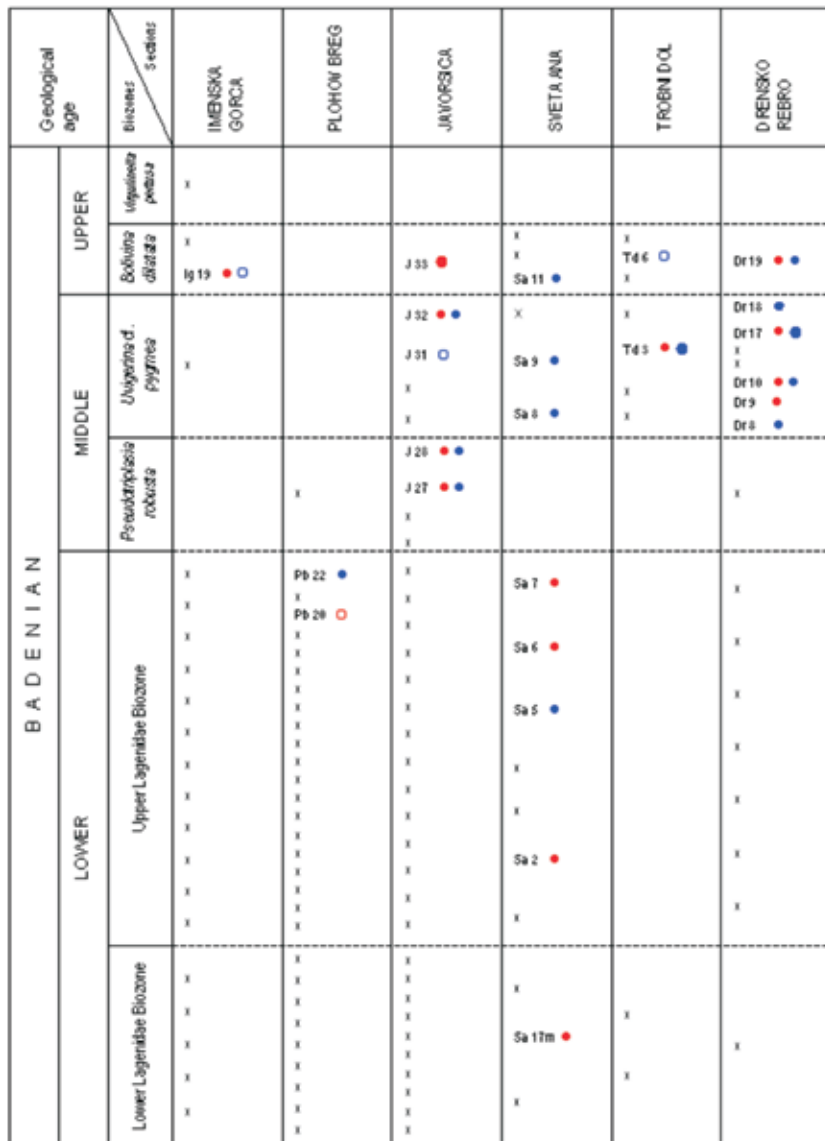
Species *Ceratobulimina contraria* and *Hoeglundina elegans* were found in all six sections (Figure 1). *C. contraria* appears in 15 samples from the Lower Badenian (Lower Lagenidae Zone) to Upper Badenian (*Bolivina dilatata* Zone). In Plohov breg and Sveta Ana sections, it is delimited to the Lower Badenian; in the early Lower Badenian (Lower Lagenidae Zone) it was found only in the sample Sa 17m of the Sveta Ana section, while in the late Lower Badenian (Upper Lagenidae Zone) it becomes more common in both sections.

In other four sections: Imenska Gorca, Javoršica, Trobni Dol and Drensko Rebro, the species appears in the Middle and Upper Badenian only. The highest abundance is seen in the Upper Badenian sample J 33. *H. elegans* appears in 16 samples from the Lower Badenian Upper Lagenidae Zone to Upper Badenian *Bolivina dilatata* Zone. It is more common in the Middle and Upper Badenian with highest abundances being seen in Middle Badenian samples Td 3 and Dr 17. In sections Imenska Gorca, Javoršica, Trobni Dol and Drensko Rebro, the co-occurrence of both species is noted.

CONCLUSIONS

In Kozjansko (Eastern Slovenia), the foraminiferal suborder Robertinina is represented with two species; *Ceratobulimina contraria* (Reuss) and *Hoeglundina elegans* (d'Orbigny). Both species were found in samples from the Lower to Upper Badenian. They are scarce in the Early Lower Badenian (Lower Lagenidae Zone) but increased abundance is noted in the Middle and Upper Badenian. Highest abundances are seen in the late Middle Badenian (*Uvigerina cf. pygmea* Zone) and in the early Upper Badenian (*Bolivina dilatata* Zone).

Due to their occurrence throughout whole sections the species have little stratigraphic value for the Badenian, which coincides with previous studies of the Central Paratethys (CICHA ET AL., 1998). Moreover, occurrence of the species *Ceratobulimina contraria* in Upper Badenian samples points to its even wider stratigraphic range; the last appearance data of the species is moved from the Middle Badenian (CICHA ET AL., 1998) to early Upper Badenian (this study). Both species are described, imaged, classified and represented by their exact occurrence through the sections for the first time in Slovenia.



LEGEND

- x sample without robertininas
- J 32 sample containing robertininas
- ● ● rare, frequent, numerous *Ceratobulimina contraria*
- ● ● rare, frequent, numerous *Hoeglundina elegans*

Figure 1. Frequence distribution of robertininas in the sections (after OBLAK, 2006); samples are listed in stratigraphic sequence

Slika 1. Pojavljanje robertinin v profilih (po OBLAK, 2006); vzorci si sledijo v stratigrafskem zaporedju

POVZETKI

Foraminiferni podred Robertinina iz badenija na Kozjanskem (vzhodna Slovenija)

V prispevku je predstavljen foraminiferni podred Robertinina iz badenijskih plasti Kozjanskega. Podred Robertinina je bil opisan zadnji izmed dvanajstih foraminifernih podredov, ki jih zajema foraminiferna klasifikacija LOEBLICHA in TAPPANOVE (1987). Podred vključuje foraminifere s planispiralno do trohospiralno zavitimi hišicami, večinoma notranje predeljenimi kamricami in steklasto porozno steno, zgrajeno iz struktorno in optično žarkovitega aragonita (LOEBLICH & TAPPAN, 1987). Stene hišic vseh preostalih steklastih foraminifer, z izjemo v mezozoiku izumrlega podreda Involutinina, so namreč kalcitne. V podred Robertinina je po omenjeni klasifikaciji (LOEBLICH & TAPPAN, 1987) uvrščenih 48 rodov, s stratigrafskim razponom od zgornjega triasa do danes. Iz srednjega miocena je poznanih šest rodov, od tega v Evropi le štirje; *Ceratobulimina* Toula, 1915, *Lamarckina* (Berthelin, 1881), *Hoeglundina* Brotzen, 1948 in *Robertina* d'Orbigny, 1846. Glede na relativno majhno vrstno diverzitetno v srednjemiocenskih sedimentih je podred Robertinina kot takson v literaturi manj poznan. V Sloveniji je bila iz miocenskih plasti doslej določena le vrsta *Hoeglundina elegans* (RIJAVEC, 1975, 1976, 1977 in 1984, PETRICA ET AL., 1995, DOZET ET AL., 1999).

Na Kozjanskem je bilo vzorčenih šest profilov; Imensa Gorca, Plohov breg, Javoršica, Sveta Ana, Trobni Dol in Drensko Rebro (OBLAK, 2006), ki pripadajo Planinski sinklinali, oziroma zahodnemu obrobju nekdanje Centralne Paratetide (BUSER, 1977& 1979, ANIČIĆ & JURIŠA 1984, ANIČIĆ & JURIŠA 1985, ANIČIĆ ET AL., 2004). Iz 128 vzorcev laporja in laporastega kalkarenita je bilo določenih 187 foraminifernih vrst iz sedmih podredov. Red Robertinina je zastopan z vrstama *Ceratobulimina contraria* (Reuss) in *Hoeglundina elegans* (d'Orbigny) in se pojavlja v vseh šestih profilih (slika 1). *C. contraria* je prisotna v vzorcih od starejšega spodnjega badenija (spodnja lagenidna biocona) do starejšega zgornjega badenija (biocona *Bolivina dilatata*), medtem ko se pojavlja *H. elegans* od mlajšega spodnjega badenija (zgornja lagenidna biocona) dalje. Obe vrsti sta najpogostejsi v mlajšem srednjem badeniju (biocona *Uvigerina cf. pygmea*) in starejšem zgornjem badeniju (biocona *Bolivina dilatata*), kjer je opazen tudi trend skupnega pojavljanja.

Prisotnost *C. contraria* v zgornjebadenijskih vzorcih kaže na širši stratigrafski razpon kot je bil za območje Centralne Paratetide poznan doslej. Glede na dosezanje raziskave naj bi živila vrsta na tem območju namreč le do konca srednjega badenija (CICHA ET AL., 1998). Iz srednjemiocenskih sedimentov Slovenije vrsta še ni bila poznana. *H. elegans*, ki je bila iz srednjega miocena Slovenije že določena, je v prispevku prvič opisana, upodobljena in uvrščena v sistem.

Acknowledgements

I would like to express my thanks to Ivan Rakovec Institute of Palaeontology, ZRC SAZU for giving me the possibility to take SEM images.

REFERENCES

- ANIČIĆ, B., JURIŠA, M. (1984): *Osnovna geološka karta SFRJ 1:100.000, list Rogatec, L 33-68*. Zvezni geološki zavod, Beograd.
- ANIČIĆ, B., JURIŠA, M. (1985): *Tolmač k Osnovni geološki karti SFRJ 1:100.000, list Rogatec L 33-68*. Zvezni geološki zavod, Beograd, 76 str.
- ANIČIĆ, B., OGORELEC, B., DOZET, S. (2004): *Geološka karta Kozjanskega, 1:50.000*. Geološki zavod Slovenije, Mladinska knjiga, Ljubljana.
- BARKER, R. W. (1960): Taxonomic Notes on the Species Figured by H. B. Brady in his Report on the Foraminifera Dredged by H.M.S. Challenger During the Years 1873-1876. Accompanied by a Reproduction of Brady's Plates. *Soc. Econom. Paleont. Miner.; Spec. Publ.*, Vol. 9, pp. 1-238, Tulsa.
- BASOV, I. A., KRASHENINNIKOV, V. A. (1995): *Stratigraphy and Foraminifers of the Pliocene and Quaternary Deposits of the Timor Trough (the Indian Ocean)*. Naučni mir, Moskva, 112 pp.
- BOLLI, H. M., BECKMANN, J.-P., SAUNDERS, J. B. (1994): *Benthic foraminiferal biostratigraphy of the south Caribbean region*. Cambridge University Press, Cambridge, 408 p.
- BRAGA, G., GRÜNING, A. (1975): Foraminiferi bentonici dell'Eocene superiore. In: Braga, G., De Biase, R. Grünig, A. & Proto Decima, F., Foraminiferi bentonici del Paleocene ed Eocene della sezione di Possagno. *Schweizerische Paläontologische Abhandlungen*; Vol. 97, pp. 85-199, Basel.
- BUSER, S. (1977): *Osnovna geološka karta SFRJ 1:100.000, list Celje L 33-67*. Zvezni geološki zavod, Beograd.
- BUSER, S. (1979): *Tolmač k Osnovni geološki karti SFRJ 1:100.000, list Celje L 33-67*. Zvezni geološki zavod, Beograd, 72 str.
- CICHA, I., RÖGL, F., RUPP, C., CTYROKA, J. (1998): Oligocene - Miocene foraminifera of the Central Paratethys. *Abh. Senckenberg. Naturforsch. Ges.*; Vol. 549, 325 p., Frankfurt am Main.
- CICHA, I., ZAPLETALOVÁ, I., PAPP, A., CTYROKA, J., LEHOTAYOVA, R. (1971): Die Foraminiferen der Eggenburger Schichten-gruppe (incl. Arcellinida). In: Steininger, F. & Seneš, J. (Eds.), *Chronostratigraphie und Neostratotypen, Miozän der Zentralen Paratethys*. Bd. II, Eggenburgien, VEDA, Bratislava, pp. 234-355.
- CIMERMAN, F., LANGER, M. R. (1991): Mediterranean Foraminifera. *Dela IV. razreda SAZU*; Vol. 30, 118 str., Ljubljana.

- CIMERMAN, F., JELEN, B., SKABERNE, D. (2006): Late Eocene benthic foraminiferal fauna from clastic sequence of the Socka - Dobrna area and its chrono-stratigraphic importance (Slovenia). *Geologija.*; Vol. 49/1, pp. 7-44, Ljubljana.
- DIECI, G. (1959): I foraminiferi tortoniani di Montegibbio e Castel Vetro. *Paleontographia Italica.*; Vol. LIV (n. ser. vol. XXIV), pp. 1-113, Pisa.
- DONDI, L., BARBIERI, R. (1982): *Foraminiferi Padani, Atlante iconografico e distribuzione stratigrafica (Terziario e Quaternario)*. AGIP S.p.A., Milano, 52 pls.
- DOZET, S., RIJAVEC, L., GRAD, K. (1999): Western Kozje Area Tertiary (Eastern Slovenia). *Rudarsko metalurški zbornik.*; Vol. 46, No. 3, pp. 475-489, Ljubljana.
- GOHRBANDT, K. (1961): Die Kleinforaminiferenfauna des obereozänen Anteils der Reigruber Serie bei Bruderndorf (Bezirk Korneuburg, Niederösterreich). *Mitt. Geol. Ges.*; Vol. 54, pp. 55-145, Wien.
- GRÜNIG, A. (1985): Systematical description of Eocene benthic foraminifera of Possagno (Northern Italy), Sansoain (Northern Spain) and Biarritz (Aquitaine, France). *Memorie di Scienze Geologiche, Inst. Geol. Mineal. Uni. Padova.*; Vol. XXXVII, pp. 251-302, Padova.
- LANGER, W. (1969): Beitrag zur Kenntnis einiger Foraminiferen aus dem mittleren und oberen Miozän des Nordsee-Beckens. *N. Jb. Geol. Paläont. Abh.*; Vol. 133, pp. 23-78, Stuttgart.
- LÉVY, A., MATHIEU, R., POIGNANT, A., ROSET-MOULINIER, M. (1998): 44. Data Report: Distribution of Pleistocene Benthic Foraminifers from the Eastern Equatorial Atlantic Ocean. In: Massale, J., Lohmann, G. P. & Moullade, M. (Eds), *Proceedings of the Ocean Drilling Program, Scientific Results.*; Vol. 159, pp. 605-610, Texas.
- LI, Q., McGOWRAN, B. (2000): Miocene foraminifera from Lakes Entrance Oil Shaft, Gippsland, southeastern Australia. *Memoir of the Association of Australasian Palaeontologists.*; Vol. 22, pp. 1-142, Canberra.
- LOEBLICH, A. R. JR., TAPPAN, H. (1984): Suprageneric classification of the Foraminiferida (Protozoa). *Micropaleontology.*; Vol. 30, No. 1, pp. 1-70, New York.
- LOEBLICH, A. R. JR., TAPPAN, H. (1987): *Foraminiferal Genera and their Classification.*; Vol. 1-2, 970 p., 847pls., Van Nostrand Reinhold, New York.
- d'ORBIGNY, A. (1826): Tableau Méthodique de la Classe des Céphalopodes. *Ann. Sci. D'Hist. Nat.*; Ser. 7, pp. 7-150, Paris.
- OBLAK, K. (2006): *Foraminiferna taksonomija, biostratigrafija in paleoekologija badenija v Planinski sinklinali (vzhodna Slovenija, Centralna Paratetida)*: Ph.D. Thesis. Ljubljana: University of Ljubljana 2006; 310 p, 60 pls.
- PAPP, A., SCHMID, M. E. (1985): Die Fossilen Foraminiferen des Tertiären Beckens von Wien. Revision der Monographie von Alcide d'Orbigny (1846). *Abh. Geol. Bundesanst.*; Vol. 37, 311 p., Wien.

- PETRICA, R., RIJAVEC, L., DOZET, S. (1995): Stratigraphy of the Upper Oligocene and Miocene beds in the Trobni Dol area (Kozjansko). *Rudarsko metalurški zbornik.*; Vol. 42, No. 3-4, pp. 127-141, Ljubljana.
- POPESCU, G. (1975): Études des foraminifères du miocène inférieur et moyen du nord-ouest de la Transylvanie. *Mémoires Inst. Géol. Géophys.*; Vol. XXIII, pp. 5-121, Bucarest.
- REISER, H. (1987): Die Foraminiferen der bayrischen Oligozän - Molasse; Systematik, Stratigraphie und Paläobathymetrie. *Zitteliana.*; Vol. 16, pp. 3-131, München.
- REUSS, A. E. (1851): Über die fossilen Foraminiferen und Entomostraceen der Septarienthone der Umgegend von Berlin. *Zeitsch. Deut. Geol. Gesel.*; Vol. 3, pp. 49-92, Berlin.
- RIJAVEC, L. (1975): *Korelacija miocenskih plasti v vzhodni Sloveniji, II. faza.* Arhiv geološkega zavoda Slovenije, 63 p., Ljubljana.
- RIJAVEC, L. (1976): *Korelacija miocenskih plasti v vzhodni Sloveniji, III. faza.* Arhiv geološkega zavoda Slovenije, 52 p., Ljubljana.
- RIJAVEC, L. (1977): *Korelacija miocenskih plasti v vzhodni Sloveniji, IV. faza.* Arhiv geološkega zavoda Slovenije, 56 p., Ljubljana.
- RIJAVEC, L. (1984): *Oligocen i miocen područja izmedju Rudnice i Boča (istočna Slovenija) na osnovi mikrofosila: Ph.D. Thesis.* Zagreb: Sveučilište u Zagrebu, Prirodoslovno-matematički fakultet Zagreb 1984, 141 p.
- ROBERTSON, B. E. (1998): Systematics and paleoecology of the benthic Foraminifera from the Buff Bay section, Miocene of Jamaica. *Micropaleontology*; Vol. 44, No. 2, 266 p., New York.
- RÖGL, F. (1969): Die miozäne Foraminiferenfauna von Laa an der Thaya in der Molassezone von Niederösterreich. *Mitt. Geol. Ges.*; Vol. 61, pp. 63-123, Wien.
- SGARRELLA, F., MONCHARMONT ZEI, M. (1993): Benthic foraminifera of the Gulf of Naples (Italy): systematics and autoecology. *Boll. Soc. Paleont. Ital.*; Vol. 32, No. 2, pp. 145-264, Modena.
- SZTRÁKOS, K. (1979): La stratigraphie, paléoécologie, paléogéographie et les Foraminifères de l'Oligocène du nord-est de la Hongrie. *Cahiers Micropaléontologie*; Vol. 3, 95 p., Paris.
- WENGER, W. F. (1987): Die Foraminiferen des Miozäns der bayerischen Molasse und ihre stratigraphische sowie paläogeographische Auswertung. *Zitteliana.*; Vol. 16, pp. 173-340, München.
- YASSINI I., JONES, B. G. (1995): *Recent Foraminifera and Ostracoda from estuarine and shelf environments on the southeastern coast of Australia.* The University of Wollongong Press, Wollongong, 484 p.

Geological characteristics of the terrain along Vc corridor between Sava river and Sarajevo town

MIRZA BAŠAGIĆ¹, NIJAZ ŠKRIPIĆ¹, FERID SKOPLJAK¹

¹ Civil Engineering Faculty of University of Sarajevo, Geology Institute, Stjepana Tomića st. 3, 71000 Sarajevo, B&H; E-mail: mbasagic@lol.ba.

Received: March 25, 2007

Accepted: August 20, 2007

Abstract: On the basis of analyzed geological, tectonic, seismic-tectonic, hydro and engineering geological characteristics of terrain, in this paper are reviewed geotechnical conditions for construction of highway, as a part of Vc Corridor through Bosnia and Herzegovina, between Sava river in the north and Sarajevo, i.e. Tarčin town in the south. Along northern half of BH-highway, 165 km long, it would be necessary to construct 37 tunnels in total length of 30.2 km and 119 bridges (viaducts) with 13 road junctions. Highway route mainly extends along river Bosna valley, in terrain with heterogeneous geological structure and complex structural-tectonic structure. It diagonally crosses structure of Dinaric Alps and active seismic-tectonic zones with intensity of up to 7 EMS. In regards to structural-geologic relations, subjects of change are also hydrogeological categories, porosity and functions of rock masses. However, highway is not in collision with water supply systems or significant water source areas. Regarding the fact that hard and stable rock masses are dominant in terrain, up to 3/4 of considered terrain belongs to favourable category for construction works. Exceptions are zones with thick covers along notches and particularly unstable landslide zones within Zenica and Kakanj areas. Those parts, unfavourable for construction works are placed in about 1/4 of considered route.

Key words: highway, corridor, geological structure, tectonic structure, seismic-tectonic zones, hydrogeological and engineering geological characteristics, stability, and favourability for construction works

INTRODUCTION

In the aim of establishment of direct road connection between Baltic and Adriatic Sea, in other words between countries of north, central and south Europe, construction of a highway in Corridor Vc is

planned (Baltic-Adriatic). South part of future highway is also placed through Bosnia and Herzegovina, in length of 330 km. From the north state border, from the bridge across Sava river near Svilaj, highway is placed along river Bosna valley and in the area near Modriča, Doboj, Tešanj,

Zenica, Sarajevo and Mostar cities, in its south part, along valleys of river Neretva, it connects to Adriatic - Ionic motorway in Republic of Croatia. North half part of BH corridor, in length of 164.93 km extends between Sava River and Sarajevo (Tarčin). Inside mentioned section, 37 tunnels in total length of 30,253 m shall be constructed

as well as 119 bridges (viaducts), in other words structures, and 13 junctions (road loops). This paper represents review of geological-tectonic, seismic-tectonic and hydrogeological-engineering geological characteristics of terrain and geotechnical conditions for construction of highway along mentioned section.

RESULTS AND DISCUSSION

Physical and geographic characteristics

Relief between Svilaj and Tarčin is uneven in morphologic aspect. Up to Doboj it belongs to a plain south edge of Pannonia lowland. From Doboj to Tarčin, road route in its main part extends along the valley of river Bosna, inside Dinaric Alps massif with hilly-mountain relief. The lowest altitudes are in the north, along riverbeds of Bosna and Sava, between 85 - 120 m a.s.l. In south direction, in the area of mountain ranges, altitude increases from 500 to over 1000 m a.s.l.

Geological structure

In geological structure, rock systems of Phanerozoic

- Palaeozoic rock systems (Pz) compose south part of reviewed terrain. They are composed of philite, quartz-sericite schist with lenses of lidite, quartzite, quartz-porphyre, dolomite, limestone and marble of Devonian (D), and Permian conglomerate, sandstone and shale (P), and to Permian Triassic (P,T) belong shaly marly limestone in the area of Tarčin.

- Mesozoic rock systems (Mz) compose middle part of terrain. They are characterized with great variety of facies.
- Within lower Triassic (T_1) represented are sandstone, schist, marl and limestone, and both stages of middle Triassic (T_2) are composed of limestone and dolomite of Anisian (T_2^1), and igneous-sedimentary formation of Ladinian (T_2^2). Massive microsparite belongs to upper Triassic (T_3).
- Jurassic sediments (J) are extended from river Rudanka and Doboj, to Nemila. Dominant is igneous-sedimentary formation, more precisely ophiolite "mélange".
- Transitional horizons of Jurassic and Cretaceous (J, K) are represented in flysch like rocks, as "Nemila" (1J,K) and "Vranduk" sediments (2J,K).
- Upper Cretaceous (K_2) is characterised with so called "carbonate flysch" (limestone, breccia, subordinating pelite-alevrolite and marl in exchange).
- Cainozoic (Kz) is represented with sediments of Palaeogene, Neogene and Quaternary, which are extended in Posavina and along valley of Bosna.

- Palaeogene, more precisely Palaeocene-Eocene sediments (Pc,E) are developed in clastic and carbonate facie, and Eocene sediments (E) are composed of limestone-sandstone and facie of flysch.
- Oligocene-Miocene sediments (Ol, M) are represented with conglomerate, sandstone, marl, clay and travertine limestone.
- Neogene (N) is composed of sediments of Miocene and Pliocene. Miocene (M) sediments are conglomerate, sandstone, clay, marl and limestone with occurrences of coal in Sarajevo-Zenica and Šeher-Žepče basin. Pliocene and Pliocene-Quaternary rock systems (Pl; Pl,Q) are sand, gravel and clay, and in Pliocene, coal also occurs.
- Quaternary surface covers of detritus-sand-clay composition have significant extension, especially in Posavina and on the slopes along river valleys, especially in parts where basic terrain structure is composed of clastic, clayey-marly sediments.

Tectonic structure

In tectonic aspect, the area of road route belongs to a region of inner Dinaric Alps and it extends over so called "zone of Palaeozoic schist and Mesozoic limestone", with central ophiolitic zone. Main folding structure is represented with fold of Bosnian flysch which crosses middle part of road route near Nemila. As main fault structures, determined are Spreča-Kozara and Busovača deep faults. Besides deep faults, there are also faults of the first category (Neo tectonic faults), and faults of the

second category that crosses surface parts of terrain along the road route.

Seismic-tectonic zones

Deep fractures represent areas of contemporary tectonic movements that are the most common causes of occurrence of earthquakes. In that aspect, there are following seismic-tectonic zones: Sava - Modriča; Modriča - Doboj; Usora - Maglaj; Žepče - Vranduk and Sarajevo – Zenica basin. Within those zones, prognosticated intensity of earthquakes for returning period of 500 years is $6^{\circ} - 7^{\circ}$ EMS.

Hydrogeological relations

According to hydrogeological categories, porosity and functions of rock masses, in terrain are represented water permeable and watertight rocks. Water permeable rocks are characterised with crack-cavernous and intergranular porosity structures, and according to permeability and functions there are highly water permeable and moderately water permeable underground and surface aquifers. Springs occur mainly in carbonate rocks of crack-cavernous porosity. In rocks of intergranular porosity, formed are "free" water bearing layers out of which water is used for water supply, like they are water sources in Odžak, Rudanka near Doboj, Jelah near Tešanj, near Žepče, Zenica, Kakanj, Sarajevo, etc. Watertight igneous, metamorphic and clayey-marly sedimentary rocks, in dependence of structural position, have a function of hydrogeological barriers in terrain.

Engineering geological characteristics

According to engineering geological clas-

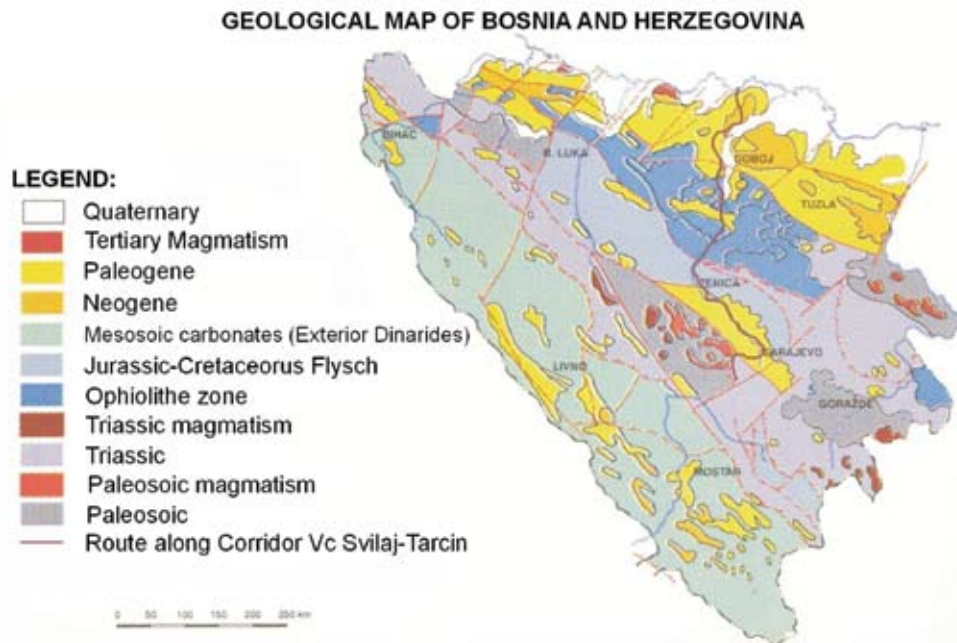


Figure 1. Geological map of Bosnia and Herzegovina (HRVATOVIĆ, H., 1999)

sification, rock masses are divided as main mapped units and selected in taxonomic units as: lithological types (LT), complexes (LC) and suites (LS). According to grade of diagenesis and strength of bonds of mineral aggregates, selected units are divided into two basic groups:

- hard and soft rocks, in other words masses of geological substrata, and
- coherent and incoherent soil, in other words surface covers of different genesis types.

Within group of hard and soft rocks, selected are 22 lithological complexes (LC) and 13 lithological types (LT). And within group of coherent and incoherent soil, se-

lected are 6 lithological complexes (LC). On the basis of engineering geological characteristics, performed was classification and definition of rock masses as real environments where highway would be constructed. According to stability and endangerment of contemporary exodynamic and techno-genetic processes and occurrences, and satisfaction for construction, selected are three categories:

- the first category: instable areas, unsatisfactory for constructions;
- the second category: conditionally stable areas, conditionally satisfactory for constructions;
- the third category: stable areas, satisfactory for constructions.

In reviewed section that is 164.93 km long, 3/4 of road route is placed in stable terrain, satisfactory for construction, and only 1/4 of road route is placed in conditionally, and instable terrain.

Geotechnical conditions for constructions

In aspect of geotechnical conditions for construction, the following can be summarised:

- In plain parts, which are composed of gravel-sand sediments, difficulties during construction are not expected, besides local occurrence of higher levels of underground water, what should be considered during disposition of road route level.
- In aspect of satisfaction for construction, that areas belong to category of satisfactory and stable terrains.
- Middle part of road route, between Doboj and Zenica, is characterised with heterogeneous lithological composition and variable physical-mechanical characteristics of rocks that create complex geotechnical conditions for constructions.
- In that part, along road route, occurrences of disturbed stability of slopes could be expected, especially in parts where thicker covers are present as well as in parts of substrata that are more decayed, in portal parts of tunnels and zones of foundations of bridge constructions (tunnel Crni Vrh, tunnels between Ozimica - Nemila, bridges over river Bosna, etc).
- In aspect of geological-geotechnical conditions for construction, the greatest difficulties are expected in the area of bypassing city of Zenica, because road route between Donja Gračanica and Drivuša is placed along instable and conditionally stable slopes.
- Along section Drivuša - Kakanj, road route is placed in terrain that is composed of clastic sediments with formed thicker cover and decayed parts of basic substrata, and landslide Tičići should also be emphasized, which together with "Zenica" landslides represent the most important occurrence of instable parts of terrain.
- Within tertiary marly-clayey rocks along tunnel, occurrences of rock yielding, underground pressures, rock collapsing, etc. should be expected, while in carbonate-clastic zones, some better conditions could be expected.
- Along section between Vlakovo and Tarčin, road route is mainly placed inside tunnels in limestone and igneous-metamorphic rocks, but construction conditions could be evaluated as satisfactory.
- In aspect of construction of tunnels, limestone and "healthy" igneous-metamorphic rocks represent satisfactory working environment, even though fault zones could be expected in them together with scattered outbursts and occurrences of underground water.

CONCLUSIONS

On the basis of analysed relevant engineering geological parameters: lithofacie composition, conditions and characteristics of rock masses, morphologic characteristics, exodynamic geological processes and occurrences, angle of stability of natural slopes, hydrogeological and seismic characteristics along Corridor Vc in section between river Sava in the north and Sarajevo, more exactly Tarčin in the south, it can be concluded that geotechnical conditions for

construction are satisfactory in the most part. Regarding the fact that in terrain dominating are hard and stable rock masses, that means that 3/4 of reviewed section belongs to more satisfactory category for construction. Exceptions to this are zones with thicker covers in notches and especially instable zones of landslides in the area of Zenica and Kakanj. Suitability for construction is represented also with a fact that road route of future highway is not in collision with water supply systems or more significant water sources.

REFERENCES

- BAŠAGIĆ, M., LANGOF, Z., ŠKRIPIĆ, N., SKOPLJAK, F. (2005): *Highway in Corridor Vc, Planning-study documentation, Technical study, Elaborate on engineering geological, hydrogeological and geotechnical conditions for construction.* Book 2.3, LOT № 1&2, IPSA, Sarajevo, pp. 1-31.
- BRAČINAC, Z. (1966): *Basic seismic-tectonic map of SR BH, 1:200,000.* Institute for engineering geology and hydrogeology, Sarajevo.
- ČIČIĆ, S. (2002): *Geological composition and tectonic of terrain of Bosnia and Herzegovina* (in Bosnian). Sarajevo, 311 p.
- HRVATOVIĆ, H. (1999): Geological guide through Bosnia and Herzegovina, Monographic (in Bosnian). *Geological Herald.*; XXIV, Sarajevo, pp. 1-203.
- ROKIĆ, L. (1989): *Role and importance of engineering geological modifiers to engineering geological characteristics of terrain of middle Bosnia.* Institute for geotechnics and foundations, Civil Engineering Faculty of Sarajevo, Sarajevo, pp. 1-169.
- VIDOVIĆ, M., MOJIČEVIĆ, M. (1975): *General Tectonic Map of Bosnia and Herzegovina.* Seismic Institute of BH, Sarajevo.

Environmental protection and investment costs as factors of road placement

Okolje in investicijski stroški kot dejavnika za umeščanje cestne trase v prostor

HEDA KOČEVAR¹, MARKO ŠETINC¹

¹ OMEGAconsult d.o.o., Gregorčičeva ulica 7, SI-1000 Ljubljana, Slovenia;
E-mail: heda.kocevar@omegaconsult.si, marko.setinc@omegaconsult.si

Received: May 31, 2007

Accepted: September 5, 2007

Abstract: In the article, a methodology to aid the choice of the most appropriate road corridor from the standpoint of environmental protections and investment costs is presented. The methodology enables road planners to first define the route or so called corridor, which according to the selected factors is most acceptable and expert grounded, and in the next phase work out multiple combinations of previously "pure" scenarios. On the basis of additional evaluations, political preferences, financial capabilities and social acceptability, the most appropriate corridor for placement of a new road is chosen. Inside of the corridor, the most technically feasible route of new road is then drawn. The advantage of such an approach is foremost in the objectivity of the methodology and the simultaneous command of multiple factors when choosing the most appropriate corridor. The classic method of route placing has its roots in technical placement; and these alternatives are evaluated between each other from multiple perspectives.

Izvleček: V prispevku je prikazana metodologija določitve najugodnejšega cestnega koridorja z vidika varovanja okolja in investicijskih stroškov gradnje ceste. Metodologija omogoča načrtovalcu najprej definirati t.i. koridorje, ki so glede na izbrane vplive najugodnejši ter strokovno in objektivno čim bolj utemeljeni. V naslednji stopnji se lahko izdela tudi različne kombinacije prejšnjih »čistih« koridorjev. Med vsemi predlaganimi koridorji se na podlagi dodatnih vrednotenj, političnih preferenc, finančnih zmožnosti in družbene sprejemljivosti izbere tistega, ki je najbolj ustrezen. Znotraj koridorja se nato izriše tehnično najbolj ugodna trasa ceste. Prednost takega pristopa je predvsem v objektivnosti metodologije in v hkratnem obvladovanju več dejavnikov, ko izbiramo najugodnejši koridor. Klasična metoda umeščanja cestne trase v prostor namreč izhaja najprej iz tehnične umestitve, šele kasneje pa se različne variante, določene na tak način, med sabo vrednoti z različnih vidikov.

Key words: road planning, environmental vulnerability, investment costs, GIS, methodology

Ključne besede: načrtovanje cest, ranljivost okolja, investicijski stroški, GIS, metodologija

INTRODUCTION

The construction of an infrastructure network is an important task that enables development of individual parts of the country as well as of the state as a whole. In road network planning – the largest in scope and complexity in infrastructure – we generally find many different approaches. The most frequent, and also the most commonly used, is the so-called »technical« approach^[1]. With this approach, the alternative individual routes according to technical criteria are chosen first, and then are judged in view of the environmental and spatial impact later. Adequate protection measures are included in this approach. The second approach, originally introduced in Germany, and now utilized in Slovenia, is the so called “spatial” approach^[1]. The purpose of this approach is to determine the spatial and environmental vulnerability of a particular route chosen. First, the narrow, spatially acceptable corridor is chosen. Then within the corridor alternative routes are designed according to technical criteria.

A choice of factors to include in route selection modelling methodology, depend on the goals we wish to achieve. In most cases environmental vulnerability is the only factor. Environmental protection is becoming an increasingly important issue in today's world. Besides an increased public aware-

ness of the need for environmental protection, Slovenia has with joining the EU in 2004 adopted European legislation, which places an even greater emphasis on environmental protection. It is important that the construction of new road connections does not harm the natural state of the environment, or cultural heritage. With project planning it is therefore paramount that the construction of the road connection itself impacts on the environment as little as possible.

The second most important factor that influences road placement and construction are investment costs. Usually, the available funds are smaller than requested, so the goal is to find the solution which enables the greatest benefit for road users and society as a whole at the lowest cost possible.

This article represents a useful introduction to the application of GIS methodologies to solve a transportation problem. In this paper appropriate methodology which allows optimal route determination in space, with regard to both environmental protection, and investment costs is utilized. The optimization of all different constraints is very important in road design, because a suitable initial approach results in substantial savings (in terms of both money and the environment) when it comes to further realization of plans and projects.

METHODOLOGY

In a broader sense the geographic information system (GIS) is an information system specializing in the input, storage, manipulation, analysis and reporting of geographical (spatially related) information^[2]. Information in GIS is often stored and represented as layers, which are sets of geographical features linked with their attributes. Before a GIS can be used to solve the problems, data must be properly chosen and represented in a digital computing environment.

Route selection or road planning is an example of the impact of multiple geographical constraints in nature. The route selection process is in fact a multi-criteria decision making process where a final decision is made by considering different types of information.

The task is to define a route linking the previously identified start and end points. The goal is to insure that the road route chosen is the shortest, least expensive (i.e. presents minimum investment costs), and does the least harm to the environment (i.e. maximum environmental preservation). Some criteria are self reinforcing, such as road length and investment costs, while others are mutually exclusive, such as road length and environmental damage. An appropriate balance which tries to satisfy divergent interests must be found.

The methodology for the optimal corridor or route selection can be divided into 5 steps. The first three are used for new data layer synthesis, for each factor separately (environment, costs, etc.), while the last two are used for optimal corridor modelling of all the factors combined (Figure 1).

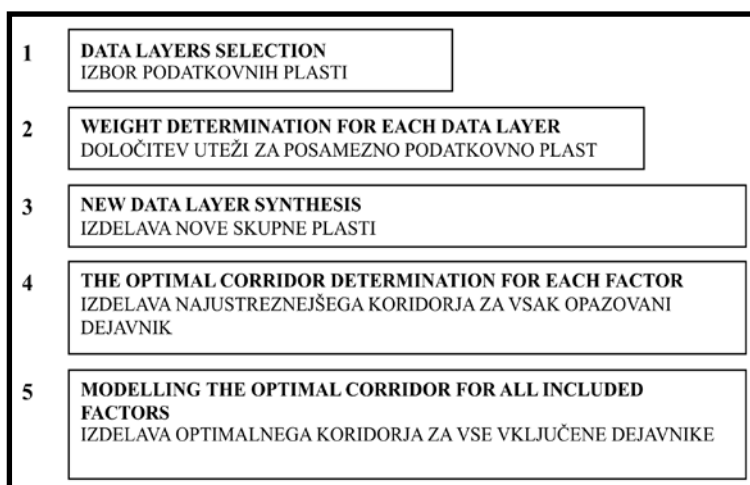


Figure 1. Schematic representation of methodology for route selection

Slika 1. Shematska predstavitev metodologije za umeščanje cestne trase v prostor

In the first stage data layer selection on an environmental protection basis is performed. The layers represent protected areas as defined by legislation or otherwise designated as protected. At this point, digital data layers of the space in question are collected and modified with the use of GIS tools. Areas where protection of the environment is called for are generally areas less (or not at all) appropriate for the placement of new road.

In the second stage, depending on the meaning of a particular area, the weights for each individual layer are assigned. The more that a certain area needs to be protected, the larger the weight assigned to that layer. The weight actually shows how much longer a route between two points will be drawn, as opposite to the most direct path of the route. If too large weight is assigned, the environment is more protected (because the route will take the path across less protected areas); however the investment costs will be significantly higher, and the new road too long.

In the third stage, vector data is converted to raster data. Every point is assigned a value, which represents the sum of the values of individual layers (layers, selected in the first stage and weights, assigned in the second). Areas with the highest values are least appropriate for new road determination from the standpoint of protection of the environment.

Cost analysis is performed in a similar way as the environmental protection analysis. In the first stage, layers which lead to increased costs of construction of the new road are determined. For example, a large

change in above sea level elevation (influence on the construction of tunnels and viaducts), potential avalanche areas or other geologically and hydrologically inappropriate areas on which the construction of roads is much more difficult. At this stage the expert geological opinion and judgement is very important. Individual layers are weighted in the second stage, with an eye as to how much they increase the total costs of construction of the new road connection. In the third stage, individual layers in raster form are combined and the values of individual overlapping areas summarized.

In the fourth stage, the most environmentally appropriate corridor is placed. The new road is placed in a location which cumulatively has the least negative impact on the environment. This is determined with the help of appropriate GIS tools. In the same way a corridor which from a construction standpoint is lowest in cost is drawn.

The two corridors determined in the fourth stage can have a similar path or can be considerably different. In the case of a considerable difference, a new corridor is determined, which represents the most optimal route between the two, in other words the most appropriate route of the new road, which would attain the lowest possible cost while not neglecting protection of the environment. In this process, every factor (environmental, cost analysis) can be assigned a weight, which is an expression of the degree of importance we assign to each perspective. Differing weights can fundamentally alter the placement of the new road route.

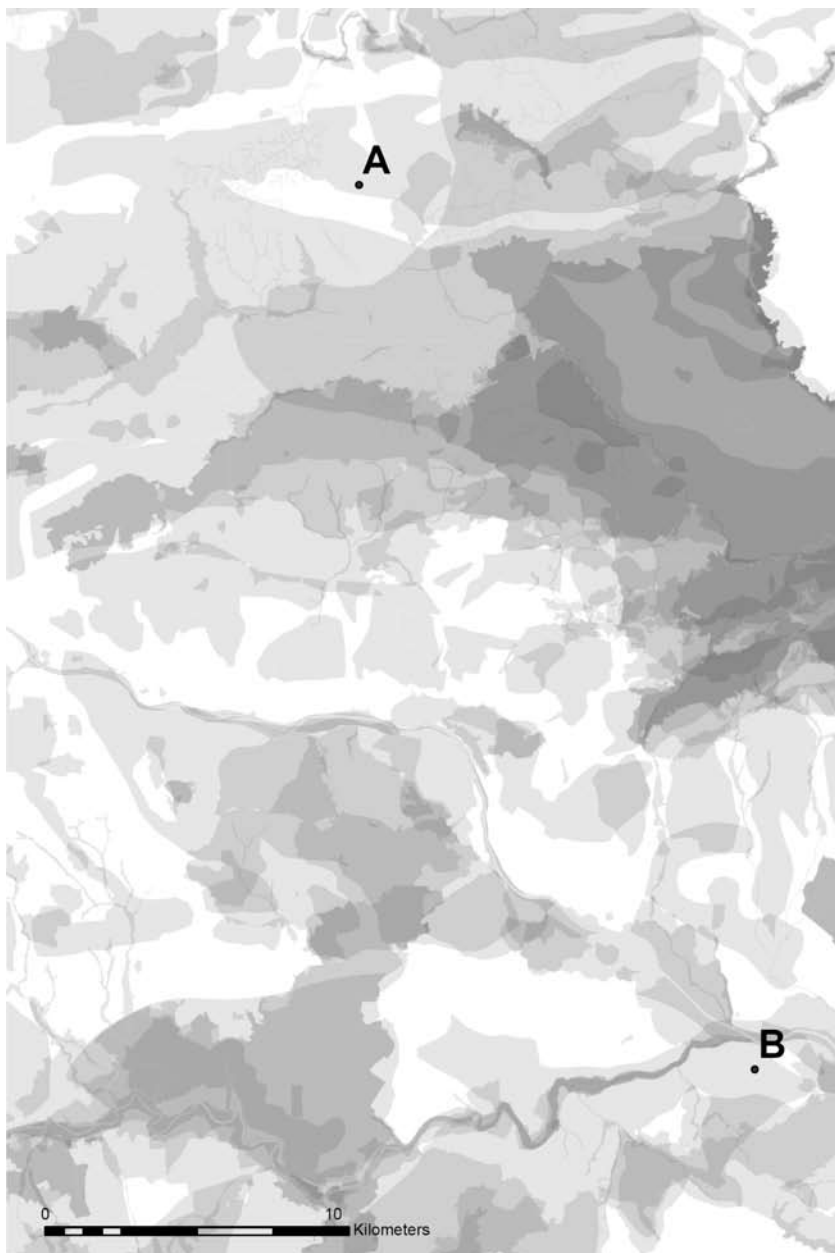


Figure 2. Composite map of environmental layers

Slika 2. Karta, sestavljena iz posameznih plasti varovanih delov okolja

RESULTS AND DISCUSSION

For the presentation of the introduced methodology, a portion of southeast Slovenia was chosen. Selected digital layers for the environmental protection analysis included:

- Natura 2000 areas,
- protected areas of nature,
- valuable natural features,
- ecologically important zones,
- water protection zones,
- cultural heritage.

For definition of a favourable corridor with regard to road construction cost analysis, the following layers were applied:

- relief (slope),
- sensible regions (flooded areas, erosion areas, landslide areas),
- waters and lakes,
- objects (buildings etc.).

In this paper, all selected data layers have equal weight. If the importance or influence of certain data is determined to be greater than that of other data, the assigned weight should be heavier. In Figure 2, the composite map of all environmental layers is presented. The darker zones correspond to several protected areas. These are the areas less suitable for new road construction. The most appropriate areas for new road placement are in white.

In the next stage, data is converted from vector format into raster format, and the most appropriate new road corridor from the environmental protection as well as cost perspective is drawn with the help of appropriate GIS tools. In Figure 3, the first

picture on the top left is environmentally the most appropriate corridor, while the last picture on the bottom right is the most appropriate route from a cost perspective. The goal of the new road planner is to find a solution which will protect the environment to the highest degree possible at the lowest possible cost.

Because two conditions that aren't directly comparable need to be satisfied in the final and most optimal corridor, there are many solutions which can be represented graphically (Figure 4 - gray and black points). The best solutions are the black points, which lay along the Pareto^[3] curve. The Pareto trade-off curve is the curve made up of Pareto points that represent possible solutions. For all the points on the curve it holds true that in giving more importance to one factor it is automatically assigned less importance to the other. All the points present an equal solution to the problem - no particular one is better than any other.

If we apply the Pareto model to the display of determination of the most appropriate corridor for road placement from an investment costs as well as environmental protection perspective (Figure 3), it can be determined that all the solutions displayed correspond to points on the Pareto curve. The next goal is to find the solution, which will be utilized in actual practice.

Comparison of the individual pictures in Figure 3 show that the model of proportions varies from costs 80 %: environment 20 % to costs 10 %: environment 90 % show territory which is in common to all the models. This territory can thus be tak-

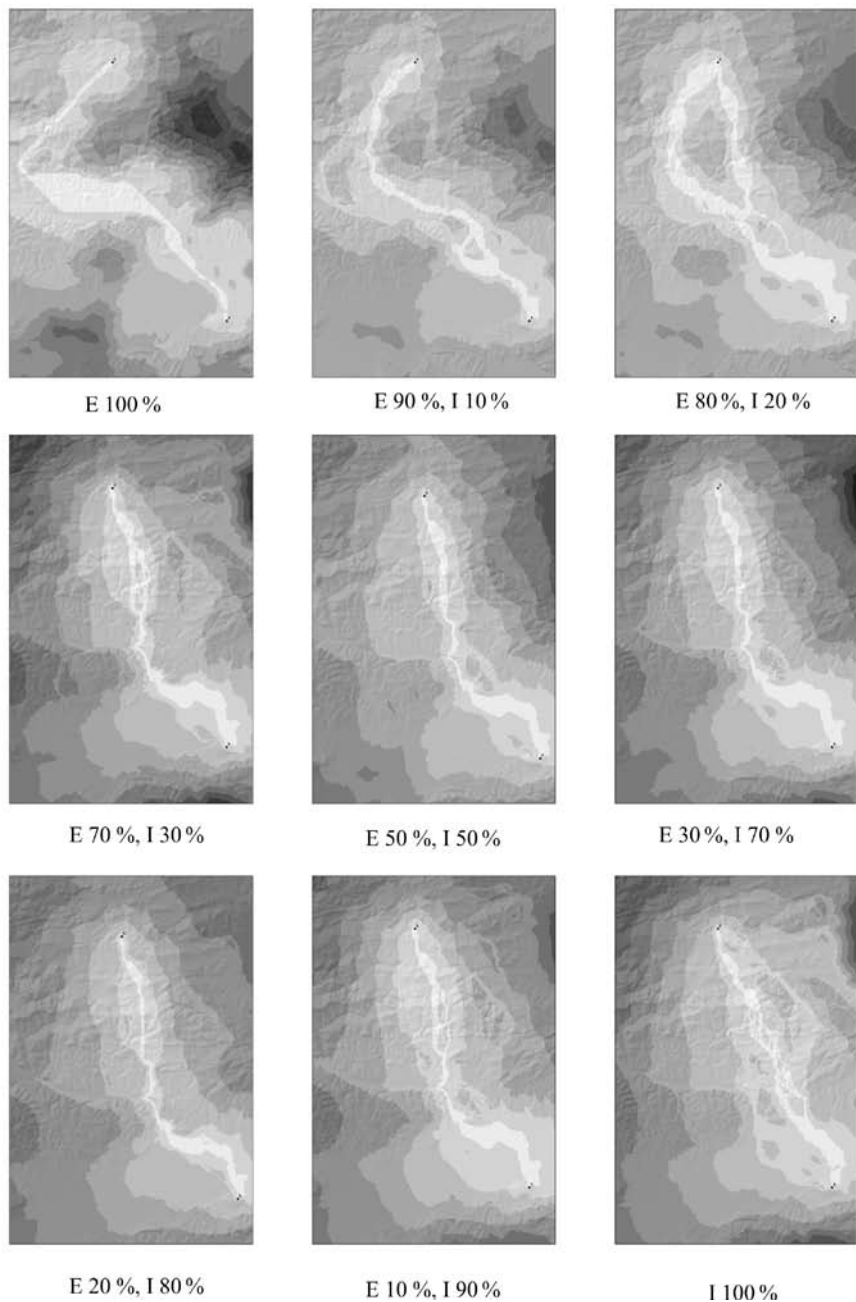


Figure 3. Optimal road corridors as a result of the corridor modelling (E – environment, I – investment)

Slika 3. Modelsko določeni optimalni koridorji poteka ceste (E – okolje, I – investicija)

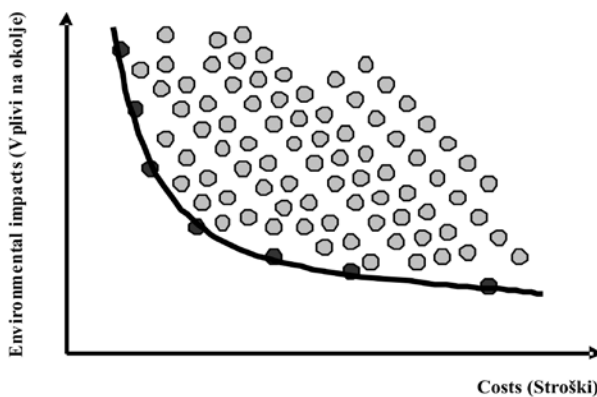


Figure 4. Pareto optimality curve
Slika 4. Paretova optimizacijska krivulja

en as the most convenient corridor for the construction of a new road. Inside of this corridor various alternatives can be determined, evaluated and compared with each other in classic approach.

The choice of the most optimal route for a new road as demonstrated above is not always simple. In a way it is a political decision, because it entails deciding how important protection of the environment is in financial terms. Social acceptance plays an important role within this process, as does the influence the new road would have on the development of a particular area. The methodology demonstrated allows for individual alternatives which enter the political foray to be expertly and objectively supported to the maximum extent possible.

In the demonstrated model two groups of limitations (environmental protection and investment costs) are included, even though more groups could be included. Possible limitations, which could also be included in the model, are:

- limitations of space (for example, neighbourhoods - limiting factor regarding the construction of road, though at the same time also a factor of attractiveness in space),
- physical barriers (unfavourable terrain, geological or hydrological conditions, water streams, lakes),
- economic potential (industrial zones, tourist zones, accessibility and the connectedness of town centres),
- political limitations and social acceptance.

CONCLUSIONS

In construction of transport infrastructure the question of how to intervene with minimal impact on the environment yet at the same time in a technically most feasible and cost effective way is a common problem. Every intervention into nature affects the environment. The planner's task is to pick the solution which will do the least harm to the environment while providing the greatest economical benefit.

In the article, a methodology to aid the choice of the most appropriate road corridor from the standpoint of the environment protections and investment costs is presented. The methodology enables road planners to determine the route or corridor, which according to the selected factors is most acceptable, and in the next phase work out multiple combinations of previously »pure« scenarios. On the basis of additional evaluations, political preferences, financial capabilities and social accept-

ability, the most appropriate corridor for placement of a new road is chosen. Inside of the corridor, the most technically feasible route of new road is then drawn.

In spite of computer support importance for methodology execution, preparing the input data needs an expert knowledge and cooperation of different specialists. Selection and data layers synthesis needs the knowledge of geology, hydrology, civil engineering, environment, legislation, land use, etc. Only professional prepared and grounded input data enable optimal results.

The advantage of such an approach is foremost in the objectivity of the methodology and the simultaneous command of multiple factors when choosing the most appropriate corridor. The classic method of placing the road route in space has its roots in technical placement; only later are alternatives evaluated between each other from multiple perspectives.

POVZETKI

Okolje in investicijski stroški kot dejavnika za umeščanje cestne trase v prostor

Pri gradnji prometne infrastrukture se vedno srečujemo z dilemo kako poseči v prostor, da bo okolje kar najmanj prizadeto, in hkrati najti tehnično najugodnejšo rešitev, ki bo tudi stroškovno ugodna. Vsak poseg v okolje prizadene tudi naravo. Načrtovalčeva naloga je, da izbere tako rešitev, ki ponuja ob najmanjši prizadetosti okolja,

največjo ekonomsko korist.

Izbor posameznih dejavnikov, ki jih vključimo v metodologijo za določitev sprejemljivega infrastrukturnega koridorja, je lahko zelo različen, odvisno od cilja, ki ga želimo doseči. Večinoma je tak dejavnik samo eden, to so različna varovana območja okolja. V tem primeru projektant izriše traso ceste tako, da poteka čim manjši meri čez varovana območja. V metodologijo pa lahko vključimo tudi druge dejavnike. V prispevku je prikazana metodologija določitve najugodnejšega cestnega koridorja z

vidika varovanja okolja in investicijskih stroškov gradnje ceste.

Predlagana metodologija za umeščanje cestne trase v prostor vsebuje več stopenj (slika 1):

1. Določi se področja, ki so povezana z varovanjem okolja. To so varovana območja, določena v zakonskih ali podzakonskih aktih, ali pa jim je na kakšen drug način pripisan varovalni pomen. Na tej stopnji se zbere plasti digitalnih prostorskih podatkov in se jih ustreznno obdela z orodji GIS (slika 2).
2. Glede na pomen posameznega področja se določi utež za posamezno plast. Bolj ko želimo neko območje ali dobrino varovati, večjo utež dobi. Če določimo preveliko utež, okolje sicer bolj varujeмо (ker bo izrisana pot prečkala malo varovanih območij), a bo nova cesta daljsa in investicijski stroški bistveno višji.
3. Vektorske podatke pretvorimo v rastrske. Vsaki točki pripisemo vrednost, ki predstavlja vsoto vrednosti posameznih plasti (plasti, izbranih v prvi stopnji in uteži, izbranih v drugi stopnji). Področja z najvišjo vrednostjo so najmanj primerena za izdelavo nove cestne povezave z vidika varovanja okolja.

Na podoben način kot okoljski vidik se izdela tudi stroškovnega. V prvi stopnji se določi plasti, ki vplivajo na povečanje stroškov pri izgradnji cestne povezave. To so na primer velika sprememba nadmorske višina (vpliva na gradnjo tunelov in viaduktov), plazovita območja oz. geolo-

ško in hidrogeološko neugodna območja, na katerih je gradnja ceste bistveno zahtevnejša. V tej stopnji je zelo pomembna tudi strokovna geološka ocena. Posamezne plasti se v drugem delu ustreznno uteži. V tretji stopnji se posamezne plasti v rastrski obliki združi in vrednosti na posameznih prekrivajočih področjih sešteje.

4. Na podlagi ovrednotenih površin iz trete točke se s pomočjo ustreznega GIS orodja izdela najustreznejši koridor z vidika varstva okolja in koridor, ki je z vidika stroškov izgradnje cestnega odseka najugodnejši.
5. Koridorja, dobljena v četrti stopnji, sta si po poteku lahko podobna ali pa se bistveno razlikujeta. V primeru bistvene razlike se izdela še koridor, ki predstavlja optimum med obema »čistima« koridorjem, torej kje je najprimernejši potek cestne trase, ko bi z najnižjimi stroški dosegli največje varovanje narave. Pri tem postopku lahko vsakemu od vidikov (okolje, stroški) določimo poljubno utež, ki je odraz tega, kateremu vidiku dajemo večji pomen. Različne uteži lahko bistveno spremenijo potek trase.

Na sliki 3 je na prvi sliki prikazan okoljsko najprimernejši koridor, na zadnji sliki pa investicijsko najugodnejši koridor. Cilj načrtovalca cestne povezave je najti tako rešitev, ki bo ob najnižjih stroških najbolj okoljsko ugodna. Ker v končnem koridorju združujemo dve lastnosti, ki nista neposredno primerljivi, obstaja veliko rešitev, kar lahko ponazorimo tudi grafično (slika 4 - sive in črne točke). Najboljše rešitve so črne točke, ki ležijo na t.i. Paretovi

krivulji^[3]. Za vse točke na tej krivulji je značilno, da če hočemo eno lastnost izboljšati, se pri tem druga poslabša. Pri tem vse te točke predstavljajo enakovredne rešitve problema - nobena ni boljša od druge.

Če prenesemo Paretov model na prikaz izdelave najbolj ugodnega koridorja izgradnje cestne povezave tako s stroškovnega kot tudi okoljskega vidika (slika 3), lahko ugotovimo, da vse prikazane rešitve ustrezajo točkom na Paretovi krivulji. Naslednji cilj je torej najti rešitev, ki jo bomo uporabili v praksi. Primerjava posameznih slik pokaže, da vsebujejo vsi modeli od razmerja okolje: stroški 80 %:20 % do razmerja 10 %:90 % v okviru najugodnejšega koridorja tudi ozemlje, ki je vsem tem modelom skupno. To ozemlje lahko zato pojmemojmo kot najbolj ugodni koridor za izgradnjo ceste. Znotraj tega koridorja pa kasneje projektant izriše več variant, ki jih vrednotimo in primerjamo med sabo na klasičen način.

Kljub pomembnosti računalniške podpore pri izpeljavi metodologije je potrebno pri pripravi vhodnih podatkov veliko strokovnega znanja in sodelovanje strokovnjakov z različnih področij. Izdelava in izbira podatkovnih plasti zahteva znanja s področja geologije, hidrogeologije, gradbeništva, okolja, poznavanja zakonodaje, rabe tal, urejanja prostora itd. Le strokovno pripravljeni in utemeljeni vhodni podatki omogočajo optimalne rezultate.

Zgoraj prikazana izbira najugodnejšega koridorja ni vedno enostavna. Dejansko je to »politična« odločitev, saj se moramo odločiti, koliko nam pomeni varovanje okolja v denarnem smislu. Pri tem igra pomembno vlogo tudi družbena sprejemljivost in pa vpliv, ki bi ga imela nova cesta na razvoj območja. Prikazana metoda pa omogoča, da so posamezne različice, ki pridejo v »politično« presojo, čim bolj strokovno in objektivno utemeljene.

REFERENCES

- [1] RADAHOVIČ, M., MARUŠIČ, J., JUVANC, A. (2006): Načrtovanje cestne povezave na podlagi ranljivosti okolja. *Ssimpozij 3. razvojna os – slovenski projekt 3. tisočletja*. Maribor, 21.3.2006, Fakulteta za gradbeništvo: Društvo za ceste Maribor, pp. 77-82.
- [2] RODRIGUE, J.-P., COMTOIS, C., SLACK, B. (2006): *The geography of transport systems*. Routledge, London and New York, 284 pp.

- [3] HEYDEMANN, K., BODIN, F.: Iterative Compilation for Two Antagonistic Criteria: Performance and Code Size Case Study [cited 17.1.1007]. Dostopno na svetovnem spletu: <www-valoria.univ-ubs.fr/jp-ifsic/2006/pdf/expos-es/FBMercredi.ppt>

Designing a national groundwater quantity monitoring network on groundwater bodies with alluvial aquifers in Slovenia

Načrtovanje državne mreže za spremljanje količin podzemne vode na vodnih telesih podzemne vode z aluvialnimi vodonosniki

PETRA SOUVENT¹, ZLATKO MIKULIČ¹, MIŠO ANDJELOV¹, VLADO SAVIĆ¹

¹ Environmental Agency of the Republic of Slovenia, Vojkova cesta 1b, SI-1000 Ljubljana, Slovenia; E-mail: petra.souvent@gov.si, zlatko.mikulic@gov.si, miso.anjelov@gov.si, vlado.savic@gov.si

Received: July 31, 2007

Accepted: October 4, 2007

Abstract: Five out of 21 groundwater bodies (GWBs), which have been delineated in Slovenia with regard to the EU Water Framework Directive (WFD), comprehend mostly alluvial high permeability aquifers. They cover approximately 10 % of the country area but contribute to about 50 % of all groundwater abstraction and to about 40 % of all drinking water to the Slovenian water supply system. The existing groundwater quantity monitoring network (GWQMN) mostly covers the areas within the GWBs which are of drinking water pumping interest. To meet all the requirements of WFD and to enable reliable assessments of the quantity status of GWBs, the existing old network has been redesigned with the help of GIS tools with the great emphasis on hydrogeological, geological and pedological characteristic of GWB. Described method of network design leads to 36 new monitoring sites on GWBs with alluvial aquifers. Redesigned national GWQMN provides better coverage of spatial differences within GWBs and shall provide data needed to better understand the groundwater regime in the GWBs.

Izvleček: Za potrebe ocenjevanja stanja podzemnih voda in njihovega upravljanja je bilo v Sloveniji določenih 21 vodnih teles podzemne vode v skladu z Vodno direktivo. Pet vodnih teles podzemne vode, s pretežno visoko prepuštnimi aluvialnimi vodonosniki, se razprostira na približno 10 % Slovenije, vendar se iz njih črpa okoli 50 % podzemne vode, oziroma 40 % vse pitne vode. Obstojeca državna mreža za spremljanje količin podzemne vode je do sedaj dobro pokrivala le področja, ki so pomembna z vidika vodooskrbe. Glede na nove prostorske enote ocenjevanja stanja voda je bilo potrebno državno mrežo za spremljanje količin podzemnih vod izpopolniti in zadovoljiti zahtevam metodologije ocenjevanja količinskega stanja.

Uporabili smo prostorsko analitično metodologijo v GIS tehnologiji, ki je upoštevala hidrogeološko, geološko in pedološko homogenost danega ozemlja ter pri analiziranju prostora upoštevali različne tipe in režime varovanja. Z opisano metodo smo določili 36 novih merilnih mest na vodnih telesih s pretežno aluvialnimi vodonosniki. Izpopolnjena državna mreža za spremeljanje količin podzemne vode nudi boljšo pokritost prostorsko in hidrološko različnih območij znotraj vodnega telesa in zagotavlja boljše razumevanje režima podzemne vode v danem vodnem telesu.

Key words: groundwater, groundwater monitoring, groundwater monitoring network design, groundwater quantity, alluvial aquifer

Ključne besede: podzemna voda, monitoring podzemne vode, načrtovanje mreže, količina podzemne vode, aluvialni vodonosnik

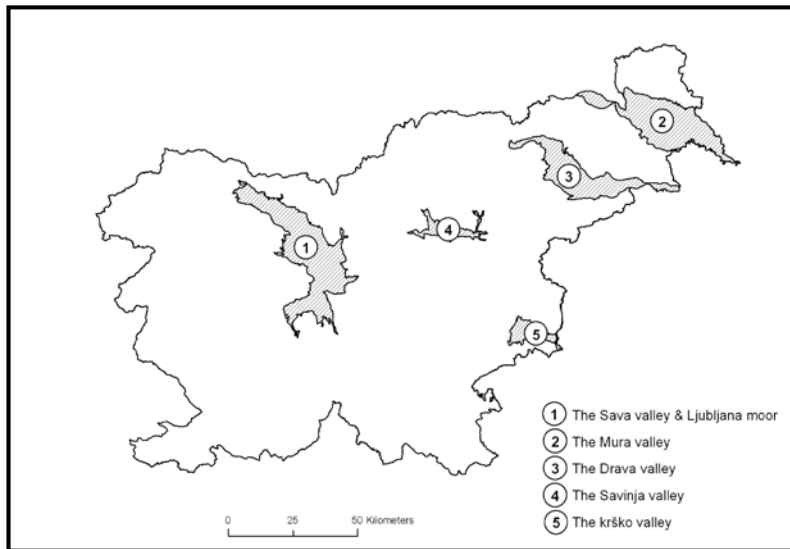
INTRODUCTION

Under the EU Water Framework Directive^[1], a total of 21 groundwater bodies^[2] have been delineated in Slovenia, with mostly karst and fissured porosity aquifers (68.9 %), followed by aquifers with intergranular porosity (26.2 %) and special case of aquifers in napped tectonic structures and aquitards (4.9 %). Five GWBs (Figure 1) with mostly alluvial, high permeability aquifers are of special interest in this study as they contribute about a half of Slovenian abstracted groundwater, but their area cover just approximately 10 % of the country. In the year 2005, about 467×10^6 m³ of groundwater was available and 116.4×10^6 m³ abstracted from these GWBs.

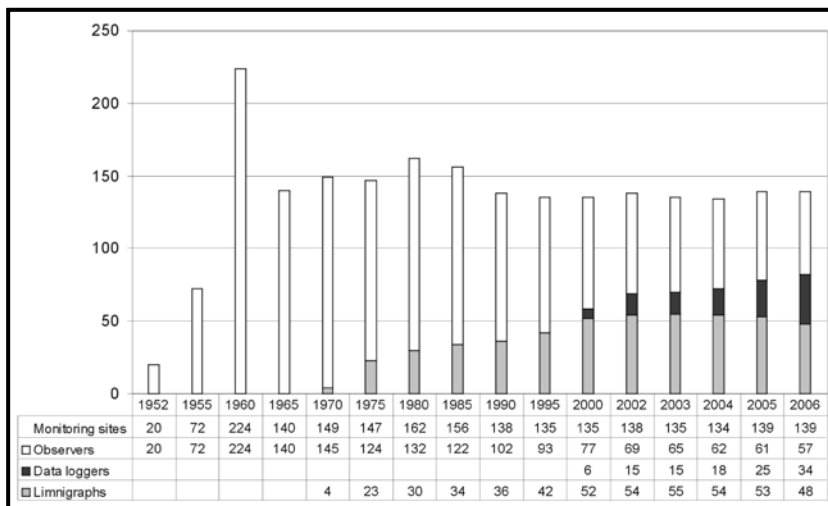
The first groundwater quantity monitoring network (GWQMN) in Slovenia was

established in the year 1952 when observers started GW level measurements in 20 private wells. This was the beginning of the national monitoring in the alluvial aquifers. The number of monitoring sites has changed with the time with regard to the Slovenian water policy. The maximum was reached in the year 1960 with 244 monitoring sites (Figure 2). In the year 2007 the national GWQMN has 128 monitoring sites in the alluvial aquifers within 5 GWBs.

So far, the existing groundwater quantity monitoring network mostly covered the areas within the GWBs which are of drinking water supply interest. To meet all the needs of WFD and to enable reliable assessments of the quantity status of GWBs, the existing network has been redesigned using GIS tools^[3].

**Figure 1.** GWBs with mostly alluvial high permeability aquifers

Slika 1. Vodna telesa podzemne vode (VTPoDv) s pretežno aluvialnimi vodonosniki

**Figure 2.** Development of the national groundwater quantity monitoring network in Slovenia

Slika 2. Razvoj državne mreže za spremljanje količin podzemne vode

DESIGNING THE GROUNDWATER QUANTITY MONITORING NETWORK

The leading idea was to divide the area of GWBs into logical units according to the hydrogeological, geological and pedological characteristics (Figure 3) and afterwards to add areas protected by law. These protected areas include Natura 2000 sites established under the EU Habitats Directive (92/43/EEC)^[4] and the EU Birds Directive (79/409/EEC)^[5] as well as Drinking Water Protected Areas established under Article 7^[6] of the WFD.

Hydrogeological spatial data layer comprises all known hydrogeologically distinct units within specific GWB and distinguish between different hydrological regimes, such as: areas with direct infiltration of rainfall into alluvial aquifer were separated

from the areas fed by the runoff from the hills, as well as recharge from rivers and inflow from other aquifer systems. Perched aquifers were defined and delineated too. They overlay the lower hydrogeological unit. On Figure 4, an example of hydrogeologically distinct units is presented for the GWB Mura valley.

For each GWB pertaining catchment area was determined. Catchment area was divided in sub-catchment areas that represent catchments for each logically separated spatial unit. On Figure 5, as best and clear example among alluvial GWBs, a catchment area and its sub-catchment areas are presented for the GWB Savinja valley. In the case of trans-boundary GWB, the areas of groundwater inflow from another country and groundwater outflow from Slovenia were separated too.

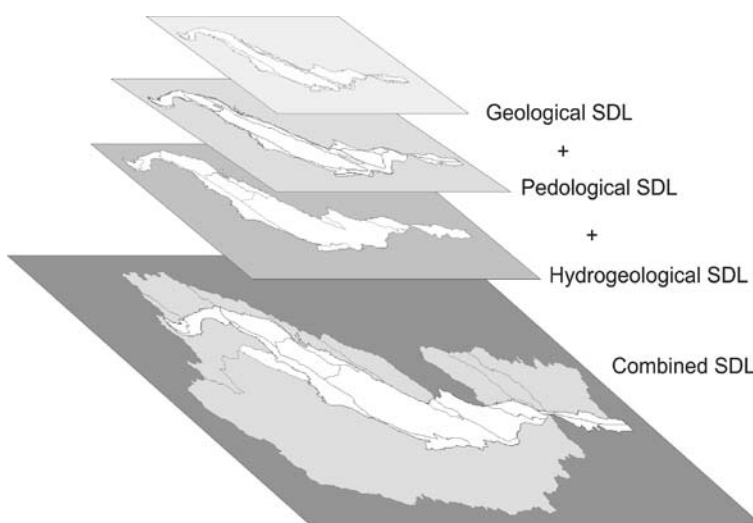


Figure 3. Concept of joining spatial data layers (SDL) into one logical subsystem of GWB

Slika 3. Koncept združitve prostorskih podatkovnih slojev (PPS) v homogeni podsistem vodnega telesa

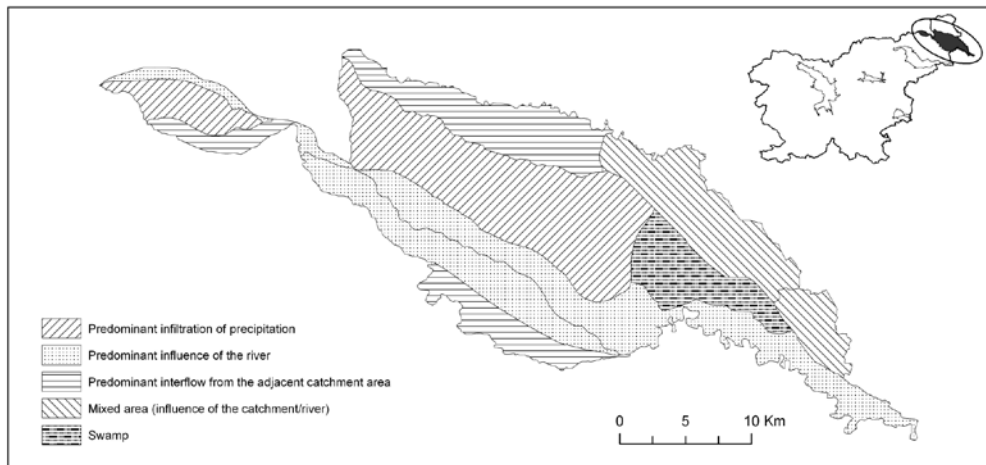


Figure 4. Hydrogeologically distinct units within GWB Mura valley
Slika 4. Hidrogeološko različna območja znotraj mej VTPodV Murska kotlina

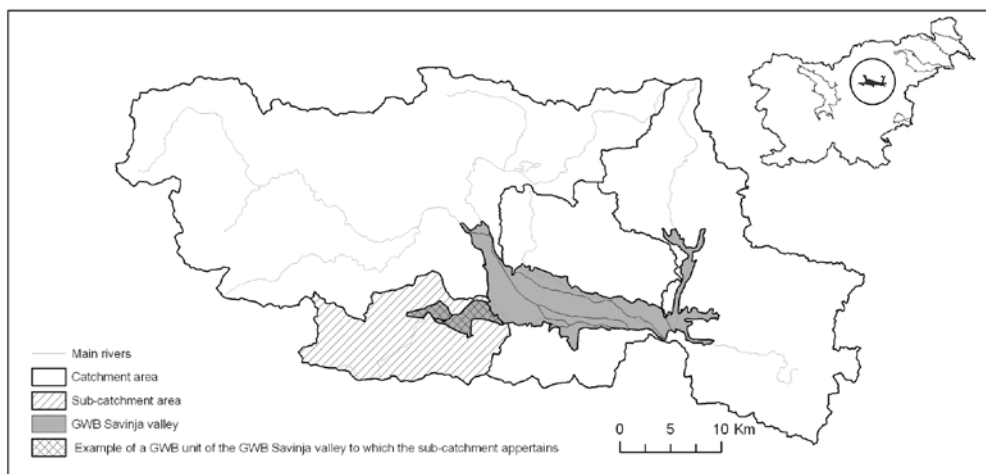


Figure 5. Catchment area and sub-catchments areas for the GWB Savinja valley
Slika 5. Zaledje in podenota zaledja prikazana za primer VTPodV Savinjska kotlina

The geological spatial data layer was constructed with the help of geological maps^[7] (1:100000) and lithological cross sections, if available. In this layer, each GWB was divided into geological units according to the surface geology (Figure 6). Lithological cross sections were used for better understanding of the sub-surface geology.

Pedological spatial data layer consists of areas defined due to soil characteristic (Figure 7). The source of information in this process were the general digital pedological map of Slovenia^[8] with soil types, map of mean soil depth^[8] and map of mean textural soil classes in Slovenia^[8].

All three spatial data layers were combined into one composite layer (Figure 3) with GWB units, representing areas with a similar hydrogeological regime, geology and pedology (Figure 8). Such an analysis of GWBs has enabled selection of new monitoring sites by the principle: each logically separated spatial GWB unit should have at least one groundwater monitoring site. Within these units, protected areas were also separated, represented by one monitoring site as a rule. In the areas with no hydrological data of groundwater monitoring, the area of the groundwater body was divided due to aquifer systems defined by Geological Survey of Slovenia^[9], and the density of network was adjusted accordingly.

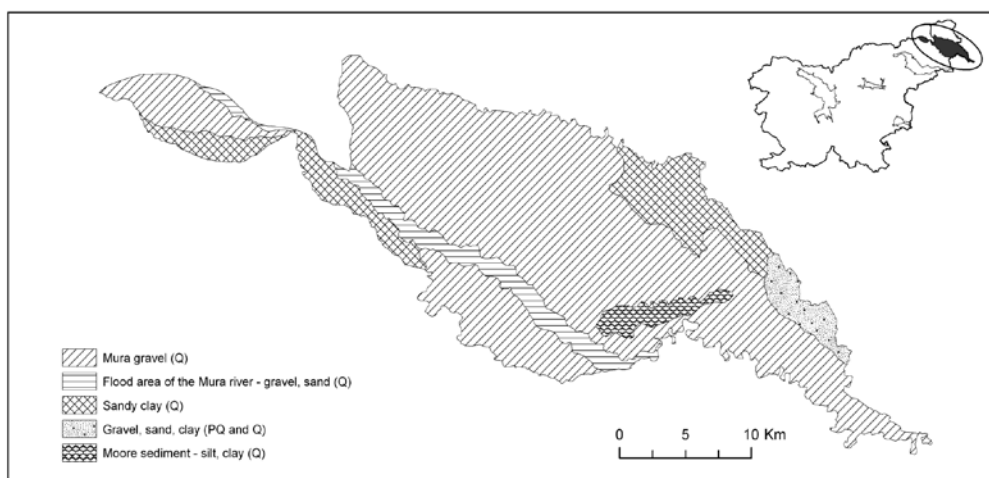


Figure 6. Geological units within GWB Mura valley

Slika 6. Geološke enote znotraj mej VTPodV Murska kotlina

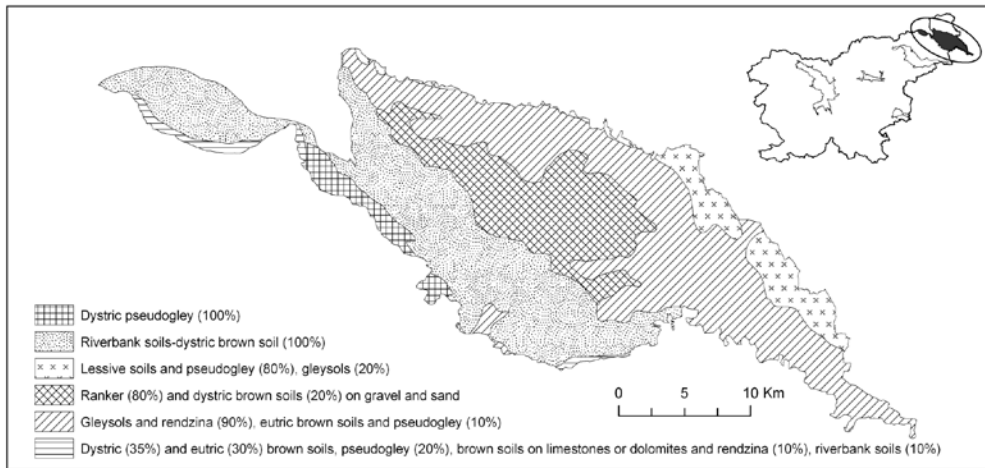


Figure 7. Soil Characteristics within GWB Mura valley
Slika 7. Tipi tal znotraj mej VTPodV Murska kotlina

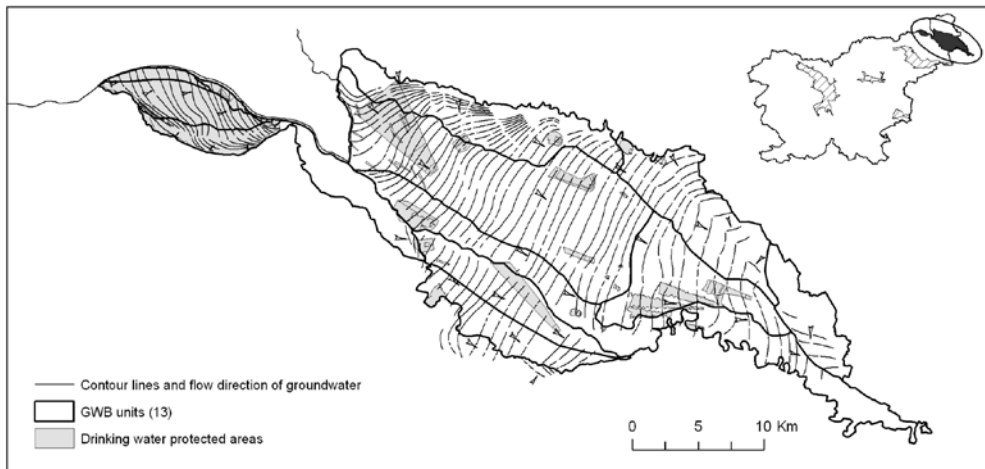


Figure 8. Spatial data layer with the GWB units (13) indicating the similar hydrological regime, geology and pedology (example for GWB Mura valley)
Slika 8. Prostorski podatkovni sloj z območji (13), kjer je podoben hidrološki režim, geologija in pedologija (primer za VTPodV Murska kotlina)

Table 1. Main alluvial GWBs (Figure 1) with existing and new monitoring sites

Tabela 1. VTPodV s pretežno aluvialnimi vodonosniki (slika 1) z obstoječimi in novimi merilnimi mesti

	The Sava valley & Ljubljana moor	The Mura valley	The Drava valley	The Savinja valley	The Krško valley
Area in km ²	774	591	429	109	97
Number of areas with the similar hydrological regime, geology and pedology (GWB units)	28	13	12	7	6
Number of existing monitoring sites (GW monitoring program 2007)	41	24	18	19	26
Number of new monitoring sites	28	1	3	2	2
Total number of monitoring sites	69	25	21	21	28

RESULTS AND DISCUSSION

Checking the existing GWQMN with the help of described method has shown that majority of the existing monitoring sites within relevant GWB fits well into this new concept of network design. Anyhow, redesign of existing national GWQMN still led to certain number of new monitoring sites (Table 1) which will be added to the GWQMN. On Figure 9, for example, the existing and planned monitoring sites

are presented for the GWB Sava valley and Ljubljana moor.

Following the design study phase in the office, field inspection has begun and is still in progress, with the purpose to confirm or to reject the chosen new locations. The GWQMN will be completed with the new monitoring sites gradually, till the year 2013, within the project: “Upgrading of hydro-meteorological system for monitoring and analysis of waters in Slovenia”^[10].

CONCLUSIONS

Described method of network design has enabled easier selection of monitoring sites and has facilitated the set up of better GWQMN. Redesigned national GWQMN shall provide better data needed to under-

stand groundwater regime in the GWBs, enable reliable assessments of the quantitative status of a GWB, shall facilitate the national groundwater quality monitoring network redesign and offer additional data for a modeling of groundwater flow in the alluvial aquifers.

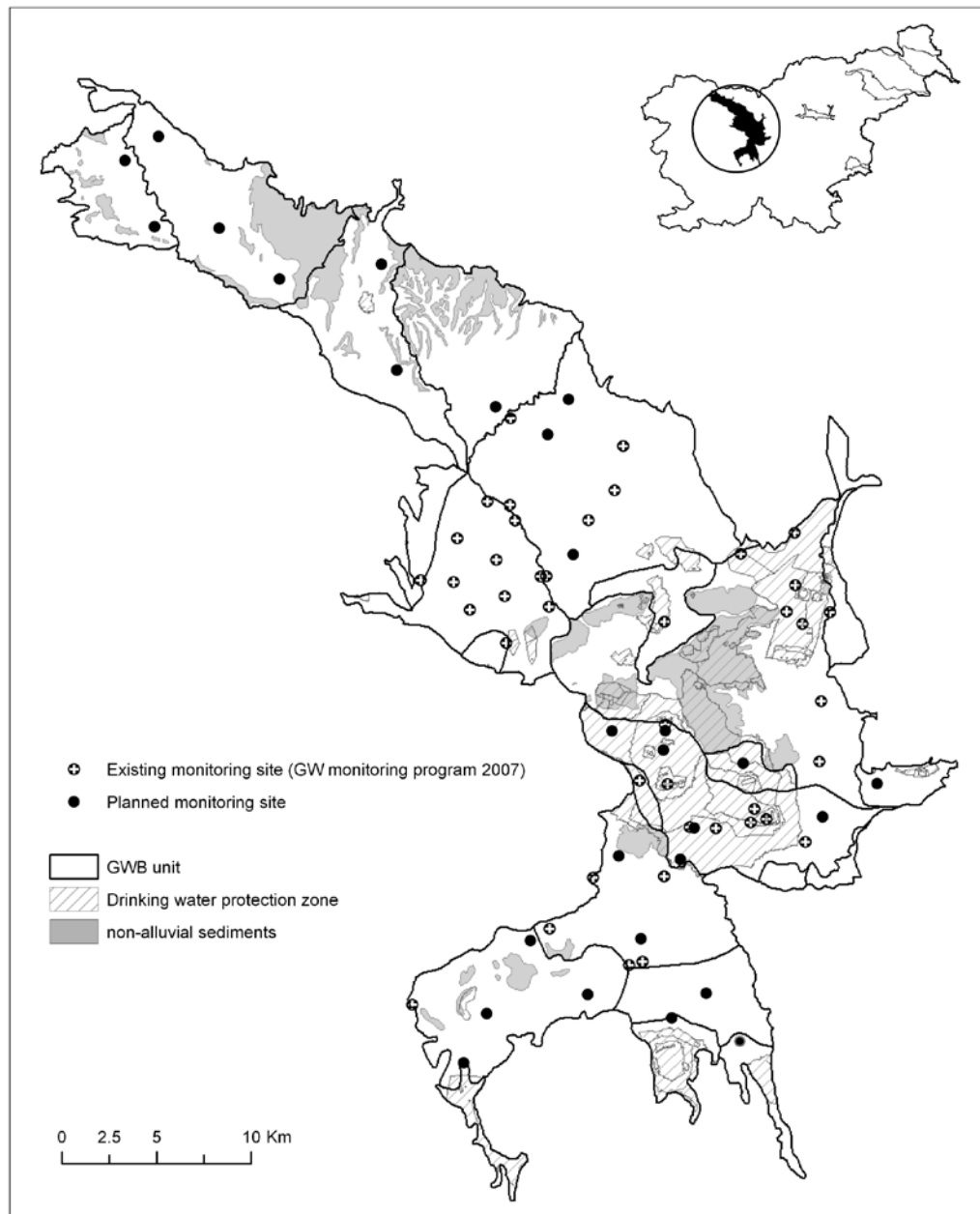


Figure 9. Existing (41) and planned (28) monitoring sites for the GWB Sava valley and Ljubljana moor

Slika 9. Obstojeca (41) in planirana (28) merilna mesta na VTPodV Savska kotlina in Ljubljansko barje

POVZETKI

Načrtovanje državne mreže za spremljanje količin podzemne vode na vodnih telesih podzemne vode z aluvialnimi vodonosniki

Državna mreža za spremljanje količin podzemne vode na vodnih telesih podzemne vode s pretežno aluvialnimi vodonosniki (slika 1), vključuje večinoma obstoječe objekte, kot so: piezometri, vrtani vodnjaki in kopani vaški vodnjaki, ki prvotno niso bili namenjeni za spremljanje globine do podzemne vode v sklopu državne mreže. Državna mreža je bila v preteklosti usmerjena predvsem na območja, ki so bila pomembna za vodooskrbo. S sprejetjem Evropske vodne direktive - VD (EU Water Framework Directive (WFD)) in z definiranjem 21 vodnih teles podzemne vode na območju Slovenije, se je koncept za spremljanje količin podzemne vode prilagodil VD. Da bi zadostili potrebam VD, mora Slovenija spremljati in oceniti količinski status vodnih teles v skladu z zahtevami VD in z mrežo optimalno pokriti celotno vodno telo podzemne vode. Tako smo z novim pristopom načrtovanja državne mreže za spremljanje količin podzemne vode na vodnih telesih s pretežno aluvialnimi vodonosniki preverili, kako dobra je pokritost vodnih teles z dosedanjemrežo in v primeru nezadostne pokritosti optimalno pokrili območja znotraj vodnih teles z novimi meritnimi mesti. Pri tem smo uporabili prostorsko analitično metodologijo v GIS tehnologiji, ki je upoštevala hidrogeološko, geološko in pedološko homogenost danega ozemlja ter pri analizi-

ranju prostora upoštevali različne tipe in režime varovanja.

Vodilna ideja metodologije je bila razdeliti območja vodnih teles na logične enote glede na hidrogeološke, geološke in pedološke karakteristike danega ozemlja. Tako smo za vsako vodno telo s pretežno aluvialnimi vodonosniki (za 5 teles – slika 1) kreirali tri prostorske podatkovne sloje, ki smo jih potem združili v skupen prostorski podatkovni sloj:

- Hidrogeološki prostorski podatkovni sloj,
- Geološki prostorski podatkovni sloj,
- Pedološki prostorski podatkovni sloj.

Hidrogeološki prostorski podatkovni sloj

Hidrogeološki prostorski podatkovni sloj vključuje vsa znana hidrogeološko različna območja znotraj danega vodnega telesa in tako razlikuje med različnimi hidrološkimi režimi. Izdvojena so bila tudi območja z visečo podtalnico. Območja s prevladujočo direktno infiltracijo padavin v aluvialni vodonosnik smo tako ločili od območij, ki se večinoma napajajo iz zaledja. Izdvojili smo območja, kjer reka napaja vodonosnik in območja, kjer je dotok podzemne vode iz drugih vodonosnih sistemov. Slika 4 prikazuje hidrogeološke enote znotraj VTPodV Murska kotlina. Za vsako vodno telo smo definirali odgovarjajoče zaledje, ki je razdeljeno na več pod-zaledij. Vsako pod-zaledje odgovarja enemu izdvojenemu območju znotraj vodnega telesa. Na sliki 5 je primer zaledja in pod-enote zaledja prikazan za VTPodV Savinjska kotlina. Ločili smo tudi cone dotoka podzemne vode iz sosednjih držav ter cone iztoka podzemne vode iz Slovenije.

Geološki prostorski podatkovni sloj

Geološki prostorski podatkovni sloj je nastal na podlagi osnovne Geološke karte, znanih litoloških presekov vodnih teles in litologije pridobljene iz vrtin iz baz GeoZS in Oddelka za hidrologijo podzemnih voda. V tem podatkovnem sloju je vodno telo razdeljeno na območja glede na geologijo na površju vodnega telesa. Litološke preseke smo uporabili za boljše razumevanje geologije pod površjem. Na sliki 6 so prikazane geološke enote znotraj mej VT-PodV Murska kotlina.

Pedološki prostorski podatkovni sloj

Pedološki prostorski podatkovni sloj je sestavljen iz območij, ki smo jih določili glede na karakteristike tal določenega vodnega telesa. Podatke o tipih tal smo pridobili iz osnovne pedološke karte Slovenije, karte o povprečni globini tal v Sloveniji ter karte o povprečnem teksturnem razredu tal v Sloveniji. Na sliki 7 so prikazani tipi tal znotraj mej VTPodV Murska kotlina.

Združitev vseh treh prostorskih podatkovnih slojev

Vsi trije podatkovni sloji so bili združeni v en prostorski sloj, ki predstavlja območja s podobnim hidrogeološkim režimom, geologijo in pedologijo. Združen prostorski podatkovni sloj je prikazan za primer VTPodV Murska kotlina na sliki 8.

Takšen pristop k izpopolnitvi mreže nam je omogočil preveritev obstoječe mreže in izbor novih merilnih mest oz. lokacij

po načelu: vsaka logično izdvojena enota na vodnem telesu mora biti pokrita z vsaj enim merilnim mestom. Na območjih, na katerih ne razpolagamo s hidrogeološkimi podatki, so bila območja znotraj vodnega telesa izdvojena na podlagi vodonosnih sistemov, ki jih je določil GeoZS, temu primerno je bila prilagojena gostota mreže.

Preveritev državne mreže za spremljanje količin podzemne vode na vodnih telesih z opisano metodo je pokazala, da se večina obstoječih merilnih mest znotraj danega vodnega telesa dobro vklaplja v opisani koncept izpopolnitve mreže. Opisana metoda je pripeljala do 36 novih lokacij na petih vodnih telesih s pretežno aluvialnimi vodonosniki. Po končanem kabinetnem delu smo začeli s terenskimi ogledi novih lokacij z namenom, da potrdimo ali ovržemo le-te.

Opisana metoda omogoča lažjo izbiro novih lokacij oz. merilnih mest in olajšuje postavitev optimalne državne mreže za spremljanje količin podzemne vode na vodnih telesih s pretežno aluvialnimi vodonosniki. Takšna mreža nam bo zagotovljala bolj kakovostne podatke za poznavanje hidroloških režimov na danih vodnih telesih in bo omogočala zanesljivo oceno količinskega stanja vodnih teles. Olajšala bo izpopolnitev državne mreže za spremljanje kvalitete podzemne vode in zagotovila dodatne podatke, ki jih potrebujemo za modeliranje toka podzemne vode v aluvialnih vodonosnikih.

REFERENCES

- [1] Directive 2000/60/EC of the European Parliament and of the Council (WFD). *Official Journal of the European Communities*. 2000, 72 p.
- [2] URL RS 63/05 (2005): *Pravilnik o določitvi vodnih teles podzemnih voda* (Rules on determining water bodies of groundwater).
- [3] SOUVENT, P., GALE, U., MIKULIČ, Z., ANDJELOV, M., TRIŠIČ, N., SAVIČ, V. (2007): *Strokovna izhodišča za izpopolnitve merilne mreže za spremljanje količin podzemne vode*. Interno gradivo Sektorja za hidrologijo, (Hydrogeological Guidelines for Upgrading Groundwater Quantity Monitoring Network), 104 str.
- [4] Council Directive 92/43/EEC of 21 May 1992 on the conservation of natural habitats and of wild fauna and flora.
- [5] Council Directive 79/409/EEC of 2 April 1979 on the conservation of wild birds.
- [6] Article 7 of the WFD (2000): Waters used for the abstraction of drinking water. *Official Journal of the European Communities*, p. 12.
- [7] Geological map of Slovenia (23 separate sheets) in GIS environment (2003). Geological survey of Slovenia.
- [8] Soil data of Slovenia (2007), Centre for Soil and Environmental Sciences of Biotechnical Faculty. Dostopno na svetovnem spletu http://www.bf.uni-lj.si/cpvo/Novo/main_PodatkiTalSlovenije.htm.
- [9] Geološki zavod Slovenije (2004): Nacionalna baza hidrogeoloških podatkov za opredelitev teles podzemne vode Republike Slovenije. *Sklepno poročilo 3. faze*. (Geological Survey of Slovenia (2004): National base of hydrogeological data for groundwater body determination in Slovenia).
- [10] Agencija RS za okolje (2006): *Projekt: Nadgradnja sistema za spremljanje in analiziranje stanja vodnega okolja v Sloveniji (SSSV)*. (Environmental Agency of the Republic of Slovenia (2006): Project: Upgrading of hydro-meteorological system for monitoring and analysis of waters in Slovenia).

A contribution to construction monitoring with simultaneous application of various types of observations

Prispevek k spremljanju objektov s simultanimi meritvami različnih tipov

MILIVOJ VULIĆ¹, GREGOR URANJEK²

¹ University of Ljubljana, Faculty of Natural sciences and Engineering, Department of Geotechnology and Mining Engineering, Aškerčeva cesta 12, SI-1000 Ljubljana, Slovenia;
E-mail: milivoj.vulic@ntf.uni-lj.si

² Premogovnik Velenje d.d., Partizanska cesta 78, 3320 Velenje, Slovenia;
E-mail: gregor.uranjek@rlv.si

Received: September 2, 2007

Accepted: September 25, 2007

Abstract: The presented observations, adjustment and analysis of the spatial heterogeneous local network initial epoch will serve together with following epochs for object's characteristic points mutually spatial position monitoring. Spatial heterogeneous local network is observed with simultaneous observations of various types. Observations between characteristic points could not be applied. From the initial epoch results is concluded that on the base of precision estimations of slope distances between object's characteristic points is expected that will be possible to monitor slope distance changes larger than 10 mm in any direction in space (at $\tau = 2$, the probability is 95.45 %). If the most favorable condition are considered, it will be possible to monitor slope distance changes larger than 3 mm (at $\tau = 2$, the probability is 95.45 %).

Izvleček: Predstavljena je izmera, izravnava in analiza začetne terminske izmere prostorske heterogene merske mreže, ki bo skupaj z naslednjimi terminskimi izmerami služila za analizo spremljanja medsebojnih prostorskih položajev karakterističnih točk objektov. Heterogena prostorska mreža je merjena s simultanimi meritvami različnih tipov. Meritve poševnih razdalj med karakterističnimi točkami niso bile mogoče. Iz rezultatov začetne terminske izmere je zaključeno, da se bodo lahko na osnovi ocen natančnosti poševnih razdalj med karakterističnimi točkami spremeljale spremembe poševnih razdalj večje kot 10 mm v poljubni smeri v prostoru pri $\tau = 2$ (verjetnost je 95,45 %). Ob upoštevanju najugodnejših primerov pa se pričakuje, da se bodo lahko zaznale spremembe poševnih razdalj večje od 3 mm pri $\tau = 2$ (verjetnost je 95,45 %).

Key words: spatial heterogeneous networks, 3D adjustment, estimation of the precision, monitoring of mutual spatial relations, characteristic points, confidence pedaloid (surface)

Ključne besede: prostorska heterogena mreža, 3D izravnava, ocena natančnosti, spremljanje medsebojnih prostorskih položajev, spremljanje medsebojnih prostorskih relacij, karakteristične točke, pedaloid (ploskev) pogreškov

INTRODUCTION

The discussed example deals with simultaneous observations and simultaneous adjustment of spatial heterogeneous local network. The purpose of the local network will be monitoring of mutual spatial positions of characteristic points, with a possibility of constraining local network into the existing network. Observations between object's characteristic points could not be applied.

Slope distances between characteristic points are afterwards determined from

adjusted characteristic points spatial coordinates. Estimation of slope distances precision is based on variance-covariance matrix of unknowns $\Sigma_{\hat{x}\hat{x}}$ of the observed network which is the result of the adjustment.

For the construction (pillars) monitoring purpose four characteristic points (one per pillar) and two auxiliary points in pillars proximity have been reconnaissanced and materialized. Characteristic points are observed from auxiliary points which are observed from existing network points.

OBSERVATION METHOD OF HETEROGENEOUS LOCAL NETWORK

Heterogeneous observation system is combined from different types of observation systems. Heterogeneous observation system contains observed points, observations, network adjustment and results interpretation. Regardless the observations types and observation systems, respectively, which are containing heterogeneous observation system all observations, are simultaneously adjusted.

Simultaneous observations of heterogeneous local network contain three observa-

tion systems:

- baselines of static DGPS observations (Differential Global Positioning System),
- height differences of differential leveling,
- microtriangulation and microtrilateration:
 - horizontal directions,
 - zenith distances,
 - slope distances.

From existing network points ($X1/A1$ and $X5$) the auxiliary points ($Pom1$ and $Pom2$) are observed with baselines of DGPS observation and height differences of differ-

ential leveling and from auxiliary points characteristic points ($STk1$, $STk2$, $STk3$ and $STk4$) are observed with combined resections (Figure 1) (horizontal directions, zenith distances and slope distances) using the sets of angles method.

The results of local network observation are most probable values and *a priori* precision estimations of individual observations.

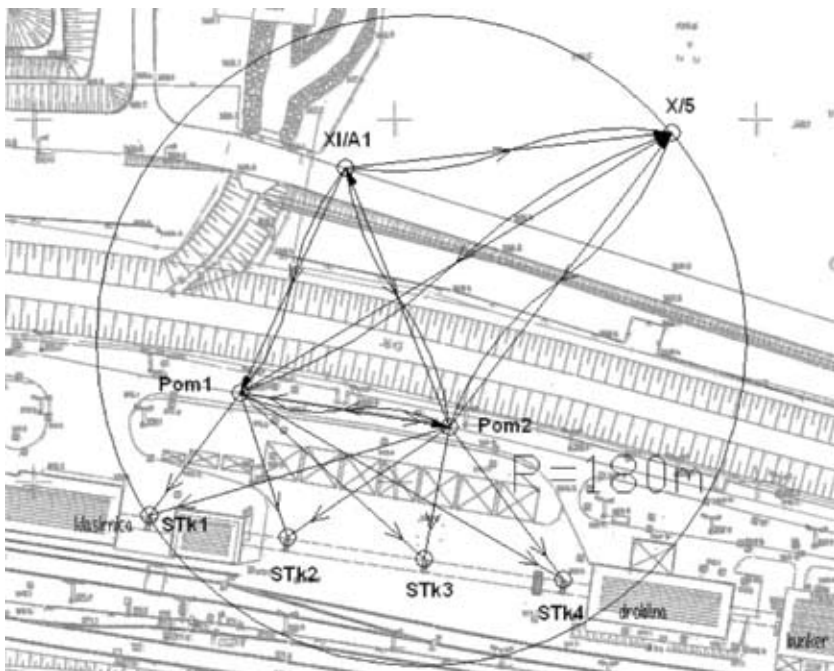


Figure 1. Heterogeneous local network
Slika 1. Lokalna heterogena mreža

ADJUSTMENT OF LOCAL NETWORK

The entering adjustment data are known points' coordinates of the existing network and the approximate coordinates of characteristic and auxiliary points and most probable values and *a priori* precision estimations of individual observations.

Adjustment strategy of local network

The simultaneous adjustment procedure of terrestrial and GPS observations is realized in three steps:

- observation testing with adjustment of inner constrained or minimally constrained networks upon individual observation types or observation systems,

- quality known points control of the existing network which is illustrated with combined adjustment comparison (GPS network and leveling network) in minimally constrained network and

fully constrained network in which the known points are datum,
- combined adjustment of terrestrial and GPS observations.

ADJUSTMENT OF HETEROGENEOUS LOCAL NETWORK WITH PROGRAMME PACKAGE Leica GEO OFFICE 5.0

Local network, which is observed with terrestrial and GPS observations, is adjusted as spatial (3D) network with orthometric heights in programme package *Leica Geo Office 5.0* (module *Adjustment*). *Leica Geo Office 5.0* in module *Adjustment* is using processing kernel *MOVE3 3.4* of well known programme for network adjustment *MOVE3*. Module *Adjustment* is one of the programme package *Leica Geo Office 5.0* modules and it is suitable for the design, adjustment and quality control of 3D, 2D and 1D measuring networks.

3D model for combined adjustment of terrestrial and GPS observations (Local geodetic) in the programme package *Leica Geo Office 5.0*, is in ellipsoidal coordinates (φ, λ, h) in local coordinate system. This kind of 3D model, which is implemented in programme package *Leica Geo Office 5.0*, has following advantages (BOEKELO, 1996):

- The mathematical model is “truly” 3D;

designed to model 3D reality (in stead of the 2D map), it complies with the modern surveying needs.

- The model does not require reductions to sea level or to the horizontal plane, nor corrections for earth curvature or for the projection.
- As mapping/projection is an auxiliary process there is no model-constraint limiting the network size.
- The model is best suited for the combination of GPS and terrestrial measurements.
- Original observations are tested (in stead of derivatives) using an uncompromised statistical model.

In programme package *Leica Geo Office 5.0* the precision estimation of 3D position is visualized in two parts so that the standard deviation of plane position (X, Y) is presented with confidence ellipse, and standard deviation of height (H) is presented separately with a bar in the same scale as confidence ellipse (Figures from 2 to 5). Precision estimation of observations is presented only with relative confidence ellipse (2D).

OBSERVATION TESTING

In order to test observations regarding to blunders (gross errors), the observation

systems are adjusted separately in inner constrained networks or minimally constrained networks. With this procedure the known points influence is unabled.

All observations have been tested with standardized residuals with observations *a priori* variances (VULIĆ, 2005/2006):

$$v_{ni} = \frac{v_i}{\sigma_{ll_i}} \quad (1)$$

v_{ni} - standardized residual with *a priori* observation variances

v_i - observation residual

σ_{ll_i} - *a priori* observation variance

Separately observations have been tested with statistical tests F-test (global test) and W-test (datasnooping test), which are programme package *Leica Geo Office 5.0* tools. The results of all observation tests show that observations are blunders free.

QUALITY CONTROL OF KNOWN POINTS

Known points acquired data unfortunately did not include *a posteriori* precision estimation of known points. The known points influence on *a posteriori* precision estimation of auxiliary points is illustrated with combined network (DGPS baselines and height differential leveling differences) adjustments comparison in minimally constrained network and fully constrained net-

work in which the known points are datum. The *a posteriori* precision estimation of auxiliary points at minimally constrained network adjustment is influenced only by observations incompatibility (Figure 2) and the *a posteriori* precision estimation of auxiliary points at fully constrained network adjustment is influenced with observations incompatibility and mutual position of known points quality (Figure 3).

COMBINED ADJUSTMENT OF TERRESTRIAL AND GPS OBSERVATIONS

Objects will be monitored with slope distances changes between characteristic points. For that matter the slope distances precision is important. For precise slope distances determining the quality of auxiliary points mutual position is important. From known points quality control is concluded, that the known points are determined with centimeter's precision at best. Observation testing show that the characteristic points can be determine with millimeter's precision by combined resections from auxiliary points.

From known points quality control and observation testing is obvious that carrying errors from known points to local network are not reasonable. Because of the stated findings the simultaneous adjustment of terrestrial and GPS observations is executed in two steps. In first step the datums in adjustment are existing network points (Figure 4). With first step the auxiliary points mutual position is determined. In second step the datums in adjustment are auxiliary points adjusted coordinates determined in first step. With second step the adjusted (Figure 5) characteristic points coordinates and variance-covariance matrix of unknowns is determined.

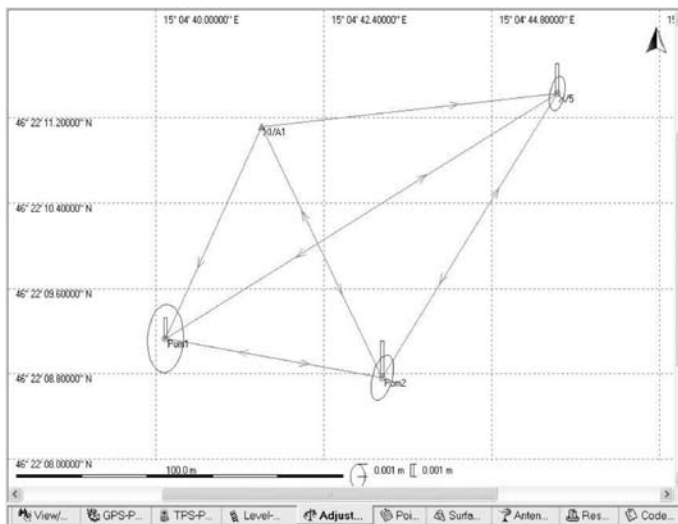


Figure 2. Adjustment of DGPS baselines and differential leveling height differences in minimally constrained network

Slika 2. Izravnava minimalno vpete mreže baznih vektorjev in višinskih razlik geometričnega nivelmana

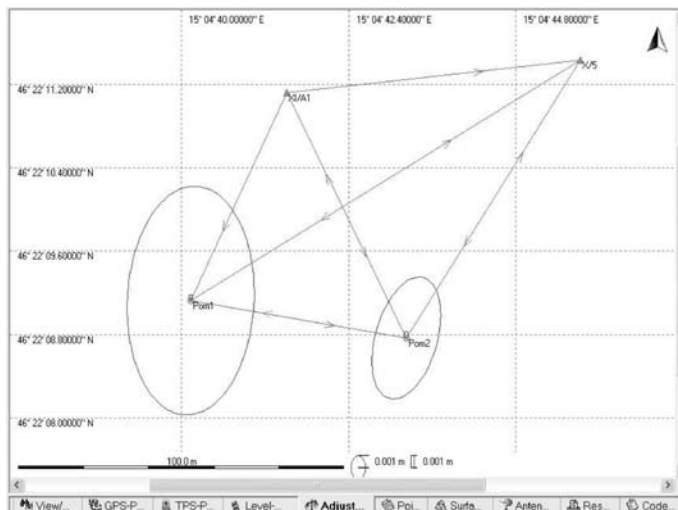


Figure 3. Adjustment of DGPS baselines and differential leveling height differences in fully constrained network

Slika 3. Izravnava vpete mreže baznih vektorjev in višinskih razlik geometričnega nivelmana

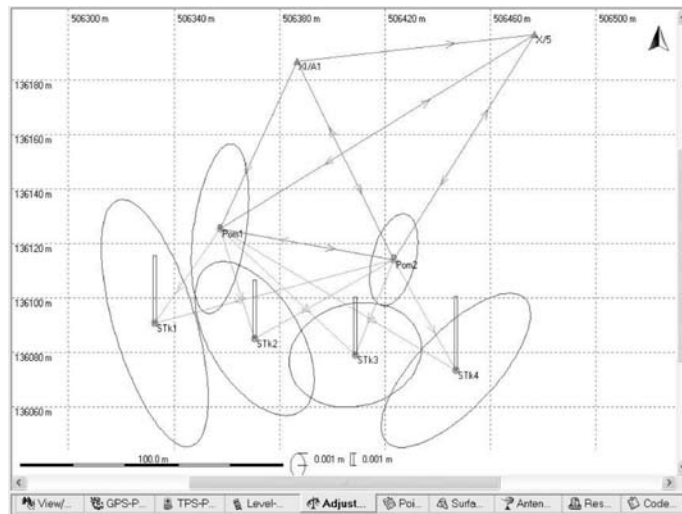


Figure 4. First step of terrestrial and GPS observations simultaneous adjustment

Slika 4. Prvi korak skupne izravnave terestričnih in GPS opazovanj

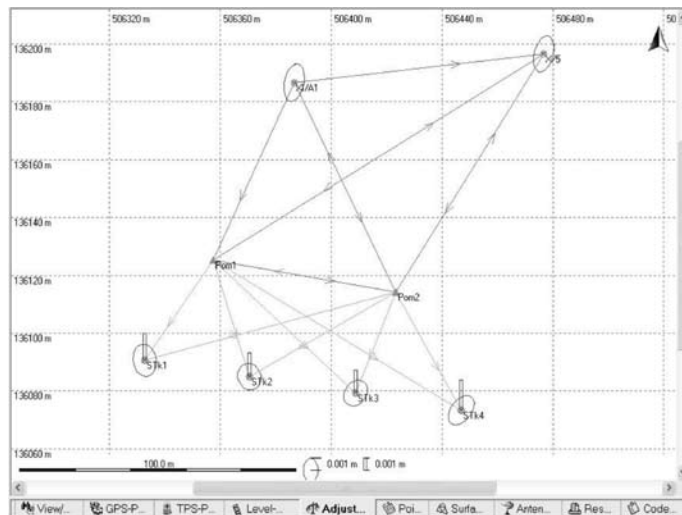


Figure 5. Second step of terrestrial and GPS observations simultaneous adjustment

Slika 5. Drugi korak skupne izravnave terestričnih in GPS opazovanj

DETERMINATION AND PRECISION ESTIMATION OF SLOPE DISTANCES BETWEEN CHARACTERISTIC POINTS

Adjusted characteristic points spatial coordinates are determined with 3D adjustment model in ellipsoidal coordinates (φ, λ, h), which are then projected on a plane (Gauss-Krüger projection). Heights are defined with orthometric heights. Characteristic points plane coordinates (Y, X) and orthometric heights (H) are adopted in further calculations as spatial coordinates (Y, X, H) because of the small local network dimensions (Figure 1).

From adjusted characteristic points coordinates are determined slope distances $d_{slope\ ij}$ between characteristic points with expres-

$$d_{slope\ ij} = \sqrt{(Y_j - Y_i)^2 + (X_j - X_i)^2 + (H_j - H_i)^2} \quad (2)$$

Index i is for slope distance starting point and index j is for slope distance finishing point.

A posteriori precision estimation of slope distances between characteristic points is acquired from variance-covariance matrix of unknowns Σ_{xx} (Figure 6) which is adjustment product (simultaneous adjustment of all observations). Variance-covariance matrix Σ_{xx} is containing information about *a posteriori* precision estimation of all points' spatial coordinates (variances) which are taking part in adjustment and interdependence between all points' spatial coordinates (covariances).

Upon our suggestion¹ the programme package *Leica Geo Office* producer has add variance-covariance matrix $\Sigma_{\Delta ij}$ between module *Adjustment* results in version 5.0.

At network adjustment the variance-covariance matrix Σ_{xx} elements are saved in separated ASCII file (AdjVar2).

From variance-covariance matrix Σ_{xx} (Figure 6) submatrixes (3×3) the covariance matrixes $\Sigma_{\hat{x}\hat{x}}$ for each slope distance are composed, for which the precision estimation is wanted. The belonging slope distance covariance matrix $\Sigma_{\Delta ij}$ is then determine with taking into consideration the variance-covariance propagation law for random variables linear functions (VULIĆ, 206).

$$\Sigma_{\Delta ij} = \mathbf{J}_{ij} \cdot \Sigma_{ij} \cdot \mathbf{J}_{ij}^T$$

$$\Sigma_{\Delta ij} = \begin{bmatrix} -\mathbf{I}_{3 \times 3} & \mathbf{I}_{3 \times 3} \end{bmatrix} \cdot \begin{bmatrix} \Sigma_{\hat{x}_i \hat{x}_i} & \Sigma_{\hat{x}_i \hat{x}_j} \\ \Sigma_{\hat{x}_j \hat{x}_i}^T & \Sigma_{\hat{x}_j \hat{x}_j} \end{bmatrix} \cdot \begin{bmatrix} -\mathbf{I}_{3 \times 3} \\ \mathbf{I}_{3 \times 3} \end{bmatrix} \quad (3)$$

$$\Sigma_{\Delta ij} = \begin{bmatrix} \Sigma_{\Delta ij_{xx}} & \Sigma_{\Delta ij_{xy}} & \Sigma_{\Delta ij_{xz}} \\ \Sigma_{\Delta ij_{yx}} & \Sigma_{\Delta ij_{yy}} & \Sigma_{\Delta ij_{yz}} \\ \Sigma_{\Delta ij_{zx}} & \Sigma_{\Delta ij_{zy}} & \Sigma_{\Delta ij_{zz}} \end{bmatrix}$$

\mathbf{J}_{ij} - the Jacobian matrix for slope distance's components functions
 $d_{slope\ ij}$

$\Sigma_{\hat{x}_i \hat{x}_i}, \Sigma_{\hat{x}_j \hat{x}_j}, \Sigma_{\hat{x}_i \hat{x}_j}, \Sigma_{\hat{x}_j \hat{x}_i}$ - submatrixes (3×3) of covariance matrix Σ_{xx} of parameters
 $\Sigma_{\Delta ij}$ - covariance matrix $\Sigma_{\Delta ij}$ of slope distance between characteristic points i and j

After all slope distances covariance matrixes determination $\Sigma_{\Delta ij}$ it is proceeded to confidence surface's defining elements

¹ We purchased programme package *Leica Geo Office 4.0* in which the complete cofactors matrix \mathbf{Q}_{xx} ($\Sigma_{xx} = \hat{\sigma}_0^2 \cdot \mathbf{Q}_{xx}$) extraction is not supported. If we have to determine cofactors matrix \mathbf{Q}_{xx} by our selves (as we did before purchase) the programme package is unnecessary because we must execute complete adjustment to determine cofactors matrix \mathbf{Q}_{xx} which is one of the adjustment results. After contact with producer's technical support, they added the complete variance-covariance matrix Σ_{xx} between module Adjustment results in version 5.0 and they upgraded our programme package to *Leica Geo Office 5.0*.

Σ_{xx}	1	2	3	4	5	6	7	8	9	10	11	12	13	14	15	16	17	18	19	20	21	22	23	24
Pon1	X	Y	H	X	Y	H	X	Y	H	X	Y	H	X	Y	H	X	Y	H	X	Y	H	X	Y	H
1	Pon1	X	0	0	0	0	0	0	0	0	0	0	0	0	0	0	0	0	0	0	0	0	0	0
2	Pon1	Y	0	0	0	0	0	0	0	0	0	0	0	0	0	0	0	0	0	0	0	0	0	0
3	Pon1	H	0	0	0	0	0	0	0	0	0	0	0	0	0	0	0	0	0	0	0	0	0	0
4	Pon2	X	0	0	0	0	0	0	0	0	0	0	0	0	0	0	0	0	0	0	0	0	0	0
5	Pon2	Y	0	0	0	0	0	0	0	0	0	0	0	0	0	0	0	0	0	0	0	0	0	0
6	Pon2	H	0	0	0	0	0	0	0	0	0	0	0	0	0	0	0	0	0	0	0	0	0	0
7	STR1	X	0	0	0	0	0	0	0	0	0	0	0	0	0	0	0	0	0	0	0	0	0	0
8	STR1	Y	0	0	0	0	0	0	0	0	0	0	0	0	0	0	0	0	0	0	0	0	0	0
9	STR1	H	0	0	0	0	0	0	0	0	0	0	0	0	0	0	0	0	0	0	0	0	0	0
10	STR2	X	0	0	0	0	0	0	0	0	0	0	0	0	0	0	0	0	0	0	0	0	0	0
11	STR2	Y	0	0	0	0	0	0	0	0	0	0	0	0	0	0	0	0	0	0	0	0	0	0
12	STR2	H	0	0	0	0	0	0	0	0	0	0	0	0	0	0	0	0	0	0	0	0	0	0
13	STR3	X	0	0	0	0	0	0	0	0	0	0	0	0	0	0	0	0	0	0	0	0	0	0
14	STR3	Y	0	0	0	0	0	0	0	0	0	0	0	0	0	0	0	0	0	0	0	0	0	0
15	STR3	H	0	0	0	0	0	0	0	0	0	0	0	0	0	0	0	0	0	0	0	0	0	0
16	STR4	X	0	0	0	0	0	0	0	0	0	0	0	0	0	0	0	0	0	0	0	0	0	0
17	STR4	Y	0	0	0	0	0	0	0	0	0	0	0	0	0	0	0	0	0	0	0	0	0	0
18	STR4	H	0	0	0	0	0	0	0	0	0	0	0	0	0	0	0	0	0	0	0	0	0	0
19	X5	X	0	0	0	0	0	0	0	0	0	0	0	0	0	0	0	0	0	0	0	0	0	0
20	X5	Y	0	0	0	0	0	0	0	0	0	0	0	0	0	0	0	0	0	0	0	0	0	0
21	X5	H	0	0	0	0	0	0	0	0	0	0	0	0	0	0	0	0	0	0	0	0	0	0
22	XIA1	X	0	0	0	0	0	0	0	0	0	0	0	0	0	0	0	0	0	0	0	0	0	0
23	XIA1	Y	0	0	0	0	0	0	0	0	0	0	0	0	0	0	0	0	0	0	0	0	0	0
24	XIA1	H	0	0	0	0	0	0	0	0	0	0	0	0	0	0	0	0	0	0	0	0	0	0

Figure 6. Variance-covarince matrix Σ_{xx} of parameters of local network
Slika 6. Variančno-kovarijančna matrika Σ_{xx} neznanih veličin lokalne mreže

calculation (confidence pedaloid defining elements). Main (characteristic) standard deviations of slope distances are determined with slope distance's covariance matrix Σ eigenvalues λ_i :

$$\begin{aligned}\hat{\sigma}_{\xi\xi} &= \sqrt{\lambda_{\xi\xi}} \\ \hat{\sigma}_{\eta\eta} &= \sqrt{\lambda_{\eta\eta}} \\ \hat{\sigma}_{\zeta\zeta} &= \sqrt{\lambda_{\zeta\zeta}}\end{aligned}\quad (4)$$

Main standard deviations components of slope distances are determined with slope distance's covariance matrix $\Sigma_{\Delta ij}$ eigen-

$$\begin{aligned}\hat{\sigma}_{\xi\xi} \cdot \mathbf{s}_{\xi\xi}^T &= \begin{vmatrix} s_{\xi x} & s_{\xi y} & s_{\xi z} \end{vmatrix} \\ \hat{\sigma}_{\eta\eta} \cdot \mathbf{s}_{\eta\eta}^T &= \begin{vmatrix} s_{\eta x} & s_{\eta y} & s_{\eta z} \end{vmatrix} \\ \hat{\sigma}_{\zeta\zeta} \cdot \mathbf{s}_{\zeta\zeta}^T &= \begin{vmatrix} s_{\zeta x} & s_{\zeta y} & s_{\zeta z} \end{vmatrix}\end{aligned}\quad (5)$$

In three-dimensional (3D) perpendicular coordinate system the confidence pedaloid is determined with main standard deviations (the half-axis confidence pedaloid values) and with main standard deviations components (the half-axis confidence pedaloid directions). The precision estimation results are in Table 1.

The slope distance's main standard deviations visualization is constructed in CAD programme *Rhinoceros* (Figures from 10 to 13) with slope distances confidence ellipsoids because in programme package *Leica Geo Office 5.0* 3D estimated 3D quantities main standard deviations visualization is limited with confidence ellipses (Y, X) and separately with heights standard deviations (H), (Figures from 2 to 5).

Confidence ellipse is confidence pedal approximation (confidence curve), analogous is confidence ellipsoid confidence pedaloid approximation (confidence surface). Confidence pedal is cross-section of confidence pedaloid and optional plane which is intersecting the confidence pedaloid's center. In programme package *Leica Geo Office 5.0* the intersecting plane is always parallel with horizontal plane YX . Confidence pedaloid (VEHOVEC, 2005) is surface which is presenting (Figures from 7 to 9) estimated quantity errors values in optional direction in space. That is important in detailed analysis at construction monitoring.

Table 1. Defining elements of slope distances confidence pedaloids (ellipsoids) between characteristic points at $\tau = 2$ (the probability is 95.45 %)

Tabela 1. Elementi pedaloidov (elipsoidov) pogreškov poševnih razdalj med karakterističnimi točkami pri $\tau = 2$ (verjetnost je 95,45 %)

From	To	a	a_x, a_y, a_H	b	b_x, b_y, b_H	c	c_x, c_y, c_H
		[m]	[m]	[m]	[m]	[m]	[m]
STk1	STk2	0,006	0,0016	0,003	0,0028	0,002	-0,0007
			0,0006		-0,0010		-0,0023
			0,0058		-0,0007		0,0005
STk1	STk3	0,006	0,0017	0,003	-0,0030	0,003	0,0002
			0,0007		-0,0001		-0,0026
			0,0058		0,0009		0,0003
STk1	STk4	0,007	0,0011	0,004	-0,0036	0,004	0,0007
			0,0006		-0,0010		-0,0026
			0,0066		0,0007		0,0001
STk2	STk3	0,006	0,0014	0,003	-0,0025	0,003	0,0009
			0,0002		-0,0009		-0,0024
			0,0054		0,0007		-0,0001
STk2	STk4	0,006	0,0008	0,003	-0,0031	0,003	0,0009
			0,0001		-0,0012		-0,0025
			0,0063		0,0005		-0,0001
STk3	STk4	0,006	0,0007	0,003	-0,0028	0,002	0,0012
			0,0001		-0,0017		-0,0020
			0,0062		0,0003		-0,0001

a - main standard deviation value (major)

b - main standard deviation value (semi)

c - main standard deviation value (minor)

a_x, b_x, c_x - main standard deviations components in direction X

a_y, b_y, c_y - main standard deviations components in direction Y

a_H, b_H, c_H - main standard deviations components in direction H

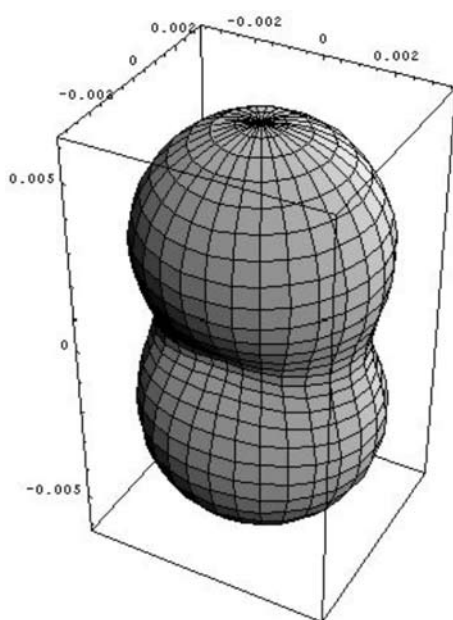


Figure 7. Confidence pedaloid (at $\tau = 2$, the probability is 95.45 %) of slope distance STk1-STk2

Slika 7. Pedaloid pogreškov (pri $\tau = 2$, verjetnost je 95,45 %) poševne razdalje STk1-STk2

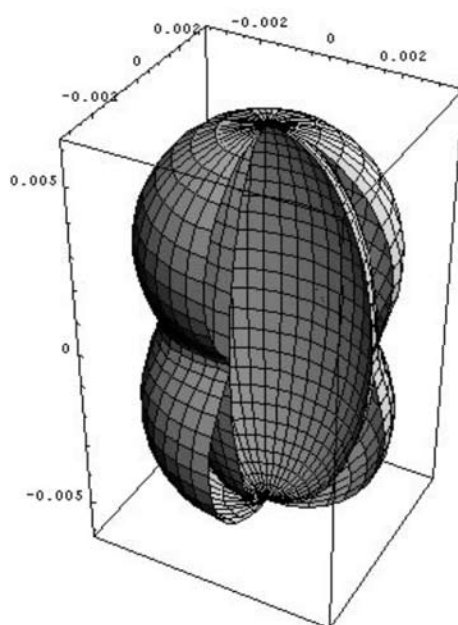


Figure 8. Confidence pedaloid and confidence ellipsoid cross-section (at $\tau = 2$, the probability is 95.45 %) of slope distance STk1-STk2

Slika 8. Presek pedaloida in elipsoida pogreškov (pri $\tau = 2$, verjetnost je 95,45 %) poševne razdalje STk1-STk2

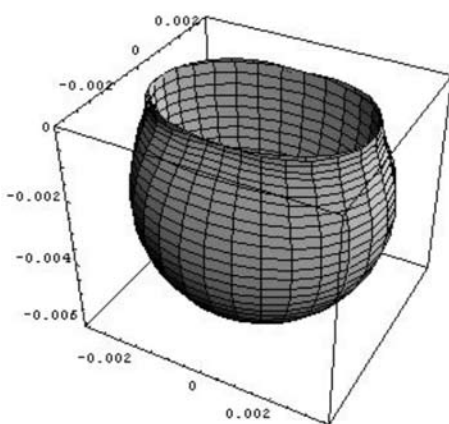


Figure 9. Slope distance STk1-STk2 confidence pedaloid and confidence ellipsoid cross-section with horizontal plane (at $\tau = 2$, the probability is 95.45 %)

Slika 9. Presek pedaloida in elipsoida pogreškov (pri $\tau = 2$, verjetnost je 95,45 %) poševne razdalje STk1-STk2 s horizontalno ravnino

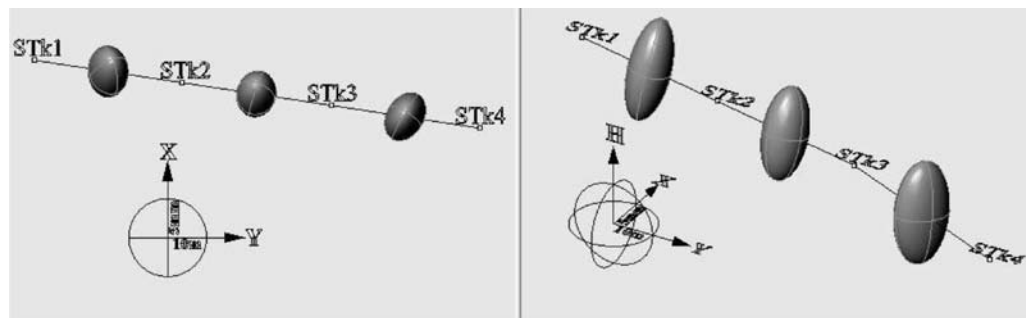


Figure 10. Confidence ellipsoids of slope distances STk1-STk2, STk2-STk3 and STk3-STk4 (at $\tau = 2$, the probability is 95.45 %) in orthogonal projection on YX plane (left) and in aksonometric projection (right)

Slika 10. Elipsoidi pogreškov poševnih razdalj STk1-STk2, STk2-STk3 in STk3-STk4 (pri $\tau = 2$, verjetnost je 95,45 %) v pravokotni projekciji na ravno YX (levo) in poševni projekciji (desno)

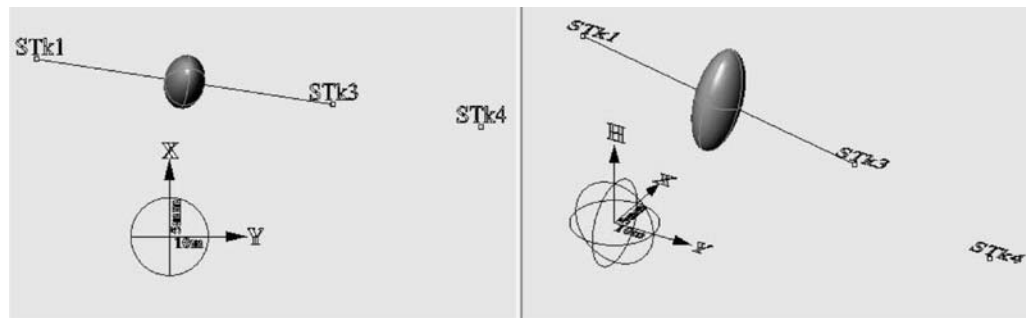


Figure 11. Confidence ellipsoid of slope distance STk1-STk3 (at $\tau = 2$, the probability is 95.45 %) in orthogonal projection on YX plane (left) and in aksonometric projection (right)

Slika 11. Elipsoid pogrešov poševne razdalje STk1-STk3 (pri $\tau = 2$, verjetnost je 95,45 %) v pravokotni projekciji na ravnino YX (levo) in poševni projekciji (desno)

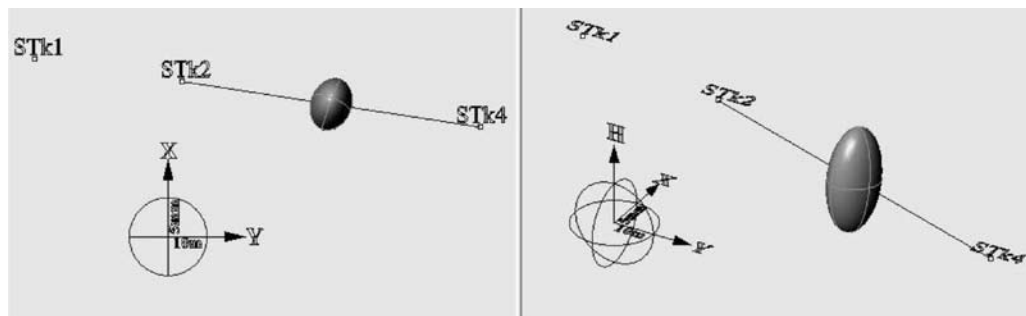


Figure 12. Confidence ellipsoid of slope distance ST_{k2}-ST_{k4} (at $\tau = 2$, the probability is 95.45 %) in orthogonal projection on YX plane (left) and in aksonometric projection (right)

Slika 12. Elipsoid pogreškov poševne razdalje ST_{k2}-ST_{k4} (pri $\tau = 2$, verjetnost je 95,45 %) v pravokotni projekciji na ravnino YX (levo) in poševni projekciji (desno)

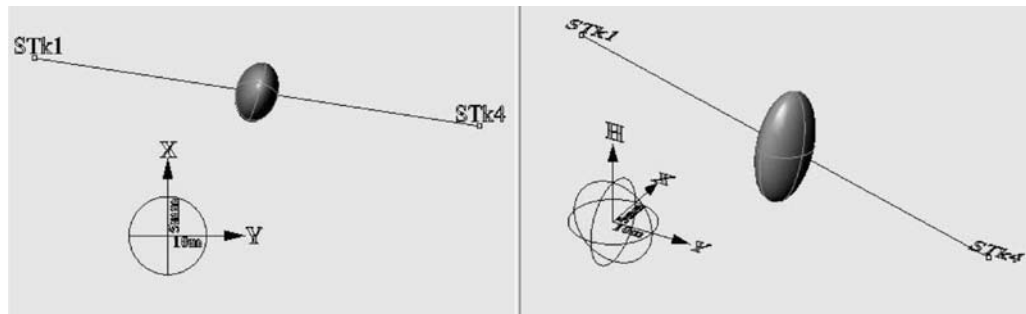


Figure 13. Confidence ellipsoid of slope distance ST_{k1}-ST_{k4} (at $\tau = 2$, the probability is 95.45 %) in orthogonal projection on YX plane (left) and in aksonometric projection (right)

Slika 13. Elipsoid pogreškov poševne razdalje ST_{k1}-ST_{k4} (pri $\tau = 2$, verjetnost je 95,45 %) v pravokotni projekciji na ravnino YX (levo) in poševni projekciji (desno)

CONCLUSIONS

Defined and estimated slope distances as described in this article, between object characteristic points at the initial epoch will be together with the following epochs, used for analyze at construction monitoring.

On base of slope distance precision estimations in two epochs and with consideration of variance propagation law for mutual independent random variables, there can be an estimation of precision made for slope distance changes between two epochs. The standard deviation values of slope distance changes between two epochs (Equation 6) are at the same time the values of minimal changes that can be monitored.

$$\hat{\sigma}_{\Delta j_{\max}}^2 = \hat{\sigma}_{i_{\max}}^2 + \hat{\sigma}_{j_{\max}}^2 \quad (6)$$

$\hat{\sigma}_{\Delta j_{\max}}$ - the maximal standard deviation of slope distance change between two epochs

$\hat{\sigma}_{i_{\max}}$ - the maximal main standard deviation of slope distances in epoch i

$\hat{\sigma}_{j_{\max}}$ - the maximal main standard deviation of slope distances in epoch j

From the initial epoch results (Table 1) and if the initial epoch results are adopted for following epoch there can be determined (Equation 7) expected minimal slope distance change that can be monitored between two epochs:

$$\hat{\sigma}_{\Delta j_{\max}} = 2 \cdot \hat{\sigma}_{\max} \quad (7)$$

$$\hat{\sigma}_{\Delta j_{\max}} = \sqrt{2} \cdot \hat{\sigma}_{\max} = \sqrt{2} \cdot 0,007 \text{ m} = 0,0099 \text{ m} = 10 \text{ mm}$$

From maximal value of slope distances main standard deviation of initial epoch (7 mm at $\tau = 2$, the probability is 95.45 %, Table 1) can be concluded that without any local network survey method improvement it will be possible to monitor slope distance changes between object's characteristic points between two epochs larger than 10 mm in any direction. If there are most favorable conditions considered (minimal main slope distance standard deviation is 2 mm at $\tau = 2$, the probability is 95.45 %, Table 1) it will be possible to monitor slope distance changes down to 3 mm.

POVZETKI

Prispevek k spremjanju objektov s simultanimi meritvami različnih tipov

Določene in ocnjene poševne razdalje, na način predstavljen v članku, med karakterističnimi točkami stebrov iz začetne terminske izmere bodo skupaj z naslednjimi terminskimi izmerami služile za analizo pri spremjanju stebrov.

Na osnovi spremembe posamezne poševne razdalje med terminskimi izmerama, katerih je ocenjena natančnost in z upoštevanjem zakona o prirastku pogreškov za medsebojno neodvisne veličine, se lahko oceni natančnost takšne spremembe. Vrednost standardne deviacije spremembe poševne razdalje $\hat{\sigma}_{\Delta j_{\max}}$ hkrati tudi pomeni vrednost minimalne spremembe, ki se jo lahko zazna:

$$\hat{\sigma}_{\Delta j_{\max}}^2 = \hat{\sigma}_{i_{\max}}^2 + \hat{\sigma}_{j_{\max}}^2$$

$\hat{\sigma}_{\Delta j_{\max}}$ - maksimalna standardna deviacija spremembe poševne razdalje med dvema terminskima izmerama

$\hat{\sigma}_{i_{\max}}$ - maksimalna glavna standardna deviacija poševne razdalje i-te terminske izmere

$\hat{\sigma}_{j_{\max}}$ - maksimalna glavna standardna deviacija poševne razdalje j-te terminske izmere

Iz rezultatov začetne terminske izmere (tabela 1) se lahko s pomočjo spodnje enačbe predvidi minimalno spremembo poševne razdalje, ki jo bo mogoče zaznati po izmeri naslednje terminske izmre:

$$\hat{\sigma}_{\Delta j_{\max}}^2 = 2 \cdot \hat{\sigma}_{\max}^2$$

$$\hat{\sigma}_{\Delta j_{\max}} = \sqrt{2} \cdot \hat{\sigma}_{\max} = \sqrt{2} \cdot 0,007m = 0,0099m = 10mm$$

Pri tem je $\hat{\sigma}_{\max}$ maksimalni glavni pogrešek poševnih razdalj med karakterističnimi točkami v začetni terminski izmeri pri $\tau = 2$ (verjetnost je 95,45 %).

Iz rezultatov začetne terminske izmre (tabela 1) se lahko sklepa, da se bodo brez izboljšanj metode opazovanja lokalne mreže, lahko spremljale spremembe poševnih razdalj večje od 10 mm v poljubni smeri pri $\tau = 2$ (verjetnost je 95,45 %). Ob upoštevanju najugodnejših primerov (minimalni glavni pogrešek poševnih razdalj je 2 mm, (tabela 1) pri $\tau = 2$ (verjetnost je 95,45 %)) pa se pričakuje, da se bodo lahko zaznale spremembe poševnih razdalj večje od 3 mm.

Acknowledgements

The realization of this project has made possible:

- The Premogovnik Velenje Ltd. company with organisation and heterogeneous network survey,
- The PVInvest Ltd. company with organisation and heterogeneous network survey,
- The Geoservis Ltd. Company:
 - with qualifying for working with programme package *Leica Geo Office 5.0*,
 - with mediation the propositions to program package producer, who made the access to total variance-covariace of unknowns $\Sigma_{\hat{x}\hat{x}}$.

REFERENCES

- BOEKELO, G. (1996): Adjustment Models and Mapping. *The Hydrographic Journal*, Issue 199607, page 3.
- GEOSERVIS d.o.o.: *Uporabniška navodila za LGO*. Ljubljana, marec 2004, 2005.
- LEICA GEOSYSTEMS AG: *Printed Documentation LGO 4.0.pdf* (Navodila za uporabo programskega paketa Leica Geo Office v elektronski obliki).
- LEICK, A. (1995): *GPS satellite surveying*. Second edition, Department of Surveying Engineering, University of Maine, Orono Main. John Wiley & sons, Inc.
- MIHAILOVIĆ, K. (1987): *Geodezija II. I deo*. Drugo izdanje, Naučna knjiga, Beograd
- STRANG, G. (Massachusetts Institute if Technology – MIT) & BORRE, K. (Aalborg University) (1997): *Linear Algebra, Geodesy and GPS*. Wellesley-Cambridge Press.
- URANJEK, G (2007): *Priloga k spremljanju objektov s simultanimi meritvemi različnih tipov*. Ljubljana, NTF, Oddlek za geotehnologijo in rудarstvo.
- VEHOVEC, A (2005): *Ugotavljanje ugrezkov terena s simultano izravnavo več termenskih izmer nivelmanske mreže s pomočjo nD relativnega elipsoida*. Ljubljana, NTF, Oddlek za geotehnologijo in rудarstvo.
- VULIĆ, M. (2006): *Metoda najmanjših kvadratov (MNK)*. Naravoslovnotehniška fakulteta, Ljubljana.
- VULIĆ, M.: *Interna predavanja 2005/2006*.
- WOLFRAM, S. (2003): *The Mathematica book*. 5th edition, Wolfram Media.

Distance reduction with the use of UDF and Mathematica

Redukcija dolžin z uporabo MS Excel–ovih lastnih funkcij in programa Mathematica

MILIVOJ VULIĆ¹, UROŠ BRECELJ²

¹ University of Ljubljana, Faculty of Natural sciences and Engineering, Department of Geotechnology and Mining Engineering, Aškerčeva cesta 12, SI-1000 Ljubljana, Slovenia;
E-mail: milivoj.vulic@ntf.uni-lj.si

² Primorje d.d., Vipavska cesta 3, 5270 Ajdovščina, Slovenia;
E-mail: uros.brecelj@primorje.si

Received: September 2, 2007

Accepted: September 26, 2007

Abstract: On market exist plenty of computer programs for distance reductions.

Mostly the programs are not for free and we do not have insight into their working. To avoid these disadvantages we can create our own program in Microsoft Excel. In Microsoft Excel is possible to create user defined functions (UDF), which we could use just like the build-in Microsoft Excel functions. With user defined functions (UDF) in combination with Add-in program it is possible to upload Excel files on our or other computers. In the sequel is review of the functions, which we need for reduction measured distance into the referential plane and later on the plane on chosen projectional plane. For all function are carried out equations for standard errors and influence of intakes on final result.

Izvleček: Na tržišču je prisotnih več programov za redukcijo dolžin, ki pa niso brezplačni, poleg tega pa nimamo vpogleda v njihovo delovanje. V izogib temu si lahko izdelamo lasten program v Microsoft Excelu. V Microsoft Excelu je mogoča izdelava lastnih funkcij, ki jih uporabljamo enako kot že izdelane Excelove funkcije. S kombinacijo lastnih funkcij in Add-in programa lahko nadgrajujemo Excelove datoteke na svojem ali na drugih računalnikih. V nadaljevanju sledi pregled funkcij, ki jih potrebujemo pri redukciji merjene dolžine na referenčno ploskev in nato na izbrano projekcijsko ravnino. Za vse funkcije so v programu Mathematica izpeljane enačbe standardnih pogreškov in njihov vpliv na končni rezultat.

Key words: distance reduction, MS Excel, user defined function (UDF), Add-in, standard error

Ključne besede: redukcija dolžin, MS Excell, lastne funkcije, Add-in, Mathematica, standardni pogrešek

DISTANCE REDUCTION

Measured distance is not adequate for direct use in mine surveying. It must be corrected for several reasons:

- Meteorological corrections: laser beam is passing through the layers of air with different density, what is reason for refraction of the laser beam and consequently measured distance.
- Geometrical corrections: show difference between space curve and slope distance on level of a ground points,

correction for refrational curve and horizontal eccentricity of distance meters.

- Projectional corrections: means transmission of slope distance on spherical arc lenght on level of referential plane and later on choosen projectional plane.

No measuring system is perfect, and so it will show more or less small deficiencies in mechanical, optical and electronical components. These instrumental errors have influence on reduced distance and therefore must be investegated.

ADD-IN PROGRAM DISTANCE REDUCTION

Purpose of the Add-in program Distance reduction is to facilitate process of reduction them which are involved in surveying distances. It is a free program, which you can download from http://www.geo.ntf.uni-lj.si/mvulic/diplome/Brecelj/Distance_reductions.xla.

Program can use everyone with basic knowledge of Excell. Design of the program enable distance reduction without knowing the theory of reduction, with simple intake of measured quantitys program return reduced distance.

ABOUT USING ADD-IN PROGRAM

Add-in is a supplemental program that adds custom commands or custom features to Microsoft Office. These commands are possible to define as a user defined functions in Microsoft Visual Basic for Applications. User defined functions are created after our own requires, we can define function which we need for our needs and is impossible to found it in build-in Excel functions. With this we save our time because once defined function is allways on disposal. Add-in is possible to use in all MS Excell files on your or on other computers that you use. Add-in have an .xla file extension, which we get in the Save as dialog box, Save as type.

After installing an add-in on your computer, you must load it into Excel. Loading an add-in makes the feature available in Excel and adds any associated commands to the appropriate menus In the Add-Ins available box, select the check box next to the add-in you want to load, and then click OK.

If you don't use often add-ins unload it to conserve memory and improve performance. Unloading an add-in removes its features and commands from Excel, but the add-in program remains on your computer so you can easily reload it. Once tested function or program is in further use as a black box.

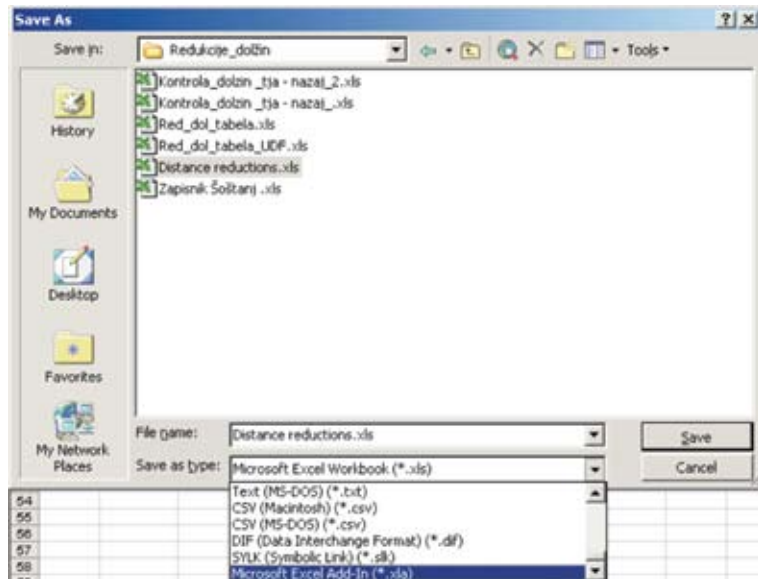


Figure 1. Saving Excel file as Add-in
Slika 1. Shranjevanje Excelove datoteke kot Add-in



Figure 2. Loading Add-in program
Slika 2. Nalaganje Add-in programa

PRESENTATION OF THE FUNCTIONS

Functions for reduction with measured zenith distance and reduction with known heights are described in following text.

mDsurvey

This function returns the value of standard error of measured distance.

Entry: measured distance [Dsurvey], accuracy of distance meter [mm] and [ppm].

Exit: standard error of measured distance [mDsurvey].

Meteorological corrections

Em

This function returns the value of saturated pressure of water steam.

Entry: constant α [alpha], constant β [beta], constant γ [gamma], wet temperature [Twet].

Exit: saturated pressure of water steam [Em].

eP

This function returns the value of partial pressure of water steam.

Entry: temperature [T], wet temperature [Twet], constant K [Kcons], air pressure [p], saturated pressure of water steam [Em].

Exit: partial pressure of water steam [Ep].

Ngroup

This function returns the value of group break quotient.

Entry: constant A [Acons], constant B [Bcons], constant C [Ccons], wavelenght [LambdaNeff].

Exit: group break quotient [Ngroup].

Nact

This function returns the value of actual break quotient.

Entry: group break quotient [Ngroup], air pressure [p], wet temperature [Twet].

Exit: actual break quotient [Nact].

distDmet

This function returns the value of distance reduced with meteorological correction.

Entry: measured distance [distDsurvey], actual break quotient [Nact], referential break quotient [N0].

Exit: distance reduced with meteorological correction [distDmet].

mDmeteoCorr

This function returns the value of standard error of distance reduced with meteorological correction.

Entry: measured distance [distDsurvey], standard error of measured distance [mDsurvey], temperature [T], standard error of temperature [mT], wet temperature [Twet], standard error of wet temperature [mTwet], air pressure [p], standard error of air pressure [mp], referential break quotient [N0], standard error of referential break quotient [mN0], wavelenght [LambdaNeff], standard error of wavelenght [mLambdaNeff], extensional coefficient of air [AlphaAir], standard error of extensional coefficient of air [mAlphaAir], constant A [Acons], standard error of constant A [mAcons], constant B [Bcons], standard error of constant B [mBcons], constant C [Ccons], standard error of constant C [mCcons], constant α [alpha], standard error of constant α [mAlpha], constant β [beta], standard error of constant β [mBeta], constant γ [gamma], standard error of constant γ [mGamma].

constant K [Kcons], standard error of constant K [mKcons].

Exit: standard error of distance reduced with meteorological correction [mDmeteoCorr], without intermediate results.

StdErrDsurveyDmet

This function returns influence of standard error of measured distance on distance reduced with meteorological correction.

Entry: standard error of measured distance [mDsurvey], referential break quotient [N0], temperature [T], wet temperature [Twet], air pressure [p], extensional coefficient of air [AlphaAir], constant A [Acons], constant B [Bcons], constant C [Ccons], wavelenght [LambdaNeff], constant α [alpha], constant β [beta], constant γ [gamma], constant K [Kcons].

Exit: influence of standard error of measured distance on distance reduced with meteorological correction [StdErrDsurveyDmet].

StdErrNoDmet

This function returns influence of referential break quotient on distance reduced with meteorological correction.

Entry: standard error of referential break quotient [mN0], measured distance [distDsurvey], temperature [T], wet temperature [Twet], air pressure [p], extensional coefficient of air [AlphaAir], constant A [Acons], constant B [Bcons], constant C [Ccons], wavelenght [LambdaNeff], constant α [alpha], constant β [beta], constant γ [gamma], constant K [Kcons].

Exit: influence of standard error of referential break quotient on distance reduced with meteorological correction [StdErrNoDmet].

StdErrPDmet

This function returns influence of standard error of air pressure on distance reduced with meteorological correction.

Entry: standard error of air pressure [mp], measured distance [distDsurvey], referential break quotient [N0], temperature [T], wet temperature [Twet], air pressure [p], extensional coefficient of air [AlphaAir], constant A [Acons], constant B [Bcons], constant C [Ccons], wavelenght [LambdaNeff], constant α [alpha], constant β [beta], constant γ [gamma], constant K [Kcons].

Exit: vpliv influence of standard error of air pressure on distance reduced with meteorological correction [StdErrPDmet].

StdErrTmet

This function returns influence of standard error of temperature on distance reduced with meteorological correction.

Entry: standard error of temperature [mT], measured distance [distDsurvey], referential break quotient [N0], temperature [T], wet temperature [Twet], air pressure [p], extensional coefficient of air [AlphaAir], constant A [Acons], constant B [Bcons], constant C [Ccons], wavelenght [LambdaNeff], constant α [alpha], constant β [beta], constant γ [gamma], constant K [Kcons].

Exit: influence of standard error of temperature on distance reduced with meteorological correction [StdErrTDmet].

StdErrTwetDmet

This function returns influence of standard error of wet temperature on distance reduced with meteorological correction.

Entry: standard error of wet temperature [mTwet], measured distance [distDsurvey], referential break quotient [N0], temperature [T], wet temperature [Twet], air

pressure [p], extensional coefficient of air [AlphaAir], constant A [Acons], constant B [Bcons], constant C [Ccons], wavelenght [LambdaNeff], constant α [alpha], constant β [beta], constant γ [gamma], constant K [Kcons].

Exit: influence of standard error of wet temperature on distance reduced with meteorological correction [StdErrTwetDmet].

StdErrAlphaAirDmet

This function returns influence of standard error of extensional coefficient of air on distance reduced with meteorological correction.

Entry: standard error of extensional coefficient of air [mAlphaAir], measured distance [distDsurvey], referential break quotient [N0], temperature [T], wet temperature [Twet], air pressure [p], extensional coefficient of air [AlphaAir], constant A [Acons], constant B [Bcons], constant C [Ccons], wavelenght [LambdaNeff], constant α [alpha], constant β [beta], constant γ [gamma], constant K [Kcons].

Exit: influence of standard error of extensional coefficient of air on distance reduced with meteorological correction [StdErrAlphaAirDmet].

StdErrKDmet

This function returns influence of constant K on distance reduced with meteorological correction.

Entry: standard error of constant K [mKcons], measured distance [distDsurvey], referential break quotient [N0], temperature [T], wet temperature [Twet], air pressure [p] extensional coefficient of air [AlphaAir], constant A [Acons], constant B [Bcons], constant C [Ccons], wavelenght [Lambda-

Neff], constant α [alpha], constant β [beta], constant γ [gamma], constant K [Kcons].

Exit: influence of standard error of constant K on distance reduced with meteorological correction [StdErrKconsDmet].

StdErrAlphaDmet

This function returns influence of constant α on distance reduced with meteorological correction.

Entry: standard error of constant α [mAlpha], measured distance [distDsurvey], referential break quotient [N0], temperature [T], wet temperature [Twet], air pressure [p], extensional coefficient of air [AlphaAir], constant A [Acons], constant B [Bcons], constant C [Ccons], wavelenght [LambdaNeff], constant α [alpha], constant β [beta], constant γ [gamma], constant K [Kcons].

Exit: influence of standard error of constant α on distance reduced with meteorological correction [StdErrAlphaDmet].

StdErrBetaDmet

This function returns influence of constant β on distance reduced with meteorological correction.

Entry: standard error of constant β [mBeta], measured distance [distDsurvey], referential break quotient [N0], temperature [T], wet temperature [Twet], air pressure [p], extensional coefficient of air [AlphaAir], constant A [Acons], constant B [Bcons], constant C [Ccons], wavelenght [LambdaNeff], constant α [alpha], constant β [beta], constant γ [gamma], constant K [Kcons].

Exit: influence of standard error of constant β on distance reduced with meteorological correction [StdErrBetaDmet].

StdErrGammaDmet

This function returns influence of constant γ on distance reduced with meteorological correction.

Entry: standard error of constant γ [mGamma], measured distance [distDsurvey], referential break quotient [N0], temperature [T], wet temperature [Twet], air pressure [p], extensional coefficient of air [AlphaAir], constant A [Acons], constant B [Bcons], constant C [Ccons], wavelength [LambdaNeff], constant α [alpha], constant β [beta], constant γ [gamma], constant K [Kcons].
Exit: influence of standard error of constant γ on distance reduced with meteorological correction [StdErrGammaDmet].

StdErrAconsDmet

This function returns influence of constant A on distance reduced with meteorological correction.

Entry: standard error of constant A [mAcons], measured distance [distDsurvey], referential break coefficient [N0], temperature [T], wet temperature [Twet], air pressure [p], extensional coefficient of air [AlphaAir], constant A [Acons], constant B [Bcons], constant C [Ccons], wavelength [LambdaNeff], constant α [alpha], constant β [beta], constant γ [gamma], constant K [Kcons].
Exit: standard error of constant A on distance reduced with meteorological correction [StdErrAconsDmet].

StdErrBconsDmet

This function returns influence of constant B on distance reduced with meteorological correction.

Entry: standard error of constant B [mBcons], measured distance [distDsurvey], referential break coefficient [N0], temperature [T], wet temperature [Twet], air pressure

[p], extensional coefficient of air [AlphaAir], constant A [Acons], constant B [Bcons], constant C [Ccons], wavelength [LambdaNeff], constant α [alpha], constant β [beta], constant γ [gamma], constant K [Kcons].
Exit: standard error of constant B on distance reduced with meteorological correction [StdErrBconsDmet].

StdErrCconsDmet

This function returns influence of constant C on distance reduced with meteorological correction.

Entry: standard error of constant C [mCcons], measured distance [distDsurvey], referential break coefficient [N0], temperature [T], wet temperature [Twet], air pressure [p], extensional coefficient of air [AlphaAir], constant A [Acons], constant B [Bcons], constant C [Ccons], wavelength [LambdaNeff], constant α [alpha], constant β [beta], constant γ [gamma], constant K [Kcons].
Exit: standard error of constant C on distance reduced with meteorological correction [StdErrCconsDmet].

StdErrLambdaNeffDmet

This function returns influence of wavelength [LambdaNeff] on distance reduced with meteorological correction.

Entry: standard error of wavelength [mLambdaNeff], measured distance [distDsurvey], referential break coefficient [N0], temperature [T], wet temperature [Twet], air pressure [p], extensional coefficient of air [AlphaAir], constant A [Acons], constant B [Bcons], constant C [Ccons], wavelength [LambdaNeff], constant α [alpha], constant β [beta], constant γ [gamma], constant K [Kcons].
Exit: standard error of wavelength on distance reduced with meteorological correction [StdErrLambdaNeffDmet].

tion [StdErrLambdaNeffDmet].

Geometrical corrections

distDr

This function returns the value of distance reduced with additional constant.

Entry: distance reduced with meteorological correction [distDmet], additional constant [Ka].

Exit: distance reduced with additional constant [distDr].

mDr

This function returns the value of standard error of distance reduced with additional constant.

Entry: distance reduced with meteorological correction [distDmet], standard error of distance reduced with meteorological correction [mDmet], additional constant [Ka], standard error of additional constant [mKa].

Exit: standard error of distance reduced with additional constant [mDr].

StdErrDmetDr

This function returns influence of standard error of distance reduced with meteorological correction on distance reduced with additional constant.

Entry: standard error of distance reduced with meteorological correction [mDmet].

Exit: influence of standard error of distance reduced with meteorological correction on distance reduced with additional constant. [StdErrDmetDr].

StdErrKaDr

This function returns influence of standard error of additional constant on distance reduced with additional constant.

Entry: standard error of additional constant [mKa].

Exit: influence of standard error of additional constant on distance reduced with additional constant [StdErrKaDr].

distDslopeZen

This function returns the value of slope distance, defined with zenith distance.

Entry: distance reduced with additional constant [distDr], height of instrument [i], height of reflector [l], height of instrument standing [Hi], zenith distance [zd], radius of Earth [R].

Exit: slope distance, defined with zenith distance [distDslopeZen].

mDslopeZen

This function returns the value of standard error of slope distance, defined with zenith distance.

Entry: distance reduced with additional constant [distDr], standard error of distance reduced with additional constant [mDr], height of instrument [i], standard error of height of instrument [mi], height of reflector [l], standard error of height of reflector [ml], height of reflector standing [Hi], standard error of height of reflector standing [mHi], zenith distance [zd], standard error of zenith distance [mzd], radius of Earth [R] , standard error of radius of Earth [mR].

Exit: standard error of slope distance, defined with zenith distance [mDslopeZen].

StdErrIDslopeZen

This function returns influence of standard error of height of instrument on slope distance, defined with zenith distance.

Entry: standard error of height of instrument [mi], distance reduced with additional constant [distDr], height of instrument [i], height of reflector [l], height of instrument standing [Hi], zenith distance [zd], radius of Earth[R].

Exit: influence of standard error of height of instrument na slope distance, defined with zenith distance [StdErrIDslopeZen].

StdErrLDslopeZen

This function returns influence of standard error of height of reflector on slope distance, defined with zenith distance.

Entry: standard error of height of reflector [ml], distance reduced with additional constant [distDr], height of instrument [i], height of reflector [l], height of instrument standing [Hi], zenith distance [zd], radius of Earth[R].

Exit: influence of standard error of height of reflector na slope distance, defined with zenith distance [StdErrLDslopeZen].

StdErrHiDslopeZen

This function returns influence of standard error of height of instrument standing on slope distance, defined with zenith distance.

Entry: standard error of height of instrument standing [mHi], distance reduced with additional constant [distDr], height of instrument [i], height of reflector [l], height of instrument standing [Hi], zenith distance [zd], radius of Earth[R].

Exit: influence of standard error of height of instrument standing on slope distance,

defined with zenith distance [StdErrHiDslopeZen].

StdErrRDslopeZen

This function returns influence of standard error of radius of earth on slope distance, defined with zenith distance.

Entry: standard error of radius of Earth [mR], distance reduced with additional constant [distDr], height of instrument [i], height of reflector [l], height of instrument standing [Hi], zenith distance [zd], radius of Earth[R].

Exit: influence of standard error of radius of Earth on slope distance, defined with zenith distance [StdErrRDslopeZen].

StdErrDrDslopeZen

This function returns influence of standard error of distance reduced with additional constant on slope distance, defined with zenith distance.

Entry: standard error of distance reduced with additional constant [mDr], distance reduced with additional constant [distDr], height of instrument [i], height of reflector [l], height of instrument standing [Hi], zenith distance [zd], radius of Earth[R].

Exit: influence of standard error of distance reduced with additional constant on slope distance, defined with zenith distance [StdErrDrDslopeZen].

StdErrZdDslopeZen

This function returns influence of standard error of zenith distance on slope distance, defined with zenith distance.

Entry: standard error of zenith distance [mzd], distance reduced with additional constant [distDr], height of instrument [i], height of reflector [l], height of instrument standing [Hi], zenith distance [zd], radius

of Earth [R].

Exit: influence of standard error of zenith distance on slope distance, defined with zenith distance [StdErrZdDslopeZen].

distDslope

This function returns the value of slope distance, defined with known heights.

Entry: distance reduced with additional constant [distDr], height of instrument [i], height of reflector [l], height of instrument standing [Hi], height of reflector standing [Hl], radius of Earth [R].

Exit: slope distance, defined with known heights [distDslope].

mDslope

This function returns the value of standard error of slope distance, defined with known heights.

Entry: distance reduced with additional constant [distDr], standard error of distance reduced with additional constant [mDr], height of instrument [i], standard error of height of instrument [mi], height of reflector [l], standard error of height of reflector [ml], height of instrument standing [Hi], standard error of height of instrument standing [mHi], height of reflector standing [Hl], standard error of height of reflector standing [mHl], radius of Earth [R], standard error of radius of Earth [mR].

Exit: standard error of slope distance, defined with known heights [mDslope].

StdErrIDslope

This function returns influence of standard error of height of instrument on slope distance, defined with known heights.

Entry: standard error of height of instrument [mi], distance reduced with additional constant [distDr], height of instrument [i],

height of reflector [l], height of instrument standing [Hi], height of reflector standing [Hl], radius of Earth [R].

Exit: influence of standard error of height of instrument na slope distance [StdErrIDslope].

StdErrLDslope

This function returns influence of standard error of height of reflector on slope distance, defined with known heights.

Entry: standard error of height of reflector [ml], distance reduced with additional constant [distDr], height of instrument [i], height of reflector [l], height of instrument standing [Hi], height of reflector standing [Hl], radius of Earth [R].

Exit: influence of standard error of height of reflector na slope distance [StdErrLDslope].

StdErrHiDslope

This function returns influence of standard error of height of instrument standing on slope distance, defined with known heights.

Entry: standard error of height of instrument standing [mHi], distance reduced with additional constant [distDr], height of instrument [i], height of reflector [l].

Exit: influence of standard error of height of instrument standing na slope distance [StdErrHiDslope].

StdErrHIDslope

This function returns influence of standard error of height of reflector standing on slope distance, defined with known heights.

Entry: standard error of height of reflector standing [mHl], distance reduced with additional constant [distDr], height of instrument [i], height of reflector [l].

Exit: influence of standard error of height of reflector standing na slope distance [StdErrHIDslope].

StdErrRDslope

This function returns influence of standard error of radius of Earth on slope distance, defined with known heights.

Entry: standard error of radius of Earth [mR], distance reduced with additional constant [distDr], height of instrument [i], height of reflector [I].

Exit: influence of standard error of radius of Earth na slope distance [StdErrRDslope].

StdErrDrDslope

This function returns influence of standard error of distance reduced with additional constanton slope distance, defined with known heights.

Entry: standard error of distance reduced with additional constant [mDr], distance reduced with additional constant [distDr], height of instrument [i], height of reflector [I], height of instrument standing [Hi], height of reflector standing [HI], radius of Earth [R].

Exit: influence of standard error of radius of Earth na slope distance [StdErrDrDslope].

Projectional corrections

distDzenDir

This function returns the value of spherical arc length on referential plane of the earth, this is a plane of referential sphere, defined with zenith distance and direct reduction.

Entry: slope distance [distDslopeZen], height of instrument standing [Hi], zenith distance [zd], radius of Earth [R], refracti-

onal coefficient [k].

Exit: spherical arc lenght [distDzenDir].

mDzenDir

This function returns the value of standard error of spherical arc length on referential plane of the earth, defined with zenith distance and direct reduction.

Entry: slope distance [distDslopeZen], standard error of slope distance [mDslopeZen], height of instrument standing [Hi], standard error of height of reflector standing [mHi], zenith distance [zd], standard error of zenith distance [mzd], radius of Earth [R], standard error of radius of Earth [mR], refraktional coefficient [k], standard error of refraktional coefficient [k].

Exit: standard error of spherical arc lenght [mDzenDir].

StdErrHiDzenDir

This function returns influence of standard error of height of instrument standing on spherical arc lenght on referential plane of Earth, defined with zenith distance and direct reduction.

Entry: standard error of height of reflector standing [mHi], slope distance [distDslopeZen], height of instrument standing [Hi], zenith distance [zd], radius of Earth [R], refraktional coefficient [k].

Exit: influence of standard error of height of reflector standing [StdErrHiDzenDir].

StdErrRDzenDir

This function returns influence of standar error of radius of Earth on spherical arc lenght on referential plane of Earth, defined with zenith distance and direct reduction.

Entry: standard error of radius of Earth [mR], slope distance [distDslopeZen], hei-

ght of instrument standing [Hi], zenith distance [zd], radius of Earth [R], refractive coefficient [k].

Exit: influence of standard error of radius of Earth [StdErrRDzenDir].

StdErrDslopeDzenDir

This function returns influence of standard error of slope distance on spherical arc length on referential plane of Earth, defined with zenith distance and direct reduction.

Entry: standard error of slope distance [mR], slope distance [distDslopeZen], height of instrument standing [Hi], zenith distance [zd], radius of Earth [R], refractive coefficient [k].

Exit: influence of standard error of slope distance [StdErrDslopeDzenDir].

StdErrZdDzenDir

This function returns influence of standard error of zenith distance on spherical arc length on referential plane of Earth, defined with zenith distance and direct reduction.

Entry: standard error of zenith distance [mzd], slope distance [distDslopeZen], height of instrument standing [Hi], zenith distance [zd], radius of Earth [R], refractive coefficient [k].

Exit: influence of standard error of zenith distance [StdErrZdDzenDir].

StdErrKDzenDir

This function returns influence of standard error of refractive coefficient [k] on spherical arc length on referential plane of Earth, defined with zenith distance and direct reduction.

Entry: standard error of refractive coefficient [mk], slope distance [distDslopeZen], height of instrument standing [Hi], height

of reflector standing [Hl], zenith distance [zd], radius of Earth [R], refractive coefficient [k].

Exit: influence of standard error of refractive coefficient [StdErrKDzenDir].

distDzenGrad

This function returns the value of spherical arc length on referential plane of the earth, this is a plane of referential sphere, defined with zenith distance and gradual reduction.

Entry: slope distance [distDslopeZen], height of instrument standing [Hi], zenith distance [zd], radius of Earth [R], height of reflector standing [Hl], refractive coefficient [k].

Exit: spherical arc length [distDzenGrad].

mDzenGrad

This function returns the value of standard error of spherical arc length on referential plane of the earth, defined with zenith distance and gradual reduction.

Entry: slope distance [distDslopeZen], standard error of slope distance [mDslopeZen], height of instrument standing [Hi], standard error of height of reflector standing [mHi], height of reflector standing [Hl], standard error of height of reflector standing [mHl], zenith distance [zd], standard error of zenith distance [mzd], radius of Earth [R], standard error of radius of Earth [mR], refractive coefficient [k], standard error of refractive coefficient [mk].

Exit: standard error of spherical arc length [mDzenGrad].

StdErrHiDzenGrad

This function returns influence of standard error of height of instrument standing on

spherical arc lenght on referential plane of Earth, defined with zenith distance and gradual reduction.

Entry: standard error of height of reflector standing [mHi], slope distance [distDslopeZen], height of instrument standing [Hi], height of reflector standing [Hi], zenith distance [zd], radius of Earth [R], refractive coefficient [k].

Exit: influence of standard error of height of reflector standing [StdErrHiDzenDir].

StdErrHiDzenGrad

This function returns influence of standard error of height of reflector standing on spherical arc lenght on referential plane of Earth, defined with zenith distance and gradual reduction.

Entry: standard error of height of reflector standing [mHi], slope distance [distDslopeZen], height of instrument standing [Hi], height of reflector standing [Hi], zenith distance [zd], radius of Earth [R], refractive coefficient [k].

Exit: influence of standard error of height of reflector standing [StdErrHiDzenDir].

StdErrRDzenGrad

This function returns influence of standard error of radius of Earth on spherical arc lenght on referential plane of Earth, defined with zenith distance and gradual reduction.

Entry: standard error of radius of Earth [mR], slope distance [distDslopeZen], height of instrument standing [Hi], height of reflector standing [Hi], zenith distance [zd], radius of Earth [R], refractive coefficient [k].

Exit: influence of standard error of radius of Earth [StdErrRDzenDir].

StdErrDslopeDzenGrad

This function returns influence of standard error of slope distance on spherical arc lenght on referential plane of Earth, defined with zenith distance and gradual reduction.

Entry: standard error of slope distance [mDslope], slope distance [distDslopeZen], height of instrument standing [Hi], height of reflector standing [Hi], zenith distance [zd], radius of Earth [R], refractive coefficient [k].

Exit: influence of standard error of slope distance [StdErrDslopeDzenDir].

StdErrZdDzenGrad

This function returns influence of standard error of zenith distance on spherical arc lenght on referential plane of Earth, defined with zenith distance and gradual reduction.

Entry: standard error of zenith distance [mzd], slope distance [distDslopeZen], height of instrument standing [Hi], height of reflector standing [Hi], zenith distance [zd], radius of Earth [R], refractive coefficient [k].

Exit: influence of standard error of zenith distance [StdErrZdDzenDir].

StdErrKDzenGrad

This function returns influence of standard error of refractive coefficient on spherical arc lenght on referential plane of Earth, defined with zenith distance and gradual reduction.

Entry: standard error of refractive coefficient [mk], slope distance [distDslopeZen], height of instrument standing [Hi], height of reflector standing [Hi], zenith distance [zd], radius of Earth [R], refractive coefficient [k].

Exit: influence of standard error of refractive coefficient [StdErrKDzenDir].

distDoDir

This function returns distance of chord in level of horizont, defined with known heights and direct reduction.

Entry: slope distance [distDslope], height of instrument standing [Hi], height of reflector standing [Hl], radius of Earth [R].

Exit: chord lenght in horizontal level [distDoDir].

mDoDir

This function returns the value of standard error of distance of chord with known heights and direct reduction.

Entry: slope distance [distDslope], standard error of slope distance [mDslope], height of instrument standing [Hi], standard error of height of instrument standing [mHi], height of reflector standing [Hl], standard error of height of reflector standing [mHl], radius of Earth [R], standard error of radius of Earth [mR].

Exit: standard error of chord lenght in horizontal level [mDoDir].

StdErrDslopeDoDir

This function returns influence of standard error of slope distance on chord lenght on horizontal level, defined with direct reduction.

Entry: standard error of slope distance [mDslope], slope distance [distDslope], height of instrument standing [Hi], height of reflector standing [Hl], radius of Earth [R].

Exit: influence of standard error of slope distance [StdErrDslopeDoDir].

StdErrHiDoDir

This function returns influence of standard error of height of instrument standing on chord lenght on horizontal level, defined with direct reduction.

Entry: standard error of height of instrument standing [mHi], slope distance [distDslope], height of instrument standing [Hi], height of reflector standing [Hl], radius of Earth [R].

Exit: influence of standard error of height of instrument standing [StdErrHiDoDir].

StdErrHlDoDir

This function returns influence of standard error of height of reflector standing on chord lenght on horizontal level, defined with direct reduction.

Entry: standard error of height of reflector standing [mHl], slope distance [distDslope], height of instrument standing [Hi], height of reflector standing [Hl], radius of Earth [R].

Exit: influence of standard error of height of reflector standing [StdErrHlDoDir].

StdErrRDoDir

This function returns influence of standard error of radius of Earth on chord lenght on horizontal level, defined with direct reduction.

Entry: standard error of radius of Earth [mR], slope distance [distDslope], height of instrument standing [Hi], height of reflector standing [Hl], radius of Earth [R].

Exit: influence of standard error of radius of Earth [StdErrRDoDir].

distDoGrad

This function returns distance of chord in level of horizont, defined with known heights and gradual reduction.

Entry: slope distance [distDslope], height of instrument standing [Hi], height of reflector standing [HI].

Exit: chord lenght in horizontal level [distDoGrad].

[Hi], height of reflector standing [HI], radius of Earth [R].

Exit: influence of standard error of height of instrument standing [StdErrHiDoDir].

mDoGrad

This function returns the value of standard error of distance of chord with known heights and gradual reduction.

Entry: slope distance [distDslope], standard error of slope distance [mDslope], height of instrument standing [Hi], standard error of height of instrument standing [mHi], height of reflector standing [HI], standard error of height of reflector standing [mHI], radius of Earth [R], standard error of radius of Earth [mR].

Exit: standard error of chord lenght in horizontal level [mDoGrad].

StdErrHiDoGrad

This function returns influence of standard error of height of reflector standing on chord lenght on horizontal level, defined with gradual reduction.

Entry: standard error of height of reflector standing [mHI], slope distance [distDslope], height of instrument standing [Hi], height of reflector standing [HI], radius of Earth [R].

Exit: influence of standard error of height of reflector standing [StdErrHiDoDir].

StdErrDslopeDoGrad

This function returns influence of standard error of slope distance on chord lenght on horizontal level, defined with gradual reduction.

Entry: standard error of slope distance [mDslope], slope distance [distDslope], height of instrument standing [Hi], height of reflector standing [HI], radius of Earth [R].

Exit: influence of standard error of slope distance [StdErrDslopeDoGrad].

StdErrRDoGrad

This function returns influence of standard error of radius of Earth on chord lenght on horizontal level, defined with gradual reduction.

Entry: standard error of radius of Earth [mR], slope distance [distDslope], height of instrument standing [Hi], height of reflector standing [HI], radius of Earth [R].

Exit: influence of standard error of radius of Earth [StdErrRDoDir].

distDrefPlane

This function returns the value of spherical arc length on referential plane of the earth, this is a plane of referential sphere, defined with known heights.

Entry: chord lenght in horizontal level [distDoDir], radius of Earth [R].

Exit: spheric arc lenght [distDrefPlane].

StdErrHiDoGrad

This function returns influence of standard error of height of instrument standing on chord lenght on horizontal level, defined with gradual reduction.

Entry: standard error of height of instrument standing [mHi], slope distance [distDslope], height of instrument standing

mDrefPlane

This function returns the value of standard error of spherical arc length on referenti-

al plane of the earth, defined with known heights.

Entry: chord lenght in horizontal level [distDoDir], standard error of chord lenght in horizontal level [mDoDir], radius of Earth [R], standard error of radius of Earth [mR].

Exit: standard error of spheric arc lenght [mDrefPlane].

StdErrRDrefPlane

This function returns influence of standard error of radius of Earth on spherical arc lenght on referential plane of Earth, defined with known heights.

Entry: standard error of radius of Earth [mR], chord lenght in horizontal level [distDoDir], radius of Earth [R].

Exit: influence of standard error of radius of Earth [StdErrRDrefPlane].

StdErrDoDirDrefPlane

This function returns influence of standard error of chord lenght on spherical arc lenght on referential plane of Earth, defined with known heights.

Entry: standard error of chord lenght in horizontal level [mDoDir], chord lenght in horizontal level [distDoDir], radius of Earth [R].

Exit: influence of standard error of chord lenght in horizontal level [StdErrDoDirDrefPlane].

distDgkm

This function returns the value of Gauss - Kruger modulate distance.

Entry: spheric arc lenght [distDrefPlane], radius of Earth [R], coordinate of instrument standing [yi], coordinate of reflector standing [yl], projectional module [module].

Exit: Gauss Krueger modulate distance [distDgkm].

mDgkm

This function returns the value of standard error of Gauss - Kruger modulate distance.

Entry: spheric arc lenght [distDrefPlane], standard error of spherical arc lenght [mDrefPlane], radius of Earth [R], standard error of radius of Earth [mR], coordinate of instrument standing [yi], standard error of coordinate of instrument standing [myi], coordinate of reflector standing [yl], standard error of coordinate of reflector standing [myl], projectional module [module], standard error of projection module [mModule].

Exit: standard error of Gauss Krueger modulate distance [mDgkm].

StdErrDrefPlaneDgkm

This function returns influence of standard error of spherical arc lenght on Gauss Kruger modulate distance.

Entry: standard error of spheric arc lenght [mDrefPlane], spheric arc lenght [DrefPlane], radius of Earth [R], coordinate of instrument standing [yi], coordinate of reflector standing [yl], projectional module [module].

Exit: influence of standard error of spherical arc lenght [StdErrDrefPlaneDgkm].

StdErrRDgkm

This function returns influence of standard error of radius of Earth on Gauss Kruger modulate distance.

Entry: standard error of radius of Earth [mR], spheric arc lenght [DrefPlane], radius of Earth [R], coordinate of instrument standing [yi], coordinate of reflector stan-

ding [yl].

Exit: influence of standard error of radius of Earth [StdErrRDgkm].

StdErrYiDgkm

This function returns influence of standard error of coordinate standing of instrument on Gauss Kruger modulate distance.

Entry: standard error of coordinate of instrument standing [myi], spheric arc lenght [DrefPlane], radius of Earth [R], coordinate of instrument standing [yi], coordinate of reflector standing [yl].

Exit: influence of standard error of coordinate of instrument standing [StdErrYiDgkm].

StdErrYIdgkm

This function returns influence of standard error of coordinate standing of reflector on Gauss Kruger modulate distance.

Entry: standard error of coordinate of reflector standing [myl], spheric arc lenght [DrefPlane], radius of Earth [R], coordinate of instrument standing [yi], coordinate of reflector standing [yl].

Exit: influence of standard error of coordinate of reflector standing [StdErrYIdgkm].

StdErrYIdgkm

This function returns influence of standard error of projectional module on Gauss Kruger modulate distance.

Entry: standard error of modula projekcije [mModule], spheric arc lenght [DrefPlane].

Exit: influence of standard error of modula projekcije [StdErrModuleDgkm].

DefHI

This function returns the value of height of

second end point.

Entry: slope distance [distDslopeZen], height of instrument standing [Hi], zenith distance [zd], radius of Earth [R].

Exit: height of second end point[DefHI].

mHI

This function returns the value of standard error of height of second end point.

Entry: slope distance [distDslopeZen], standard error of slope distance [mDslopeZen], height of instrument standing [Hi], standard error of height of instrument standing [mHi], zenith distance [zd], standard error of zenith distance [mzd], radius of Earth [R], standard error of radius of Earth [mR].

Exit: standard error of height of second end point[mHi].

StdErrHiHI

This function returns influence of standard error of height of instrument standing on height of second end point.

Entry: standard error of height of instrument standing [mHi], slope distance [distDslopeZen], height of instrument standing [Hi], zenith distance [zd], radius of Earth [R].

Exit: influence of standard error of height of instrument standing [StdErrHiHI].

StdErrRHI

This function returns influence of standard error of radius of Earth on height of second end point.

Entry: standard error of radius of Earth [mR], slope distance [distDslopeZen], height of instrument standing [Hi], zenith distance [zd], radius of Earth [R].

Exit: influence of standard error of radius of Earth [StdErrRHI].

StdErrDslopeZenHl

This function returns influence of standard error of slope distance on height of second end point.

Entry: standard error of slope distance [mDslope], slope distance [distDslopeZen], height of instrument standing [Hi], zenith distance [zd], radius of Earth [R].

Exit: influence of standard error of slope distance [StdErrDslopeHl].

StdErrZdDzenDir

This function returns influence of standard error of zenith distance on height of second end point.

Entry: standard error of zenith distance [mzd], slope distance [distDslopeZen], height of instrument standing [Hi], zenith distance [zd], radius of Earth [R].

Exit: influence of standard error of zenith distance [StdErrZdHl].

defRadiusR

This function returns the value of radius of Earth.

Entry: large half axis of referential ellipsoid [a], small half axis of referential ellipsoid

[b], ellipsoidal latitude [Phi].

Exit: radius of Earth [DefRadiusR].

mR

This function returns the value of standard error of radius of Earth.

Entry: large half axis of referential ellipsoid [a], standard error of large half axis of referential ellipsoid [ma], small half axis of referential ellipsoid [b], standard error of small half axis of referential ellipsoid [mb], ellipsoidal latitude [Phi], standard error of ellipsoidal latitude [mPhi].

Exit: standard error of radius of Earth [mR].

StdErrAR

This function returns influence of standard error of big half axis of referential ellipsoid on radius of Earth.

Entry: standard error of large half axis of referential ellipsoid [ma], large half axis of referential ellipsoid [a], small half axis of referential ellipsoid [b], ellipsoidal latitude [Phi].

Exit: influence of standard error of large half axis of referential ellipsoid [StdErrAR].

StdErrBR

This function returns influence of standard error of small half axis of referential ellipsoid on radius of Earth.

Entry: standard error of small half axis of referential ellipsoid [ma], large half axis of referential ellipsoid [a], small half axis of referential ellipsoid [b], ellipsoidal latitude [Phi].

Exit: influence of standard error of small half axis of referential ellipsoid [StdErrBR].

StdErrPhiR

This function returns influence of standard error of ellipsoidal latitude on radius of Earth.

Entry: standard error of ellipsoidal latitude [mPhi], large half axis of referential ellipsoid [a], small half axis of referential ellipsoid [b], ellipsoidal latitude [Phi].

Exit: influence of standard error of ellipsoidal latitude [StdErrPhiR].

USER DEFINE FUNCTIONS FOR REDUCTION WITHOUT INTERMEDIATE RESULTS

This function returns the value of reduced distance and standard error without intermediate results. In the function are entered all measured entrys and function directly return reduced distance.

distMeteoCorr

This function returns the value of distance reduced with meteorological correction, without intermediate result.

Entry: measured distance [distDsurvey], temperature [T], wet temperature [Twet], air pressure [p], referential break quotient [N0], wavelenght [LambdaNeff], extensional coefficient of air [AlphaAir], constant A [Acons], constant B [Bcons], constant C [Ccons], constant α [alpha], constant β [beta], constant γ [gamma], constant K [Kcons].

Exit: distance reduced with meteorological correction [distMeteoCorr].

mDmeteoCorr

This function returns the value of standard error of distance reduced with meteorological correction.

Entry: measured distance [distDsurvey], standard error of measured distance [mDsurvey], temperature [T], standard error of temperature [mT], wet temperature [Twet], standard error of wet temperature [mTwet], air pressure [p], standard error of air pressure [mp], referential break quotient [N0], standard error of referential break quotient [mN0], wavelenght [LambdaNeff], standard error of wavelenght [mLambdaNeff], extensional coefficient of air [AlphaAir], standard error of extensional coefficient of air [mAlphaAir], constant A [Acons], stan-

dard error of constant A [mAcons], constant B [Bcons], standard error of constant B [mBcons], constant C [Ccons], standard error of constant C [mCcons], constant α [alpha], standard error of constant α [mAlpha], constant β [beta], standard error of constant β [mBeta], constant γ [gamma], standard error of constant γ [mGamma], constant K [Kcons], standard error of constant K [mKcons].

Exit: standard error of distance reduced with meteorological correction [mDmeteoCorr], without intermediate results.

distGeomCorrZen

This function returns the value of distance reduced with geometrical corrections. It is a slope distance, defined with zenith distance.

Entry: distance reduced with meteorological correction [distMeteoCorr], additional constant [Ka], height of instrument [i], height of reflector [l], height of instrument standing [Hi], zenith distance [zd], radius of Earth [R].

Exit: slope distance – distance corrected with geometrical corrections, defined with zenith distance [distGeomCorrZen].

mDgeomCorrZen

This function returns the value of standard error of geometrical corrections on slope distance, defined with zenith distance.

Entry: distance reduced with meteorological correction [distMeteoCorr], standard error of distance reduced with meteorological correction [mDmeteoCorr], additional constant [Ka], standard error of additional constant [mKa], height of instrument [i], standard error of height of instrument [mi], height of reflector [l], standard error of height of reflector [ml], height of instrument

standing [Hi], standard error of height of instrument standing [mHi], zenith distance [zd], standard error of zenith distance [mzd], radius of Earth [R], standard error of radius of Earth [mR].

Exit: standard error of slope distance - distance corrected with geometrical corrections, defined with zenith distance [mDgeomCorrZen].

distGeomCorr

This function returns the value of distance reduced with geometrical corrections. It is a slope distance, defined with known heights.

Entry: distance reduced with meteorological correction [distMeteoCorr], additional constant [Ka], height of instrument [i], height of reflector [l], height of instrument standing [Hi], height of reflector standing [Hl], radius of Earth [R].

Exit: slope distance - distance corrected with geometrical corrections, defined with known heights [distGeomCorr].

mDgeomCorr

This function returns the value of standard error of distance corrected with geometrical corrections, defined with known heights.

Entry: distance reduced with meteorological correction [distMeteoCorr], standard error of distance reduced with meteorological correction [mDmeteoCorr], additional constant [Ka], standard error of additional constant [mKa], height of instrument [i], standard error of height of instrument [mi], height of reflector [l], standard error of height of reflector [ml], height of instrument standing [Hi], standard error of height of instrument standing [mHi], height of reflector standing [Hl], standard error of

height of reflector standing [mHl], radius of Earth [R], standard error of radius of Earth [mR].

Exit: standard error of slope distance - distance corrected with geometrical corrections, defined with known heights [mDgeomCorr].

distProjCorrZen

This function returns the value of distance reduced with projectional corrections. It is a Gauss - Kruger modulate distance, defined with zenith distance.

Entry: distance corrected with geometrical corrections, defined with zenith distance [distGeomCorrZen], height of instrument standing [Hi], zenith distance [zd], radius of Earth [R], refractive coefficient [k], coordinate of instrument standing [yi], coordinate of reflector standing [yl], projectional module [module].

Exit: Gauss – Krueger modulate distance - distance corrected with projectional corrections, defined with zenith distance [distProjCorrZen].

mDprojCorrZen

This function returns the value of standard error of projectional corrections on Gauss - Kruger modulate distance, defined with zenith distance.

Entry: distance corrected with geometrical corrections, defined with zenith distance [distGeomCorrZen], standard error of distance corrected with geometrical corrections, defined with zenith distance [mDgeomCorrZen], height of instrument standing [Hi], standard error of height of instrument standing [mHi], zenith distance [zd], standard error of zenith distance [mzd], radius of Earth [R], standard error of radius of Earth [mR], refractive co-

efficient [k], standard error of refractive coefficient [mk], coordinate of instrument standing [yi], standard error of coordinate of instrument standing [myi], coordinate of reflector standing [yl], standard error of coordinate of reflector standing [myl], projectional module [module], standard error of projectional module [mModule].

Exit: standard error of Gauss – Krueger modulate distance – distance corrected with projectional corrections, defined with zenith distance [mDprojCorrZen].

distProjCorr

This function returns the value of standard error of projectional corrections on Gauss - Krueger modulate distance, defined with known heights.

Entry: distance corrected with geometrical corrections [distGeomCorr], height of instrument standing [Hi], height of reflector standing [Hl], radius of Earth [R], coordinate of instrument standing [yi], coordinate of reflector standing [yl], projectional module [module].

Exit: Gauss – Krueger modulate distance - distance corrected with projectional corrections, [distProjCorr].

mDprojCorr

This function returns the value of standard error of projectional corrections on Gauss - Krueger modulate distance.

Entry: distance corrected with geometrical corrections [distGeomCorr], standard error of distance corrected with geometrical corrections [mDgeomCorr], height of instrument standing [Hi], standard error of height of instrument standing [mHi], height of reflector standing [Hl], standard error of height of reflector standing [mHl], radius of Earth [R], standard error of radi-

us of Earth [mR], coordinate of instrument standing [yi], standard error of coordinate of instrument standing [myi], coordinate of reflector standing [yl], standard error of coordinate of reflector standing [myl], projectional module [module], standard error of projectional module [mModule].

Exit: standard error of Gauss – Krueger modulate distance – distance corrected with projectional corrections [mDprojCorr].

CONCLUSIONS

In the gradual thesis was made Add-in program Distance reduction. Add-in program is designed for those, who are dealing with distance surveying. It is a free program, which we can find on internet site http://www.geo.ntf.uni-lj.si/mvulic/diplome/Brecelj/Distance_reductions.xla. In article is shown use of the user defined functions for reduction with measured zenith distance. On internet site http://www.geo.ntf.uni-lj.si/mvulic/diplome/Brecelj/Distance_reductions.xla are located functions for reduction with known height above sea level with detail description of all functions. Standard error functions are evaluated in program for symbolic mathematical Mathematica, which enable us to define partial derivative of functions.

POVZETKI

V diplomski nalogi je bil narejen Add-in program Redukcije dolžin. Brezplačni program, ki je namenjen uporabnikom, ki se ukvarjajo z merjenjem dolžin se nahaja na spletni strani http://www.geo.ntf.uni-lj.si/mvulic/diplome/Brecelj/Distance_reductions.xla, V članku je prikazana uporaba lastnih funkcij za redukcijo dolžin z merjeno zenitno razdaljo, na navedeni spletni strani pa se nahajajo tudi lastne funkcije za redukcijo z znanimi nadmorskimi višinami z detajlnim opisom vseh funkcij. Funkcije standardnih pogreškov so bile izdelane v programu za simbolično matematiko Mathematica, ki omogoča izpeljavo parcialnih odvodov funkcij.

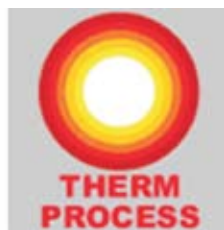
REFERENCES

- [1] KOGOJ, D. (2002): *Merjenje dolžin z elektronskimi razdaljemerji*. Fakulteta za gradbeništvo in geodezijo, Ljubljana.
- [2] BRONŠTEJN J. N., SEMENDJAJEV K. A.(1978): *Matematični priročnik*. Tehniška založba Slovenije v Ljubljani.
- [3] VIDAV, I. (1949): *Višja matematika*. Ljubljana, DZS.
- [4] VULIĆ, M. (2004): *Pogreškifunkcij*(zapiski s predavanj). Naravoslovnotehniška fakulteta, Oddelek za geotehnologijo in rudarstvo, Ljubljana.
- [5] BRECELJ, U. (2005): *Kreiranje lastnih funkcij (UDF) v Excelu zaradi redukcije dolžin in izpeljava natančnosti le teh v Mathematici*. Naravoslovnotehniška fakulteta, Oddelek za geotehnologijo in rudarstvo, Ljubljana.

Predstavitev Oddelka za materiale in metalurgijo Naravoslovnotehniške fakultete na sejmu GIFA, METEC, THERM PROCESS in NEWCAST 2007

STANISLAV KORES¹, MITJA PETRIČ¹, MAJA VONČINA¹

¹ Univerza v Ljubljani, Naravoslovnotehniška fakulteta, Oddelek za materiale in metalurgijo, Aškerčeva 12, 1000 Ljubljana; E-mail: stanislav.kores@ntf.uni-lj.si, mitja.petric@ntf.uni-lj.si, maja.voncina@ntf.uni-lj.si



METEC, 9. sejem THERM PROCESS in 2. sejem NEWCAST 2007, ki je na področju livarstva vodilen v svetu. Poleg 11-tih slovenskih podjetij se je prvkrat predstavil tudi Oddelek za materiale in metalurgijo (OMM) Naravoslovnotehniške fakultete (NTF) v Ljubljani. Pod vodstvom doc. dr. Primoža Mrvarja in doc. dr. Jožefa Medveda smo na razstavnem prostoru »Street of science« predstavljali fakulteto, znanstveno raziskovalno delo in študijske programe na oddelku. V sklopu tega razstavnega prostora, ki je bil namenjen izključno predstavitvi raziskovalnih dosežkov, je sodelovalo 14 univerz in raziskovalnih institucij, od tega 10 iz Nemčije ter po ena iz Poljske, Španije in Avstrije ter naša Fakulteta kot edina iz Slovenije.

Sejem GIFA, METEC, THERM PROCESS in NEWCAST v Düsseldorfu je tradicionalen in se odvija vsaka štiri leta.

Letošnji sejem je bil rekorden, tako po številu razstavljavcev kot tudi po številu obiskovalcev. S 1700 razstavljavci iz kar 45-ih držav sveta si je bilo možno ogledati nove tehnologije, dosežke in produkte s področja livarstva, metalurgije in toplotne tehnike. Sejem NEWCAST pa je prikazoval ulitke iz posameznih liven. Med slovenskimi podjetji so bili naslednji razstavljavci: TCG-Unitech LHT-OL, Litostroj jeklo, Livarna Goriva (LOGO), Bosio, Ferrocrtalič, Gostol, WIRE-T.S.T.,... V petih dneh si je sejem ogledalo 77.000 ljudi.

Ponosni smo, da smo na tem sejmu predstavljali tudi Oddelek za materiale in metalurgijo Naravoslovnotehniške fakultete. Posebna zahvala gre prof. dr. Milanu Trbižanu, ki je v sodelovanju z nemškim VDG priskrbel razstavni prostor na sejmu. Bili smo v družbi elitnih tehničnih univerz, kot so RTWH Aachen, TU Leoben, TU Aalen,



Slika1. Doktoranti in podiplomski študentje NTF na razstavnem prostoru OMM



Slika 2. Sestanek na razstavnem prostoru OMM; od leve proti desni: S. Kores, J. Medved, M. Vončina, B. Dremelj in P. Mrvar

TU Freiberg, TU Clausthal,... Navezali smo stike s strokovnjaki iz fakultet in izmenjali izkušnje ter predstavili raziskovalna dela in dosežke s katerimi se ukvarjam.

Razstavni prostor je bil lepo opremljen s plakati o najnovejši opremi na oddelku in delu posameznih kateder ter popestrjen z multimedijsko predstavljivijo. Izdelana je bila zloženka o delu in dosežkih na fakulteti in zloženko s predstavljivijo študijskih programov na fakulteti. Vsakemu zainteresiranemu smo z veseljem predstavili študij

in delo na naši fakulteti, za spomin pa mu podarili obesek z montanističnim znakom.

V sklopu strokovne ekskurzije, ki šteje tudi kot udeležba na zaključnih terenskih vajah, si je sejem ogledalo tudi 30 študentov visoko strokovnega študija metalurške tehnologije in univerzitetnega študija materialov in metalurgije. Bili so navdušeni nad novimi in izboljšanimi tehnologijami ter materiali. Glede na velik obseg sejma so študentje ljubljanske NTF, OMM v dveh dneh le stežka ogledali vse razstavljavce.

Author's Index

Andjelov Mišo	miso.andjelov@gov.si	235
Bašagić Mirza	mbasagic@lol.ba	217
Bombač David	david.bombac@ntf.uni-lj.si	151
Brecelj Uroš	uros.brecelj@primorje.si	265
Breskvar Bojan	bojan.breskvar@imt.si	165
Brojan Miha	miha.brojan@fs.uni-lj.si	151
Dolenec Matej	matej.dolenec@s5.net	189
Fajfar Peter	peter.fajfar@ntf.uni-lj.si	165
Kejžar Rajko	rajko.kejzar@fs.uni-lj.si	179
Kejžar Uroš	uros.kejzar@iskra-varjenje.si	179
Kočevar Heda	heda.kocevar@omegaconsult.si	223
Kores Stanislav	stanislav.kores@ntf.uni-lj.si	287
Kosec Lado	kosec@ntf.uni-lj.si	179
Krkovič Matija	matija.krkovic@kclj.si	151
Mikulič Zlatko	zlatko.mikulic@gov.si	235
Miler Miloš	mmiler@email.si	189
Oblak Katarina	katrina.oblak@ntf.uni-lj.si	203
Pavšič Jernej	jernej.pavsic@ntf.uni-lj.si	189
Petrič Mitja	mitja.petric@ntf.uni-lj.si	287
Savić Vlado	vlado.savic@gov.si	235
Skopljak Ferid		217
Souvent Petra	petra.souvent@gov.si	235
Šetinc Marko	marko.setinc@omegaconsult.si	223
Škripić Nijaz		217
Terčelj Milan	milan.tercelj@ntf.uni-lj.si	165
Turk Radomir	rado.turk@ntf.uni-lj.si	151, 165
Uranjek Gregor	gregor.uranjek@gmail.com	247
Vončina Maja	maja.voncina@ntf.uni-lj.si	287
Vulić Milivoj	milivoj.vulic@ntf.uni-lj.si	247, 265
Zalar Anton	anton.zalar@ijs.si	151

INSTRUCTIONS TO AUTHORS

RMZ-MATERIALS & GEOENVIRONMENT (RMZ- Materiali in geokolje) is a periodical publication with four issues per year (established 1952 and renamed to RMZ-M&G in 1998). The main topics of contents are Mining and Geotechnology, Metallurgy and Materials, Geology and Geoenvironment.

RMZ-M&G publishes original Scientific articles, Review papers, Technical and Expert contributions (also as short papers or letters) **in English**. In addition, evaluations of other publications (books, monographs,...), short letters and comments are welcome. A short summary of the contents in Slovene will be included at the end of each paper. It can be included by the author(s) or will be provided by the referee or the Editorial Office.

*** Additional information and remarks for Slovenian authors:**

English version with extended »Povzetek«, and additional roles (in Template for Slovenian authors) can be written. Only exceptionally the articles in the Slovenian language with summary in English will be published. The contributions in English will be considered with priority over those in the Slovenian language in the review process.

Authorship and originality of the contributions. Authors are responsible for originality of presented data, ideas and conclusions as well as for correct citation of data adopted from other sources. The publication in RMZ-M&G obligate authors that the article will not be published anywhere else in the same form.

Specification of Contributions

Optimal number of pages of full papers is 7 to 15, longer articles should be discussed with Editor, but 20 pages is limit.

Scientific papers represent unpublished results of original research.

Review papers summarize previously published scientific, research and/or expertise articles on the new scientific level and can contain also other cited sources, which are not mainly result of author(s).

Technical and Expert papers are the result of technological research achievements, application research results and information about achievements in practice and industry.

Short papers (Letters) are the contributions that contain mostly very new short reports of advanced investigation. They should be approximately 2 pages long but should not exceed 4 pages.

Evaluations or critics contain author's opinion on new published books, monographs,

textbooks, exhibitions...(up to 2 pages, figure of cover page is expected).

In memoriam (up to 2 pages, a photo is expected).

Professional remarks (Comments) cannot exceed 1 page, and only professional disagreements can be discussed. Normally the source author(s) reply the remarks in the same issue.

Supervision and review of manuscripts. All manuscripts will be supervised. The referees evaluate manuscripts and can ask authors to change particular segments, and propose to the Editor the acceptability of submitted articles. Authors can suggest the referee but Editor has a right to choose another. **The name of the referee remains anonymous.** The technical corrections will be done too and authors can be asked to correct missing items. The final decision whether the manuscript will be published is made by the Editor in Chief.

The Form of the Manuscript

The manuscript should be submitted as a complete hard copy including figures and tables. The figures should also be enclosed separately, both charts and photos in the original version. In addition, all material should also be provided in electronic form on a diskette or a CD. The necessary information can conveniently also be delivered by E-mail.

Composition of manuscript is defined in the attached Template

The original file of Template is temporarily available on E-mail addresses:

peter.fajfar@ntf.uni-lj.si,

barbara.bohar@ntfgeo.uni-lj.si

References - can be arranged in two ways:

- first possibility: alphabetic arrangement of first authors - in text: (Borgne, 1955),
or

- second possibility: ^[1] numerated in the same order as cited in the text: example^[1]

Format of papers in journals:

Le Borgne, E. (1955): Susceptibilité magnetic anomale du sol superficiel.
Annales de Geophysique, 11, pp. 399-419.

Format of books:

Roberts, J. L. (1989): Geological structures, *MacMillan, London*, 250 p.

Text on the hard print copy can be prepared with any text-processor. The electronic version on the diskette, CD or E-mail transfer should be in MS Word or ASCII format.

Captions of figures and tables should be enclosed separately. **Figures (graphs and photos)** and tables should be original and sent separately in addition to text. They can be prepared on paper or computer designed (MSExcel, Corel, Acad).

Format. Electronic figures are recommended to be in CDR, AI, EPS, TIF or JPG formats. Resolution of bitmap graphics (TIF, JPG) should be at least 300 dpi. Text in vector graphics (CDR, AI, EPS) must be in MSWord Times typography or converted in curves.

Color prints. Authors will be charged for color prints of figures and photos.

Labeling of the additionally provided material for the manuscript should be very clear and must contain at least the lead author's name, address, the beginning of the title and the date of delivery of the manuscript. In case of an E-mail transfer the exact message with above asked data must accompany the attachment with the file containing the manuscript.

Information about RMZ-M&G:

Editor in Chief prof. dr. Peter Fajfar (tel. ++386 1 4250-316) or

Secretary Barbara Bohar Bobnar, un. dipl. ing. geol. (++386 1 4704-630),

Aškerčeva 12, Ljubljana, Slovenia

or at E-mail addresses:

peter.fajfar@ntf.uni-lj.si,

barbara.bohar@ntfgeo.uni-lj.si

Sending of manuscripts. Manuscripts can be sent by mail to the **Editorial Office** address:

- RMZ-Materials & Geoenvironment
Aškerčeva 12,
1000 Ljubljana, Slovenia

or delivered to:

- **Reception** of the Faculty of Natural Science and Engineering (for RMZ-M&G)
Aškerčeva 12,
1000 Ljubljana, Slovenia
- E-mail - addresses of Editor and Secretary
- You can also contact them on their phone numbers.

TEMPLATE

**The title of the manuscript should be written in bold letters
(Times New Roman, 14, Center)**

NAME SURNAME¹,, & NAME SURNAME^X
(TIMES NEW ROMAN, 12, CENTER)

^xFaculty of ... , University of ... , Address..., Country, e-mail: ...
(Times New Roman, 11, Center)

THE LENGTH OF FULL PAPER SHOULD NOT EXCEED TWENTY (20, INCLUDING FIGURES AND TABLES) PAGES (OPTIMAL 7 TO 15), SHORT PAPER FOUR (4) AND OTHER TWO (2) WITHOUT TEXT FLOWING BY GRAPHICS AND TABLES.

Abstract (Times New Roman, Normal, 11): The text of the abstract is placed here. The abstract should be concise and should present the aim of the work, essential results and conclusion. It should be typed in font size 11, single-spaced. Except for the first line, the text should be indented from the left margin by 10 mm. The length should not exceed fifteen (15) lines (10 are recommended).

Key words: a list of up to 5 key words (3 to 5) that will be useful for indexing or searching. Use the same styling as for abstract.

INTRODUCTION (TIMES NEW ROMAN, BOLD, 12)

Two lines below the keywords begin the introduction. Use Times New Roman, font size 12, Justify alignment.

There are two (2) admissible methods of citing references in text:

1. by stating the first author and the year of publication of the reference in the parenthesis at the appropriate place in the text and arranging the reference list in the alphabetic order of first authors; e.g.:
“Detailed information about geohistorical development of this zone can be found in: Antonijević (1957), Grubić (1962), ...”
“... the method was described previously (Hoefs, 1996)”

2. by consecutive Arabic numerals in square brackets, superscripted at the appropriate place in the text and arranging the reference list at the end of the text in the like manner; e.g.:
“... while the portal was made in Zope^[3] environment.”

MATERIALS AND METHODS (TIMES NEW ROMAN, BOLD, 12)

This section describes the available data and procedure of work and therefore provides enough information to allow the interpretation of the results, obtained by the used methods.

RESULTS AND DISCUSSION (TIMES NEW ROMAN, BOLD, 12)

Tables, figures, pictures, and schemes should be incorporated in the text at the appropriate place and should fit on one page. Break larger schemes and tables into smaller parts to prevent extending over more than one page.

CONCLUSIONS (TIMES NEW ROMAN, BOLD, 12)

This paragraph summarizes the results and draws conclusions.

Acknowledgements (Times New Roman, Bold, 12, Center - optional)

This work was supported by the ***.

REFERENCES (TIMES NEW ROMAN, BOLD, 12)

In regard to the method used in the text, the styling, punctuation and capitalization should conform to the following:

FIRST OPTION - in alphabetical order

Casati, P., Jadoul, F., Nicora, A., Marinelli, M., Fantini-Sestini, N. & Fois, E. (1981): Geologia della Valle del'Anisici e dei gruppi M. Popera - Tre

- Cime di Lavaredo (Dolomiti Orientali). *Riv. Ital. Paleont.*; Vol. 87, No. 3, pp. 391-400, Milano.
- Folk, R. L. (1959): Practical petrographic classification of limestones. *Amer. Ass. Petrol. Geol. Bull.*; Vol. 43, No. 1, pp. 1-38, Tulsa.

SECOND OPTION - in numerical order

- [¹] Trček, B. (2001): *Solute transport monitoring in the unsaturated zone of the karst aquifer by natural tracers*. Ph.D. Thesis. Ljubljana: University of Ljubljana 2001; 125 p.
- [²] Higashitani, K., Iseri, H., Okuhara, K., Hatade, S. (1995): Magnetic Effects on Zeta Potential and Diffusivity of Nonmagnetic Particles. *Journal of Colloid and Interface Science* 172, pp. 383-388.

Citing the Internet site:

CASREACT-Chemical reactions database [online]. Chemical Abstracts Service, 2000, updated 2.2.2000 [cited 3.2.2000]. Accessible on Internet: <http://www.cas.org/CASFILES/casreact.html>.

POVZETEK (TIMES NEW ROMAN, 12)

A short summary of the contents in Slovene (up to 400 characters) can be written by the author(s) or will be provided by the referee or by the Editorial Board.

TEMPLATE for Slovenian Authors

**The title of the manuscript should be written in bold letters
(Times New Roman, 14, Center)**

Naslov članka (Times New Roman, 14, Center)

NAME SURNAME¹, ..., & NAME SURNAME^X (TIMES NEW ROMAN, 12, CENTER)
IME PRIIMEK¹, ..., IME PRIIMEK^X (TIMES NEW ROMAN, 12, CENTER)

^XFaculty of ..., University of ..., Address..., Country; e-mail: ...
(Times New Roman, 11, Center)

^XFakulteta..., Univerza..., Naslov..., Država; e-mail: ...
(Times New Roman, 11, Center)

THE LENGTH OF ORIGINAL SCIENTIFIC PAPER SHOULD NOT EXCEED TWENTY (20, INCLUDING FIGURES AND TABLES) PAGES (OPTIMAL 7 TO 15), SHORT PAPER FOUR (4) AND OTHER TWO (2) WITHOUT TEXT FLOWING BY GRAPHICS AND TABLES.

DOLŽINA IZVIRNEGA ZNANSTVENEGA ČLANKA NE SME PRESEGATI DVAJSET (20, VKLUČNO S SLIKAMI IN TABELAMI), KRATKEGA ČLANKA ŠTIRI (4) IN OSTALIH PRISPEVKOV DVE (2) STRANI.

Abstract (Times New Roman, Normal, 11): The text of the abstract is placed here. The abstract should be concise and should present the aim of the work, essential results and conclusion. It should be typed in font size 11, single-spaced. Except for the first line, the text should be indented from the left margin by 10 mm. The length should not exceed fifteen (15) lines (10 are recommended).

Izvleček (TNR, N, 11): Kratek izvleček namena članka ter ključnih rezultatov in ugotovitev. Razen prve vrstice naj bo tekst zamaknjen z levega roba za 10 mm. Dolžina naj ne presega petnajst (15) vrstic (10 je priporočeno).

Key words: a list of up to 5 key words (3 to 5) that will be useful for indexing or searching. Use the same styling as for abstract.

Ključne besede: seznam največ 5 ključnih besed (3-5) za pomoč pri indeksiranju ali iskanju. Uporabite enako obliko kot za izvleček.

INTRODUCTION – UVOD (TIMES NEW ROMAN, BOLD, 12)

Two lines below the keywords begin the introduction. Use Times New Roman, font size 12, Justify alignment. All captions of text and tables as well as the text in graphics must be prepared in English and Slovenian language.

Dve vrstici pod ključnimi besedami se začne Uvod. Uporabite pisavo TNR, velikost črk 12, z obojestransko poravnavo. Naslovi slik in tabel (vključno z besedilom v slikah) morajo biti pripravljeni v slovenskem in angleškem jeziku.

Figure (Table) X. Text belonging to figure (table)

Slika (Tabela) X. Pripadajoče besedilo k sliki (tabeli)

There are two (2) admissible methods of citing references – obstajata dve sprejemljivi metodi navajanja referenc:

1. by stating the first author and the year of publication of the reference in the parenthesis at the appropriate place in the text and arranging the reference list in the alphabetic order of first authors; e.g.:
 1. z navedbo prvega avtorja in letnice objave reference v oklepaju na ustreznom mestu v tekstu in z ureditvijo seznama referenc po abecednem zaporedju prvih avtorjev; npr.:
“Detailed information about geohistorical development of this zone can be found in: Antonijević (1957), Grubić (1962), ...”
“... the method was described previously (Hoefs, 1996)”

or/ali

2. by consecutive Arabic numerals in square brackets, superscripted at the appropriate place in the text and arranging the reference list at the end of the text in the like manner; e.g.:
 2. z zaporednimi arabskimi številkami v oglatih oklepajih na ustreznom mestu v tekstu in z ureditvijo seznama referenc v številčnem zaporedju navajanja; npr.;
“... while the portal was made in Zope^[3] environment.”

MATERIALS AND METHODS (TIMES NEW ROMAN, BOLD, 12)

This section describes the available data and procedure of work and therefore provides enough information to allow the interpretation of the results, obtained by the used methods.

Ta del opisuje razpoložljive podatke, metode in način dela ter omogoča zadostno količino informacij, da lahko z opisanimi metodami delo ponovimo.

RESULTS AND DISCUSSION – REZULTATI IN RAZPRAVA (TIMES NEW ROMAN, BOLD, 12)

Tables, figures, pictures, and schemes should be incorporated (inserted, not pasted) in the text at the appropriate place and should fit on one page. Break larger schemes and tables into smaller parts to prevent extending over more than one page.

Tabele, sheme in slike je potrebno vnesti (z ukazom Insert, ne Paste) v tekst na ustreznom mestu. Večje sheme in tabele je potrebno ločiti na manjše dele, da ne presegajo ene strani.

CONCLUSIONS – SKLEPI (TIMES NEW ROMAN, BOLD, 12)

This paragraph summarizes the results and draws conclusions.

Povzetek rezultatov in zaključki.

Acknowledgements – Zahvale (Times New Roman, Bold, 12, Center - optional)

This work was supported by the

Izvedbo tega dela je omogočilo

REFERENCES - VIRI (TIMES NEW ROMAN, BOLD, 12)

With regard to the method used in the text, the styling, punctuation and capitalization should conform to the following:

Glede na uporabljeno metodo citiranja referenc v tekstu upoštevajte eno od naslednjih oblik:

FIRST OPTION (recommended) – PRVA MOŽNOST (priporočena) – in alphabetical order (v abecednem zaporedju)

Casati, P., Jadoul, F., Nicora, A., Marinelli, M., Fantini-Sestini, N. & Fois, E. (1981): Geologia della Valle del'Anisici e dei gruppi M. Popera – Tre Cime di Lavaredo (Dolomiti Orientali). *Riv. Ital. Paleont.*; Vol. 87, No. 3, pp. 391-400, Milano.

Folk, R. L. (1959): Practical petrographic classification of limestones. *Amer. Ass. Petrol. Geol. Bull.*; Vol. 43, No. 1, pp. 1-38, Tulsa.

SECOND OPTION – DRUGA MOŽNOST - in numerical order (v numeričnem zaporedju)

[¹] Trček, B. (2001): *Solute transport monitoring in the unsaturated zone of the karst aquifer by natural tracers*. Ph.D. Thesis. Ljubljana: University of Ljubljana 2001; 125 p.

[²] Higashitani, K., Iseri, H., Okuhara, K., Hatade, S. (1995): Magnetic Effects on Zeta Potential and Diffusivity of Nonmagnetic Particles. *Journal of Colloid and Interface Science* 172, pp. 383-388.

Citing the Internet site:

CASREACT-Chemical reactions database [online]. Chemical Abstracts Service, 2000, updated 2.2.2000 [cited 3.2.2000]. Accessible on Internet: <http://www.cas.org/CASFILES/casreact.html>.

Citiranje Internetne strani:

CASREACT-Chemical reactions database [online]. Chemical Abstracts Service, 2000, obnovljeno 2.2.2000 [citirano 3.2.2000]. Dostopno na svetovnem spletu: <http://www.cas.org/CASFILES/casreact.html>.

POVZETEK – SUMMARY (TIMES NEW ROMAN, 12)

An extended summary of the contents in Slovene (from one page to approximately 1/3 of the original article length).

Razširjeni povzetek vsebine prispevka v Angleščini (od ene strani do približno 1/3 dolžine izvirnega članka).

No. of indexing of RMZ-M&G in singular Databases

(Število indeksiranih člankov iz RMZ-M&G v posameznih bazah)

(prepared by Fajfar, P. – from search done by Šercelj, M., CTK Ljubljana, 15.2.2007)

	DATABASE NAME	HITS
1:	Civil Engineering Abstracts	773
2:	CA SEARCH® - Chemical Abstracts® (1967- present)	760
3:	Inside Conferences	313
4:	Materials Business File	253
5:	METADEX®	164
6:	ANTE: Abstracts in New Technologies and Engineering	158
7:	GeoRef	154
8:	Aluminium Industry Abstracts	36
9:	PASCAL	30
10:	Energy Science and Technology	27
11:	TEME - Technology and Management	27
12:	Ei Compendex®	13
13:	CSA Aerospace & High Technology Database	12
14:	Computer and Information Systems	10
15:	Mechanical & Transportation Engineering Abstracts	8
16:	Engineered Materials Abstracts®	3
17:	Corrosion Abstracts	3
18:	Analytical Abstracts	1
19:	FLUIDEX	1
20:	Solid State and Superconductivity Abstracts	1
21:	Electronics and Communications Abstracts	1
		2748

ŠTOREQSTEEL

155 let

železarska c. 3 3220 Štore Slovenija
www.store-steel.si